A Technique for Real-Time Detection of Defects in Composite Structure using Carbon nanotubes, and Transfer Learning

Farzad Kashefinishabouri

A thesis

In the Department

Of

Mechanical, Industrial, and Aerospace Engineering

Presented in Partial Fulfillment of the Requirements

For the Degree of Master of Applied Science (Mechanical Engineering) at

Concordia University

Montreal, Quebec, Canada

August 2022

CONCORDIA UNIVERSITY

School of Graduate Studies

This is to certify that the thesis prepared

By: Farzad Kashefinishabouri

Entitled: A Technique for Real-Time Detection of Defects in Composite Structure using Carbon nanotubes, and Transfer Learning

and submitted in partial fulfillment of the requirements for the degree of

Master of Applied Science (Mechanical Engineering)

complies with the regulations of the university and meets the accepted standards with respect to originality and quality.

Signed by the final Examining Committee:

_____ Examiner, and Chair

Dr. Mehdi Hojjati

_____ Examiner

Dr. Abdessamad Ben Hamza

_____ Supervisor

Dr. Suong Van Hoa

Approved by _____

Dr. Martin Pugh

Chair, Department of Mechanical, Industrial & Aerospace Engineering

August 29, 2022 _____

Dr. Mourad Debbabi

Dean, Gina Cody School of Engineering and Computer Science

ABSTRACT

A Technique for Real-Time Detection of Defects in Composite Structure using Carbon nanotubes, Machine Learning Including Transfer Learning

Farzad Kashefinishabouri

Fiber-reinforced polymer composites have garnered interest in a range of industrial applications due to their outstanding mechanical characteristics and lightweight. Monitoring the health of polymer composite structures in real-time is one of the most challenging issues in the practical use of composites due to their susceptibility to many types of damage. Conventional non-destructive tests (NDT) methods such as X-ray tomography and ultrasonic may be used to assess composite materials but the drawback of conventional NDT techniques is that they cannot be implemented when the composite part is in use.

Composite plates' electrical characteristics can be to do real-time health monitoring. Carbon nanotubes (CNTs) because of their excellent conductivity characteristics, are used in composites to enhance the conductivity of resins within composites. It is shown that by monitoring the electrical behavior of composites with CNT embedded resins, defects can be detected. The issue with this approach is that numerous wires and connections are required. The weight of composite structures is greatly influenced by the number of wires and connections, which also makes the system more prone to errors because numerous connections must function well for the system to respond as intended.

To tackle this problem, in this study, the goal is to reduce the number of required probes and connections by limiting the probes to the edges of composite plates rather than throughout the plate. By having the probes on the edges of the plate, there may not be a direct correlation between defects at different locations within the plates to the measurements as it was in the previous cases. There are two approaches to tackle this problem:1. To develop a physics-based model that can precisely model the electrical behavior of composite with CNTs embedded in the resin. 2. To develop a data-driven model that can relate the measurements to the location

of the defect. As the first approach is expensive and time-consuming the second approach is picked in this study. Neural network (NN) is used to find the pattern between measurements on the edges and the location of the defect. The problem with using neural network (NN) models is that they require numerous numbers of labeled examples. To tackle this problem Transfer Learning (TL) and data augmentation is used. TL is used to reduce the number of labeled data points required for the training process as in composites it is too expensive and time-consuming to generate a huge number of data points. In the TL method that is used, the training is done in two stages, first stage the training is done based on the data generated from a similar problem that the data can be abundant, and the second stage of training is done using experimental data of the exact problem. Data augmentation is used on experimental data to increase the data points for training NN. The performance of the trained neural network in locating defects by having the probes only on the edges of the samples is promising (accuracy of 78.57% on the test set).

Also, the performance of the neural network models for different precisions and sample sizes were studied. The precision is defined as the area in which the defects can be located within.

KEYWORDS

Real-time defect detection, Neural Network, Transfer learning, Data augmentation

ACKNOWLEDGMENTS

I would like to extend my sincere gratitude to my supervisor, Professor Suong Van Hoa for giving me the opportunity to work on this project under his supervision, and for his guidance and unconditional support during my program. This work would not be possible without his advice and support.

I would like to thank all (CONCOM), for their professional support. I also, wish to show my appreciation to all my friends in particular Mr. Emad Fakhimi, Mrs. Hadis Montazerinejat, Mr. Amirreza Pakzadi, Mr. Farid Ehsani, Mr. Ali Ebrahimi, and Mr. Alireza Mousakhani for their friendship.

I also would like to thank the examining committee, Dr. Mehdi Hojjati and Dr. Abdessamad Ben Hamza.

Last but not least, I like to sincerely thank my beloved father, mother, and sister for their constant support during my life.

DEDICATION

This thesis is dedicated to my always supportive parents,

Zahra and Jahangir

Table of Contents

List of Figures ..... **x**

List of Tables ..... **xiii**

CHAPTER 1: Introduction **1**

1.1 Introduction 1

1.2 Defect Detection Methods 1

1.2.1 Ultrasonic 3

1.2.2 Vibration Technique 5

1.2.3 Acoustic Emission 7

1.2.4 X-Ray 8

1.2.5 Infrared Thermography 8

1.2.6 Fiber Optics 10

1.2.7 Shearography 10

1.2.8 Electrical conductivity along the carbon fiber direction 11

1.2.9 Embedding resistance-based sensors 11

1.3 Adding carbon nanotubes into resin 13

Chapter 2: LITERATURE REVIEW AND METHODOLOGY **17**

2.1 Artificial Neural Network in the Field of Composite Materials 17

2.2 Objective 19

2.3 Rationale for selecting Machine Learning 22

2.4 Introduction to ML approaches and Method Selection 23

2.5 Special techniques to overcome the need for large amount of data 24

CHAPTER 3: Materials, Sample preparation, and Experiments **29**

3.1 Experiments 29

3.2 Determination of Optimum CNT Concentration 30

3.2.1 Effect of amount of nanotubes on resistivity 32

3.2.2 Effect of amount of nanotubes on sensitivity to the occurrence of defects 36
3.3 Samples for Experimental Data Generation 39
3.4 Electrical Resistance Testing 43
3.5 Electrical Measurement Strategy 43
3.6 Data Acquisition System 47
3.7 Measurements and Data Treatment 49
3.8 Data Augmentation 51
3.8.1 Introduction to Data Augmentation 51
3.8.2 Data Augmentation on Experimental Data Set 53
CHAPTER 4: Simulation and Data Preparation 56
4.1 Simulation 56
4.2 LTspice 56
4.3 Python 56
4.4 Simulation of a Grid of resistors 57
4.5 Data Preparation 61
CHAPTER 5: ANN Training, Optimizing, Testing, and Results 65
5.1 Introduction to ML and Tools that are Used for ANN Model 65
5.2 Development 65
5.2.1 What is ML? 65
5.2.2 Training Deep NN model 66
5.3 Transfer Learning 67
5.3.1 Definition 67
5.4 Precision Study 73
5.5 Study of Sample Size 79
CHAPTER 6: Results, Conclusion, and Future Works 83
6.1 Results and Discussion 83
6.2 Conclusion 87

6.3 Contributions 88
6.4 Future Works 88
References 90

List of Figures

Figure 1: NDT techniques classified into Active and Passive approaches[4] 2
Figure 2: a: Ultrasonic pulse-echo method. b: Ultrasonic trough-transmission method 4
Figure 3: Lock-in thermography setup[4].....9
Figure 4: A illustration of using resistance-based sensors that are embedded in the composite structures[86] 12
Figure 5: Resistance-based conductive fiber sensors used with flexible circuit board[87]....12
Figure 6: A system using ink containing carbon nanofibers as conductive lines on the surface of the composite to sense deformation and defects [88].....13
Figure 7: Three-dimensional illustration of CNTs' penetration throughout a fiber array because of their relative scale[99].....14
Figure 8: Normalized change in surface resistivity PMMA/MWNT films for different MWCNT concentrations [100]. 14
Figure 9: A plate of composite that the electrical resistances are measured using probes on the corner of each cell. The silver circles on the corners of each cell are probes [75]. 16
Figure 10: Distribution of articles published on composite characterization using ANN during different years[109] 17
Figure 11: Illustration of probes required in the method developed by Ali Naghashpour and Hoa.[158]. Purple squires represent probes. 21
Figure 12: Illustration of the number of probes required for this study to locate the location of the defect using probes on the edges. Purple squires represent probes. 22
Figure 13: Artificial Intelligence Subcategories [159] 23
Figure 14: The schematic of the procedure 26
Figure 15: a. Composite plate with probes, b. Model as network of resistors.....27
Figure 16: CNT used to prepare samples.....30
Figure 17: Epoxy resin and Curing Agent used to prepare samples.....30
Figure 18: a. Many paths of conduction in a very conductive material. b. Few paths of conduction within a less conductive material 31
Figure 19: CNTs being dispersed in epoxy resin using three roll milling.....33
Figure 20: (a) Epoxy resin with different concentrations (Difference in viscosity is shown) (b) sample with different CNT concentrations under a vacuum bag. 33

Figure 21: Samples made with different concentrations of CNT 34
Figure 22: Experimental setup for the Van-Pauw method 35
Figure 23: The current source and voltmeter used 37
Figure 24: Sample with a dilled hole to measure the measurable difference before and after the defect 37
Figure 25: Resistivity of samples vs. CNT concentration 38
Figure 26: Sensitivity (S) vs. CNT concentration.....39
Figure 27: DSC result of the cured sample**.**.....41
Figure 28: Image of the cross section of the cured layup under microscope.....41
Figure 29: A cured sample with node numbers on the edges and cell numbers in the middle of each cell 42
Figure 30: Schematic of Numbering cells, Nodes, and Probes 43
Figure 31: Schematic diagram of a four-point probe circuit 44
Figure 32: Schematic diagram of a two-point probe circuit 45
Figure 33: A four-probe method applied for measurement on a sample plate 46
Figure 34: Measurement on the sample. 47
Figure 35: Schematic diagram of the Data Acquisition System.....49
Figure 36: Some of the simple image transformations used for image augmentation [170]..52
Figure 37: presentation of data augmentation using horizontal flipping 53
Figure 38: presentation of data augmentation using horizontal flipping 54
Figure 39: (a) The actual glass fiber reinforced Epoxy with CNTs (b) The schematic of the plate indicating cell numbers and probes and their assigned numbers 57
Figure 40:(a) A schematic of the circuit of a 6 by 6 grid of resistors used to model the composite plate (b) The circuit that is shown in Fig3 (a) modeled in LTspice software 58
Figure 41: Illustration of recording electrical voltages between 14 opposite pairs of nodes. 59
Figure 42: One cell is targeted at each run of LTspice model and the values for resistors making that cell increase from initial values (random between 1Ω-10Ω) to random values between 30-40 Ω.....60
Figure 43: Flowchart for the python code 63
Figure 44: Initial NN that is trained on simulation data 70
Figure 45: Removing the top layer of the initial NN structure. 71
Figure 46: Adding 3 new layers on the top and training the parameter based on experimental data.....72
Figure 47: The original cell classes distribution. A sample with 36 possible cell classes.....74

Figure 48: The distribution of plate with 9 cell classes by grouping 4 cells of 36 cell class distribution into one new cell.....75
Figure 49: The 4 possible cell classes from 36 possible cell class distributions. 76
Figure 50: The 2 possible cell classes from 36 possible cell class distributions. 77
Figure 51: Change of accuracy with respect to changes in the precision area 78
Figure 52: Change of gained accuracy with respect to changes in the precision area.....79
Figure 53: Samples are manufactured in different sizes: 15”by15” on the left, 12” by 12” in the middle and 9” by 9” on the right side of the picture. 80
Figure 54: Changes in the accuracy of the developed NN with respect to precision and sample size. 81
Figure 55: Changes in gained accuracy of the developed NN with respect to precision and sample size. 82
Figure 56: Changes in the accuracy of the developed NN with respect to precision and sample size. 84
Figure 57: Changes in gained accuracy of the developed NN with respect to precision and sample size. 84
Figure 58: The average performance of a random classifier with respect to the number of possible classes 85
Figure 59: The way all 4 cells in the middle (in 36 cell precision) are grouped into one cell in 9 cell class precision 86
Figure 60: The way every 4 cells in the middle (in 36 cell precision) are grouped into different cells in 4 cell class precision 87

List of Tables

Table 1: Resistivity of samples with different CNT Concentration.....39
Table 2: Different models' performance with and without data augmentation[170] 52
Table 3: Optimizing initial NN on the Dev. Set data example of simulation.....69
Table 4: Performance of initial NN model on the simulation model.....70
Table 5: the performance of final NN on the experimental development set of data.....72
Table 6: Performance of final NN model on the test set from the experimental data 73
Table 7: The performance of the developed NN model on different precision data distribution.....77
Table 8: The result of the performance of NNs on the data from testing samples with the size of 9" by 9".....80
Table 9: The result of the performance of NNs on the data from testing samples with the size of 15" by 15".....81

CHAPTER 1: Introduction

1.1 Introduction

Because of their high strength-to-weight and stiffness-to-weight ratios, good corrosion resistance, and fatigue properties compared to conventional metals, fiber-reinforced polymer composites (FRPC) are widely used in many industrial applications[1]. The applications of composites in different industries such as aerospace, automotive, and marine are growing[2]. There are factors threatening the structural health of composites such as fatigue loads, impact, humidity, and temperature[3]. A catastrophic collapse might happen if the damage is not discovered early during the operation. Because of this, it's crucial to effectively analyze composites and identify damage early during the operation. However, the anisotropic structure of composites makes it more challenging to assess the damage. The assessment of damage in composites is shown to be better served by nondestructive methods[4]. Throughout the service life, both freshly generated damage and critical damage must be tracked and found. The health monitoring approach can be used to evaluate how damage will affect the composite structure's residual life [5], [6]. This Structural Health Monitoring (SHM) decreases inspection time and prevents a structure from failing while it is in use[7]. Local and global damage detection approaches are subcategories of nondestructive damage detection methods. A local damage detection approach is used when the damage location is already known for testing. Small structures like pressure vessels and the aerospace and automobile industries both employ this method. One method for local damage detection is ultrasonic testing[8]. It is not always possible to detect the damage using local damage detection techniques, especial cases are big and complex structures and inaccessible areas. Global damage detection approaches are required in such circumstances. An instance of a global damage detection method is vibration-based damage detection[9].

1.2 Defect Detection Methods

Methods of defect detection can be classified by considering different aspects of methods. As shown in Figure 1, they can be divided into two kinds of approaches: Active Techniques and Passive Techniques[4]. When detecting damage, an active technique requires complex

equipment and less signal processing, whereas a passive approach often requires more signal processing and less sophisticated equipment[10].

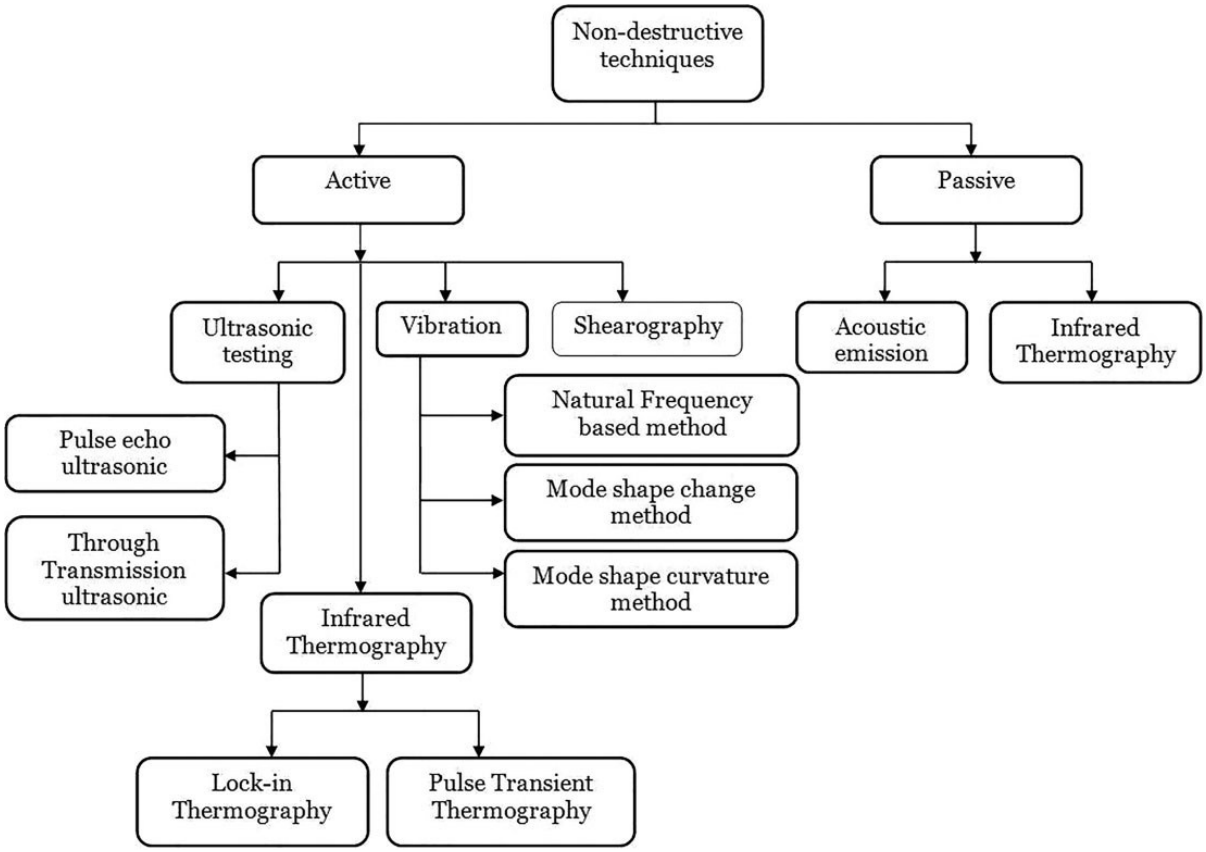

Figure 1: *NDT techniques classified into Active and Passive approaches*[4]

To find damage in composites, both destructive and non-destructive methods are employed. Due to its integration of sensors, data collecting, data transfer, computational methods, and processing power, structural health monitoring (SHM) is an improved approach of nondestructive evaluation[11],[12].

Monitoring the health of composite structures in real-time is one of the most difficult aspects in the practical application of structural composite materials in comparison to traditional metallic structures. This is due to their vulnerability to various types of damage, such as fiber fracture, matrix cracking, delamination, and fiber/matrix debonding, which can occur in various areas of composite constructions[13][14]. With a wide range of usage of composite structures in various industries, especially in aerospace, and emerging the era of

reusing spaceships for space traveling, it is an urgent need to have techniques for real-time SHM of composite structures.

For health monitoring of structural composites, various non-destructive evaluation (NDE) techniques such as ultrasound scanning, acoustic emissions, X-ray, thermography, fiber optics, shearography, electrical conductivity along the direction of carbon fibers, and resistance-based sensors have been used. However, in practice, the applications of these techniques to structural health monitoring, which is the continuous assessment of structural composite integrity, have been limited due to a variety of factors, including impracticality for real-time damage monitoring, local measurement, lack of ability for real-time inspecting large composite structures, high cost, complex data analysis tools, poor spatial resolution, limited in-situ capabilities, and equipment requirements[15]–[19]. The NDE techniques and their limitations in real-time SHM are as follows:

1.2.1 Ultrasonic

An active nondestructive approach called ultrasonic testing uses the ultrasonic wave propagation in the test object to find cracks and other damage. Based on the kind of energy (reflected or transmitted energy) used in the inspection, ultrasonic testing can be divided further into the pulse-echo technique and through-transmission technique. While the through-transmission approach uses transmitted energy to identify the damage, the pulse-echo method looks for damage using reflected energy[20].

Pulse-echo testing is shown in Figure 2(a). The signal is sent into the material via the transducer, and it is reflected off the flaws or the back wall. Two transducers are employed in through-transmission technique in order to receive the waves; one transducer is at the top of the test specimen's front surface and the other is at the rear surface. Figure 2(b) illustrates how a break or damage in the sound's travel route results from a loss in the energy delivered during transmission[4].

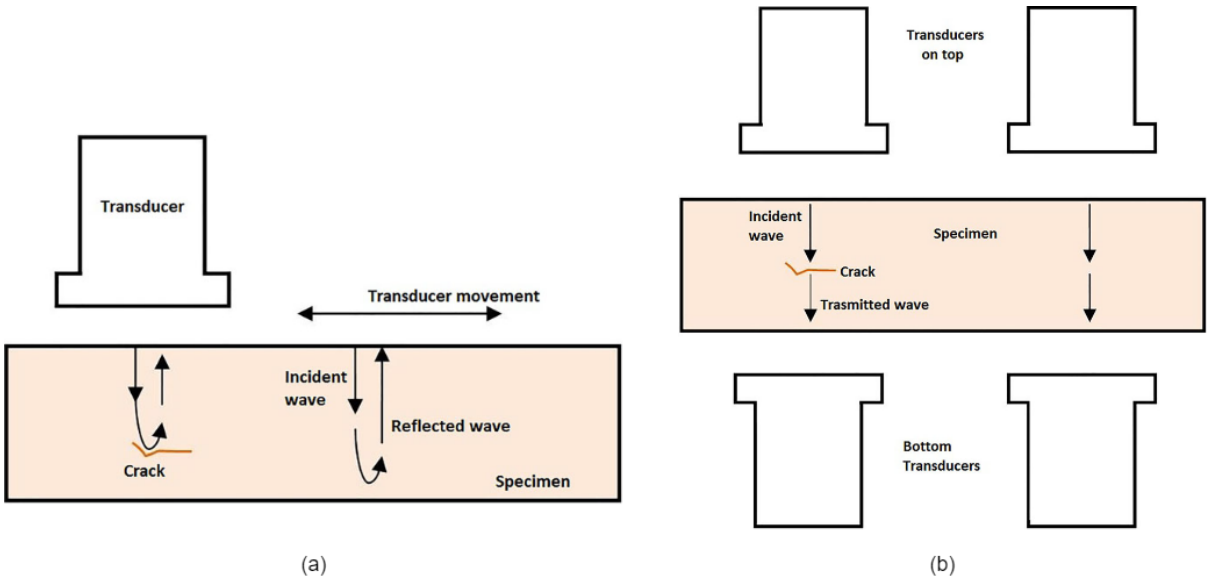

Figure 2: *a: Ultrasonic pulse-echo method. b: Ultrasonic trough-transmission method*

Ultrasonic waves are delivered across the thickness of the composite laminate in this approach. If the laminate is good, the ultrasonic wave's travel duration is short. The period of passage of the ultrasonic wave is varied if there are defects in the laminate, such as delamination or matrix cracking. A map of images from the time of travel is displayed after scanning the laminate's surface area. This image map is compared to an image map obtained over a good lamination as a reference. The region of the defect can be determined by comparing the actual map of images to the reference map of images[21]–[24].

The identification of flaws in composite materials was proposed using neural network-based processing of ultrasonic data. The neural network was utilized to identify the location and kind of the damage. This procedure was used for three different thickness of materials. Three different materials were found to have damage, and top and bottom plies were used to determine the sort of damage and its location. However, because the signals generated by damage to several plies are identical, the defect-type characterization was reduced in the middle location[25].

This method is widely used. However, there are limitations. Scanning must be done either in a lab (for small samples) or a shop (for the case of the large sample). This limits this method to be used as a real-time SHM technique. To maintain the ultrasonic beam coherently, a transfer medium is required. This medium is usually liquid. Having this liquid medium required for this method, its practical application is limited. Also, this method requires large and heavy equipment which is not appropriate for aerospace applications. The method has certain drawbacks, including the need for skilled operators and its inability to detect faults parallel to

the sound stream. Due to the thin reflecting surface, faults (delamination) parallel to the surface may go unnoticed[26].

1.2.2 Vibration Technique

Another type of method for detecting global damage is the vibration approach. Changes in the physical characteristics, like mass, stiffness, and damping result in observable changes in the modal parameters, that are used in vibration-based damage detection approaches. Natural frequency, modal damping, and mode shapes are the modal parameters that are impacted[8].

1.2.2.1 Natural frequency-based method:

The fundamental aspect of damage diagnosis in natural frequency-based approaches is the natural frequency shift. The natural frequencies are impacted by changes in the structural qualities[27]. Since the natural frequency is less sensitive to damage, it is necessary to measure the damage with better accuracy in order to obtain reliable findings. The simply supported beam and cantilever beam with a single crack's natural frequency fluctuations were discussed using the forward issue[28].

the inverse problem is used to find the location and size of damage (cracks) in cantilever and simply supported beams. The location and size of fractures in beams are determined by weightless torsion spring model. The magnitude and location of the damage in a structure are found using the inverse problem and the natural frequencies. Using a genetic algorithm, structural damage location and magnitude are inferred from natural frequency variations. As the number of recorded frequencies rises, so does the accuracy in identifying the damage and determining its severity[29].

Natural frequency shifts were used to determine the delamination size and location in fiber-reinforced composite plates. The natural frequencies change when delamination is present. Using experimentally derived values and numerically simulated frequency shifts, algorithms' performance is assessed. To generate residual frequency response functions (FRFs), the reconstruction technique was utilized to measure the frequencies of the damaged composite structure (reconstructed residual FRFs) [30]. The debonding length extent in sandwich composites and fatigue damage of composites were determined from the natural frequency and damping ratios of damaged composites utilizing the reconstructed residual FRFs[31].

For basic constructions with lesser size damage, the natural frequency-based approach can be applied. The modeling of damage and structure is the first restriction. For

the purpose of identifying damage in beam structures, fractures are treated as rotating springs. High-frequency modes and deep cracks are not good candidates for this kind of crack modeling [32]. When compared to the shift brought on by environmental and operational factors, the frequency change brought on by a minor fracture is insignificant. Because two separate damages might be causing the same change in natural frequency at two different locations, frequency change is insufficient to pinpoint structural damage[33].

1.2.2.2 Mode shape change method:

For damage identification, this approach uses changes in the mode shape of damaged structures. Natural frequency and mode shape variations can be combined to identify deterioration[34]. The difference in the mode shape between the pristine and damaged structures is used to diagnose damage using neural network-based approaches[35].

Low-velocity impact damage in composite laminates can also be identified using vibration-based approaches (model parameters)[36]. Natural frequency sensitivities and mode shapes were employed to precisely detect the damage in the cylindrical fiber-reinforced plastic (FRP) shell. The energy distribution in an intact FRP shell was used to calculate the sensitivity of natural frequency shifts based on the damage position[37]. The strain energy of the carbon fiber-reinforced polymer (CFRP) composite was determined using mode shapes, and the small change in strain energy was used as an index for the damage to detect fractures on the surface [38].

To measure mode shapes, there are large numbers of sensors required and the mode shapes are sensitive to noise contaminations[34].

1.2.2.3 Mode shape curvature method:

Small-scale damage has little effect on displacement mode forms. As a result, the second derivatives of the mode shapes are used to improve the sensitivity of damage detection [39]. Localization of the damage is achievable because they are hugely sensitive to damage. For locating the damage, the performance of displacement mode shape and mode shape curvature approaches are examined[40]. It was discovered that the curvature of the mode shape is a sensitive indicator of damage. A neural network was used to detect small damage, perforations, and debonding damage in sandwich composites using data from mode shape curvature and thermographic heat patterns[41]. The combined approach had a high degree of accuracy in detecting deterioration in sandwich composites. In beam-like structures, natural frequencies and strain mode shapes are employed as inputs to ANNs for detecting damage and determining

damage severity[42]. On composites, the broadband approach is utilized, which uses data at all frequencies and has more sensitivity than model-based methods[43].

1.2.3 Acoustic Emission

When a material experiences microstructural changes, a process known as acoustic emission happens naturally. The release of energy in the form of waves is connected to microstructural changes. The phenomenon known as Acoustic Emission (AE) is the production of elastic waves from the damaged area[44]. An artificial ear (high-frequency sensor) is fitted to the composite construction for sonic emission. When a crack appears, stress waves travel throughout the structure. A crack can be detected by reading the signal displayed by the sensor. One could find the crack by installing multiple sensors in a specific geometrical pattern on the structure's surface [15], [45]–[49]. The sensors positioned on the structure's surface or those incorporated inside the structure may both detect waves. Although the life of the host structure can be shortened by the incorporation of sensors, the sensor that is embedded is more responsive to AE monitoring than the sensor positioned on the surface[50].

De Oliverira and Marques AT [51] employed the AE approach and an artificial neural network (ANN) to detect damages in composite materials. The narrow cross-ply glass fiber polyester laminates' acoustic signals during the tensile test were subjected to the ANN. The sample size is 2.5 cm by 25 cm. Piezoelectric sensors positioned on the surface picked up the acoustic impulses. Broadband transducer utilized to better understand damage processes from AE waves[51].

Haggui M. et al. [52] discovered that throughout the test, the dissipated energy is greater in cross-ply and fast gets to the damage. In comparison to cross-ply flax fiber-reinforced laminate composite, uni-directional (UD) flax fiber-reinforced composite has a greater endurance limit. All damage mechanisms in the cross-ply laminate commence at the first stage. Fiber breakages do not show up in the UD laminate in the first stage.

Based on McCrory JP et al. [53] study: Artificial Neural Network analysis, unsupervised waveform clustering, and corrected measured amplitude ratio are the three AE approaches for classification that are used to evaluate damage in carbon fiber composite panels. These three methods of pattern identification were utilized to categorize the buckling-related damage to carbon fiber composite panels. These three methods are used to determine the damage processes, such as matrix cracking and delamination.

To evaluate the barely visible damage utilizing AE, carbon/epoxy-laminated composites were evaluated under quasi-static indentation and low-velocity impact loading. The AE results demonstrated the similarities between quasi-static indentation and low-velocity impact [54].

Extraneous noise from various sources, such as stiffener reflection and reverberation, free edges, and so on, can interfere with the desired signal. Another drawback of this method is that it is unable to find dormant cracks. Only when the cracks (flaws) are expanding can they be detected. In composite materials with complicated geometries, it is challenging to locate microscopic fractures and estimate their magnitude[55].

1.2.4 X-Ray

In this method, an X-ray photograph is taken from the samples. By observation, the defected sample can be differentiated if they are defected[19], [56]. As taking X-ray photographs requires equipment, this method can be used only in labs and not during the time of service of the structure.

1.2.5 Infrared Thermography

Thermography works on the premise that the amount of heat emitted from a structure's surface is proportional to the stress condition of the material beneath it[16]. If the material under the surface has defects, the temperature distribution on the surface will be non-uniform (down to a fraction of a degree). One can evaluate whether a sample has faults by comparing the thermal image of a reference sample to that of the sample under investigation.

The infrared (IR) energy released by the sample or specimen is detected using infrared thermography (IRT) technology. The IR energy conversion produces the thermal pictures (temperature distribution)[57]. There are primarily two types of thermography: passive thermography and active thermography. In passive thermography, a sample that is at a different temperature compared to its surroundings is subjected to the test. In active thermography, the sample's temperature gradient develops in response to an outside stimulus[58]. Lock-in thermography, pulse transient thermography, and other active thermography techniques are available depending on the external stimulation. Figure 3 demonstrates how halogen lamps are used to heat the sample during lock-in thermography in order to upset the thermal equilibrium. The input wave goes through the sample and is reflected from the specimen's rear surface or from any damaged regions. In comparison to waves in undamaged locations, waves reflected from damaged areas have a distinct phase. Different thermophysical characteristics of the damaged portions are caused by the phase delay. The reflected waves are captured by the IR

camera. In pulse transient thermography, the sample is heated over a brief period of time by a source of continuous heat flow, and then using an infrared camera the surface is observed[59]–[61].

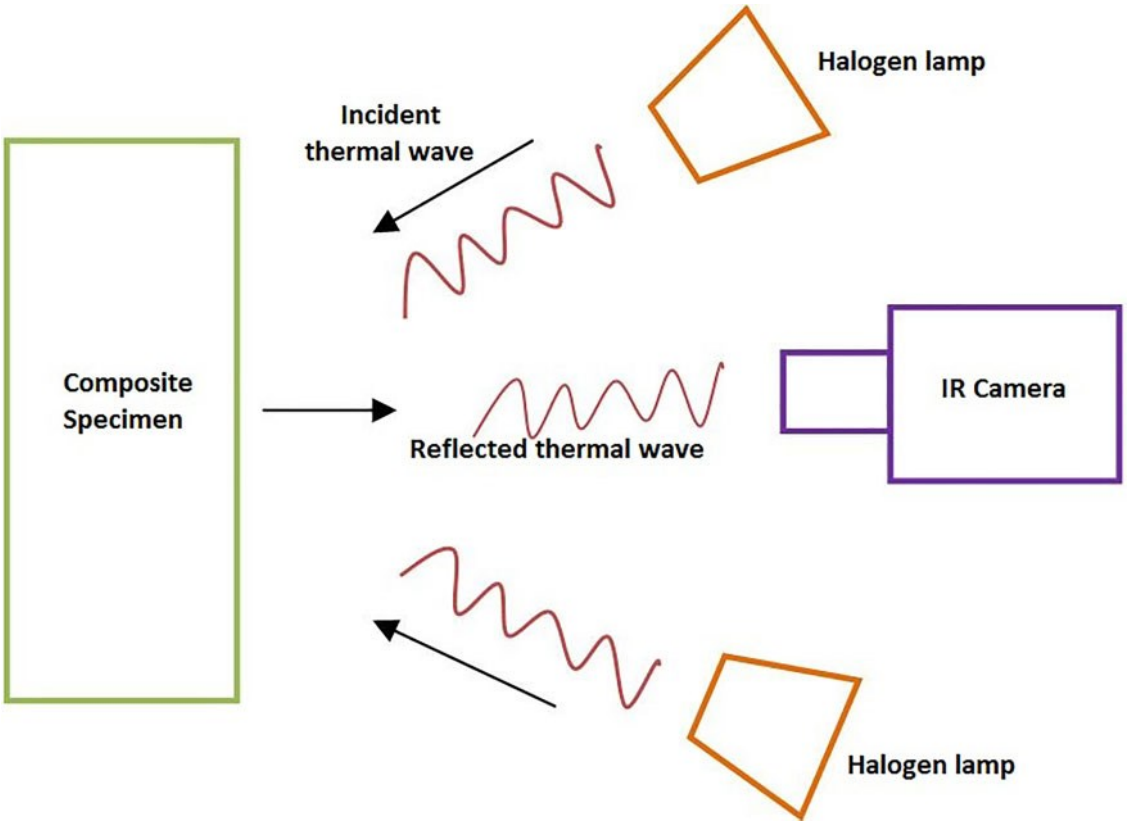

Figure 3: *Lock-in thermography setup*[4]

Harizi W, et al. [62] investigated the progression of damage in GFRP laminates under static tensile stress using passive IRT. In a study by Montesano I, et al.[63] , the relationship between braider yarn crack density and stiffness deterioration for braided carbon-reinforced polymer matrix composites was determined using the IRT. Transverse fractures were produced in the event of cyclic loading. During the cyclic loading procedure, the localized interface cracks between neighboring braiders merged with additional interface and matrix cracks. The initial loss of stiffness was caused by the commencement and saturation of braider cracks, and the loss of stiffness persisted as a result of the spread of the pre-existing interface cracks.

The significance of interfacial strength of composite under bending stress was evaluated using the passive IRT. Woven fabric glass or jute fiber-reinforced composites with polypropylene (pure or modified with a compatibilizing agent) were put to the test. A specimen made of woven glass fibers showed greater thermoelastic effects. The interface strength of composites is influenced by the reinforcing and compatibilizing agent [64]. Using passive IRT,

the fracture toughness of the carbon/epoxy UD composite laminate was calculated during compressive fiber failure[65]. The information received by IRT, in sum, aids in determining the length and position of the fracture. The temperature distribution during the growth of the fracture in the UD GFRP was also measured using IRT[66]. D'Orazio T, et al.[67], for the analysis of the series of the thermal picture for the detection of internal defects in composite materials, used the neural network approach. To extract data on internal defects (holes, knife cuts, and impact damage) in composites, a neural network was built based on composite thermographic images.

This approach can only be utilized in the lab and not as real-time monitoring. Also, some complexity like different thermal properties in different directions is part of the intrinsic nature of this technique that implies limitations for practical use for real-time monitoring[68].

1.2.6 Fiber Optics

Optical fibers with grating can be placed on the surface of the specimen or be put in the specimen to be used as a method to monitor the deformation[69]–[73]. The optical fiber receives the deformation of the material in the construction. The distance between the gratings changes according to strain in the optical fiber. The reflection of the light wave from the gratings varies as light waves are sent via fibers. The degree of strain can be determined by examining variations in the reflected wave compared to referenced signals. The approach is attractive because of the in-situ application possibilities. The problem is the size of the optical fibers and the challenges of applying them as they are fragile, and the equipment is heavy. The size of optical fibers is around 52 micrometers which are relatively huge compared to composite fibers with a diameter in the order of 10 microns.

1.2.7 Shearography

Holography and speckle interferometry are used in the optical method known as shearography[74]. The area of the object's surface that has to be illuminated is covered by an extended laser beam. It is possible to utilize the surface as is or to add a coat of paint or powder on top. A camera captures the light that the surface scatters. To create a duplicate picture of the object's surface, the camera contains a glass wedge or shearing interferometer. A reference interferogram is initially acquired in order to identify the surface deformation. As the specimen is loaded, interferograms are then captured either statically or dynamically. The displacement gradient components can be obtained from either a single camera or a multi-camera sensor. The fact that a highly precise position between the part and the camera is

needed, which might not be appropriate for field applications, is one of this technique's drawbacks. Additionally, it cannot be used to measure the material's bulk strain[75]. Shearography also has the benefit of being a highly sensitive non-contact kind of examination[76]. But also has another certain limitation, that is the need to load the specimen in order to detect flaws and the possibility of fresh damage being generated during testing. The shearing amount is another restriction. Tiny shearing amounts result in poor fringe quality yet slight shearing amounts generate a small measurement mistake[77].

1.2.8 Electrical conductivity along the carbon fiber direction

Studies have been done on using the conductivity of carbon fibers as a means for monitoring defects in composite structures[78]–[85]. Because carbon fibers are very conductive in the fiber direction, a change in electric potential can be used to detect damage in a composite specimen by providing an electric current over two probes at two points and monitoring electric potential over different two probes in the fiber direction. The drawback of this method is that resin fractures cannot be found using it since resin is not conductive. In contrast to fiber breakages, matrix cracking and delamination account for most of the damages at the comparatively modest stresses which is the case for early-stage damages. As a result, this technique's utility is constrained.

1.2.9 Embedding resistance-based sensors

Different resistance-based sensors are developed and used to monitor deformation and damage in composite structures[86]–[88]. In this set of methods, conductive sensing parts (resistance-based wire sensors or conductive ink) are embedded or out on the surface of a composite plate. These resistance-based sensors are shown to be capable of detecting small impact damages in small samples (up to 12 cm by 10 cm). The illustration of the techniques is shown in Figure 4, Figure 5, and Figure 6.

.

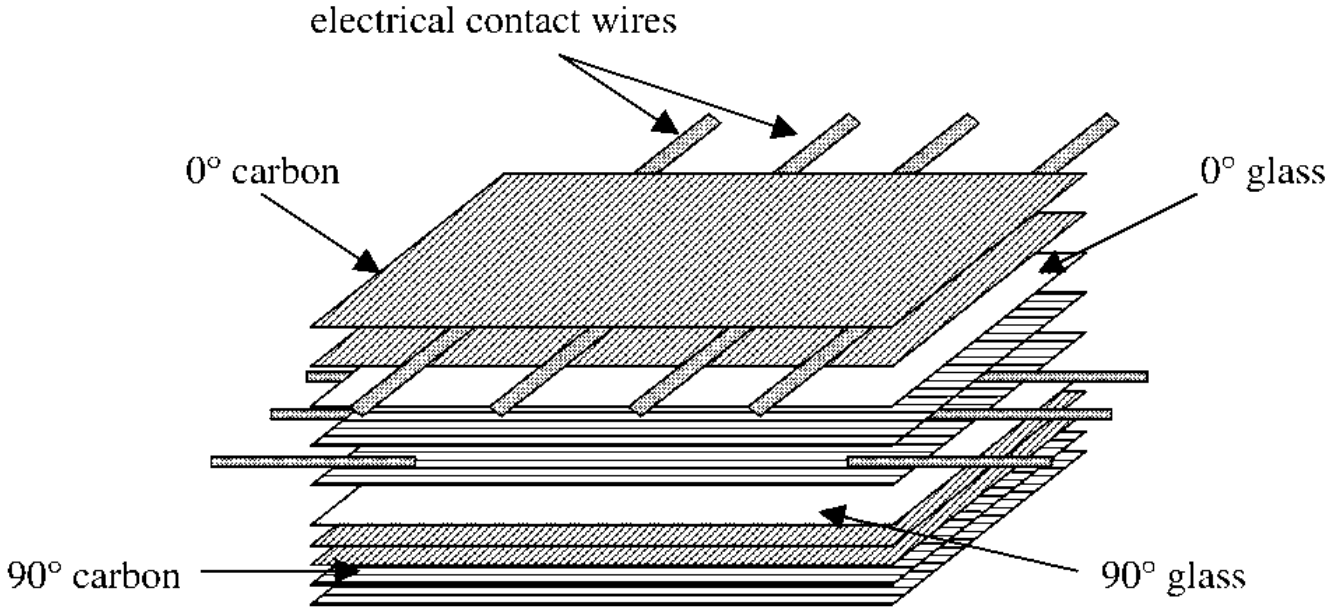

Figure 4: *A illustration of using resistance-based sensors that are embedded in the composite structures*[86]

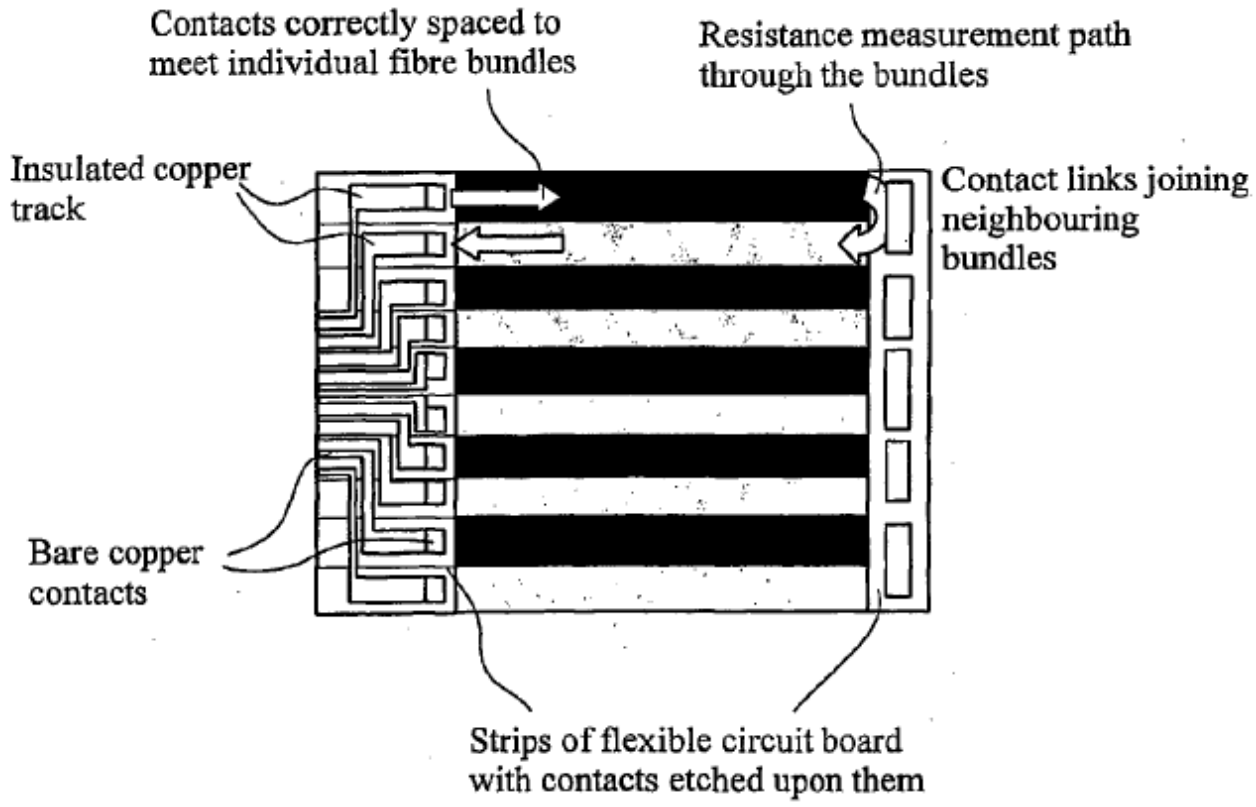

Figure 5: *Resistance-based conductive fiber sensors used with flexible circuit board*[87]

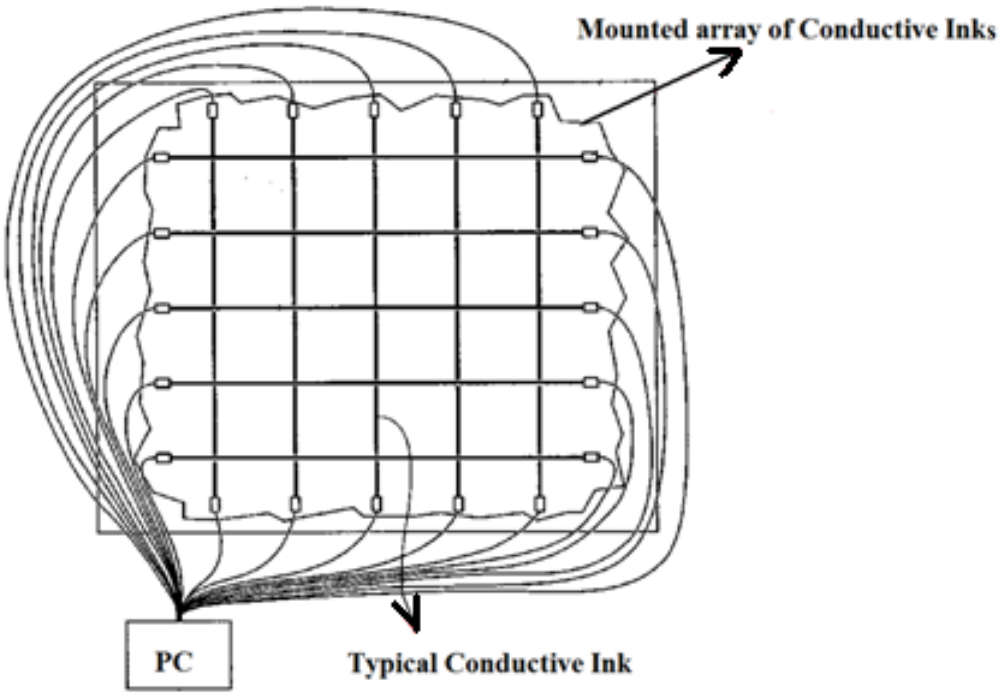

Figure 6: *A system using ink containing carbon nanofibers as conductive lines on the surface of the composite to sense deformation and defects* [88]

1.3 Adding carbon nanotubes into resin

Because of their tiny size, high aspect ratios, great electrical conductivity, thermal conductivity, and outstanding mechanical qualities, carbon nanotubes (CNTs) have been introduced as multifunctional fillers[89]–[94]. Many researchers have recently used carbon nanotubes to make the matrix of fiber-reinforced polymer composite constructions electrically conductive. Carbon Nano Tubes (CNTs) are added to resin for enhancing the mechanical properties and introducing electrical conductivity[90], [95]–[98]. The development of a network of carbon nanotubes is responsible for electrical conductivity. As the network deforms, the network's configuration is modified, and the conductivity changes when a mechanical load is applied. As sown in Figure 7, Thostenson and Chou[99] showed that CNTs penetrate in areas where the matrix content is high and between plies due to their tiny size. CNTs can be used as nonconductors to detect deformation and damage in composite laminates in this way.

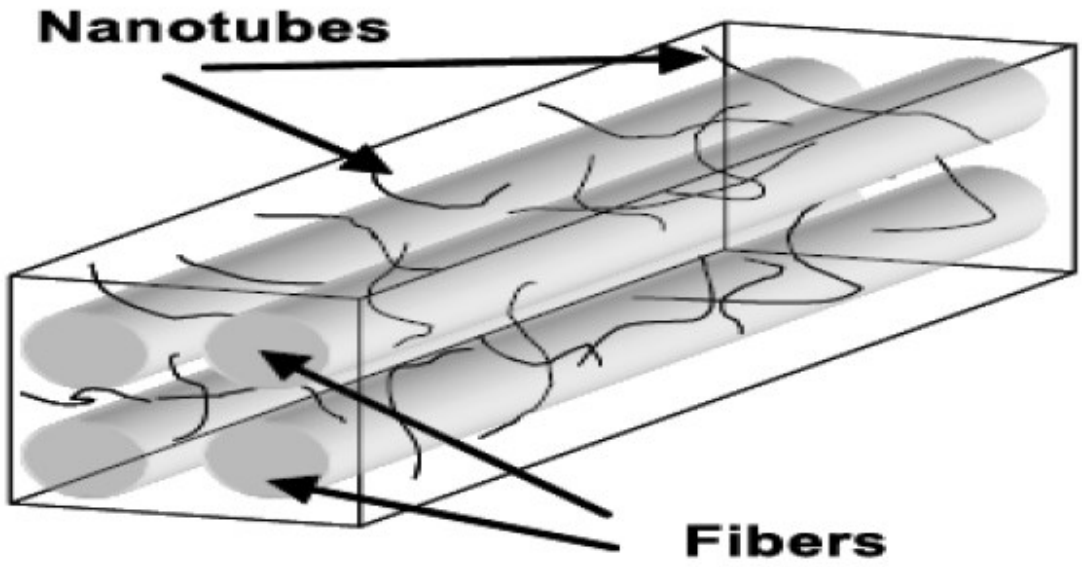

Figure 7: *Three-dimensional illustration of CNTs' penetration throughout a fiber array because of their relative scale*[99]

Pham et al. [100] studied the sensitivity of composite films with different carbon nanotube (MWCNT) concentrations. Based on this study, the sensitivity of the change in surface resistivity increases with lower MWCNT contents in nanocomposite films (Figure 8).

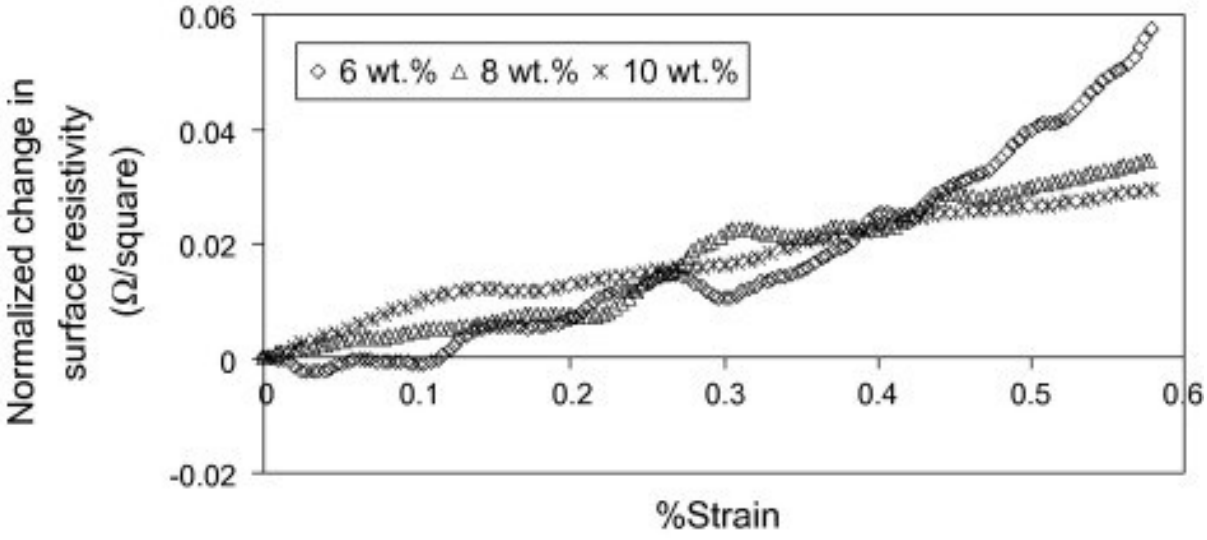

Figure 8: *Normalized change in surface resistivity PMMA/MWNT films for different MWCNT concentrations* [100].

The presented methods for detecting defects in composites provide promising results. However, they have limitations in being used as in-situ methods due to requiring the structure to be tested in labs and not being able to monitor while working.

To tackle this problem, works have been done using the change in the electrical behavior of nanocomposites. The idea is to introduce electrical conductivity to the matrix of composites structures by adding CNT. The electrical properties of the composite structure can be used as a signal to monitor the structural integrity of the structure. Ali Naghashpour and S.V. Hoa [101], developed a method that uses changes in electrical resistances in nanocomposite plates to detect the defects. They demonstrated that by using an optimal amount of carbon nanotubes, they were able to monitor the development of cracks inside the epoxy matrix at an early stage of the loading. This early detection cannot be realized using other NDT techniques, including infrared. In the method developed by Ali et al. [101] probes were placed on the grid points on composite plates to be able to measure electrical resistances throughout the entire plate (Figure 9). The method provides promising capability in real-time defect detection. The only problem with this method is the requirement for many contact points on the plate as probes. So, as using electrical behavior in composites shows a promising capability, in comparison to other NDT methods, using CNTs in composites is adopted in this study to make composite plates conductive. To overcome the limitation of practicability of the existing method, the aim of this study is to develop a method that is capable of real-time defect detection with fewer number of probes and connections.

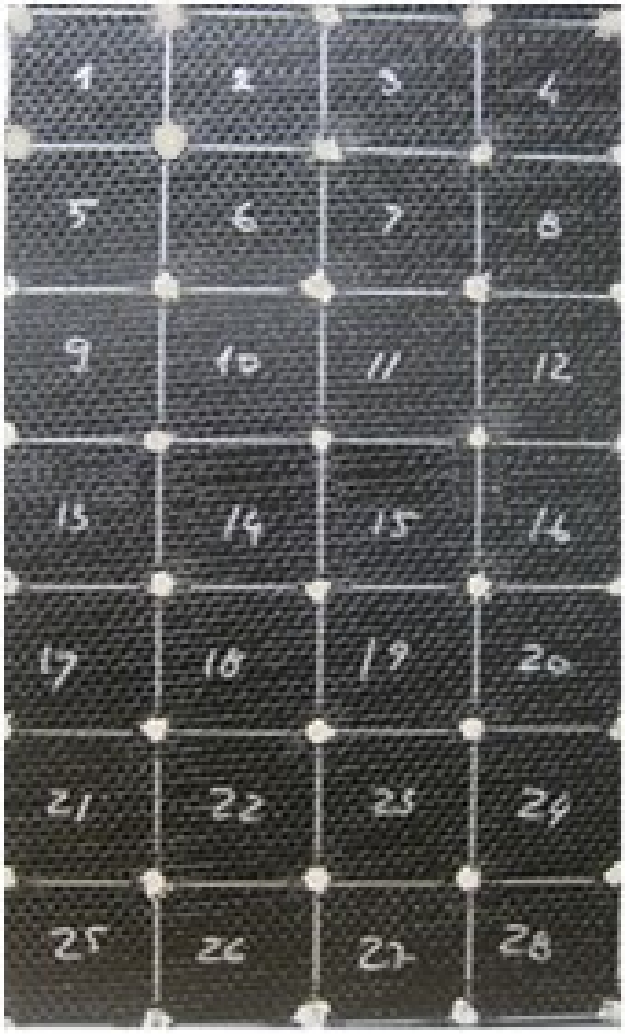

Figure 9: *A plate of composite that the electrical resistances are measured using probes on the corner of each cell. The silver circles on the corners of each cell are probes* [75].

Recently there arose many success stories about using Artificial Intelligence (AI) for the recognition of defects in biological systems [102], mechanical systems [103], and others [104]–[106]. Defect occurrences in composite materials and structures are complex phenomena. As such even though a large amount of effort has been spent in detecting, locating, and quantifying the defects in composite structures, much remains to be developed. It is the hope at the beginning of this thesis work to use AI to help in defect detection in composite structures. In particular, the intention is to use AI to help to reduce the number of probes and connections in the technique where CNTs are incorporated into the epoxy matrix to make the composite electrically conductive. There have been works where AI have been used in composites, and a survey of these work is presented in the following chapter.

Chapter 2: LITERATURE REVIEW AND METHODOLOGY

2.1 Artificial Neural Network in the Field of Composite Materials

In the previous two to three decades, technology has advanced significantly thanks to the development of artificial intelligence (AI) and its numerous applications in several industries. The efficiency and capacities of many industries that just focus on business, scientific, and technical applications have improved because of AI [107], [108]. The most promising AI technology, machine learning, is renowned for its speedy and precise simulation of human intelligence and its capacity to comprehend processes. The use of ANN in simulating the characteristics of composite materials has grown rapidly in recent years. A large percentage of the studies using ANN in composites have been done during the last four years (Figure 10). This shows the technological development in the field [109].

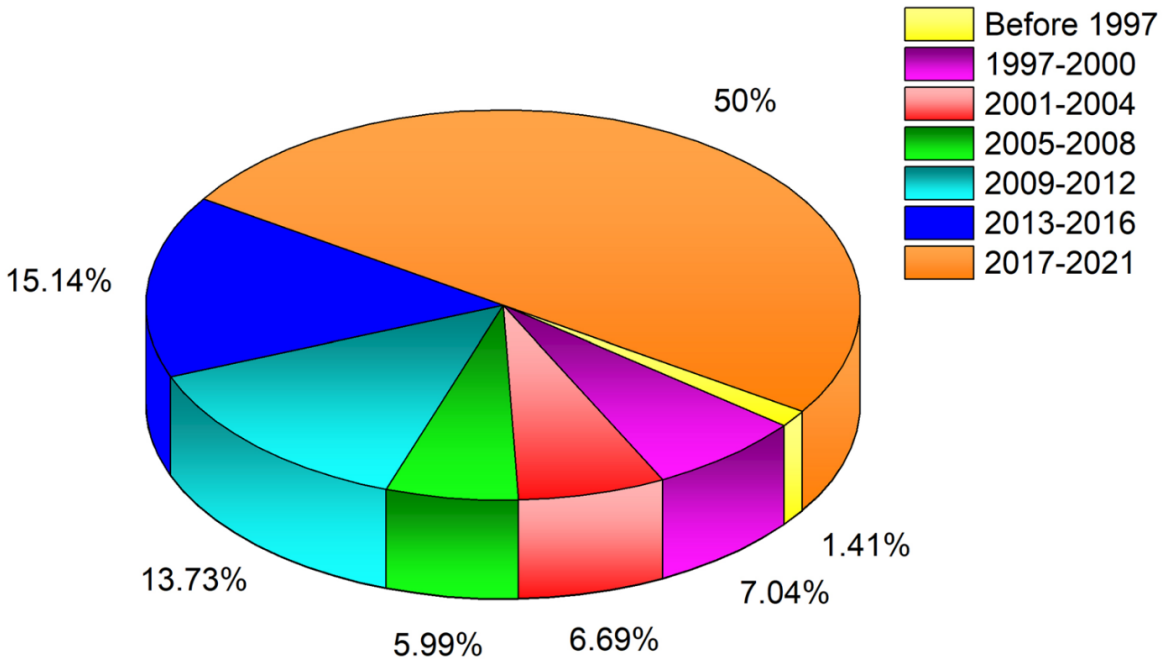

Figure 10: *Distribution of articles published on composite characterization using ANN during different years*[109]

There are studies focusing on mechanical properties of composites, like modulus, fatigue life, etc., using ANN. Some of these works are mentioned in the following paragraphs.

Gayari Vineela et al. [110] studied the ultimate tensile strength of short fiber composites. The volume fractions of short fiber were the input of the ANN. The high performance of the trained NN shows the good capability of using NN for predicting the tensile strength of composites. Hossain et al. [111] studied both tensile and compressive strength of cementitious composites. There are ten features (input) for predicting compressive strength ANN and twelve features for tensile strength. The performance of the NNs is high with R-values of 0.989 and 1.0 for compressive strength and tensile strength, respectively. Kurpinska and Kulak [112] trained a NN to predict the compressive strength of light-weight concretes. By having a NN structure of 2-11-15-1 the compressive strength of light-weight concrete was predicted with high performance. The high performance of ANNs' predictions in the strength of composites is observed in studies([113]–[117]).

The hardness of composites is also studied using ANNs. Vinoth and Datta [118] trained ANNs on the hardness of ultra-high-molecular-weight polyethylene composites with an R-value of 0.96. Nwobi-Okoye and Uzochukwu optimized ANNs to predict the hardness of A16351/eggshell composites. They considered stirring time, preheat temperature, and sitting speed as inputs (features) of the NNs. The performance of the NN modeled was measured with an R-value of 0.9982. In Devadiga et al.'s study [119], the hardness of CNT fly ash reinforced aluminum composites is predicted using ANN. The inputs are reinforcement content, ball milling time, and sintering time. The error of the trained NN is small (MAPE= 1.51%). Similar performance of ANNs is reported in other studies focusing on the hardness of composites ([120]–[125]).

The stiffness modulus of composite materials is an interesting topic for researchers to predict using ANNs. Kabbani and Kadi [126] studied Young's modulus of glass fiber polypropylene composites with different cooling rates. They predicted the stiffness of the composites using ANNs with an accuracy of 97%. Ye et al. [127] used Convolutional Neural Network (CNN) to predict both Young's modulus and Poisson's ratio of composites. The relative error of their NN is around 4%. Based on their opinion, the deep neural network is one of the best options to predict the mechanical properties of composites that have complex microstructures. There are articles that study also shear and bulk modulus of composites with high performance using ANNs ([128]–[134]).

The strength of composites under shear and flexural loading is also studied using ANN. Different tests are carried out in order to analyze and evaluate the impact of different input

factors on the shear and flexural strength of composite materials[135], [136]. However, the time and expense required for experimental tests prompted researchers to use artificial intelligence to foretell the mechanical characteristics of composite materials[109]. Shyam et al. [137] used ANNs and Deep Neural Network (DNN) to model the flexural behavior of E-glass reinforced bayan fiber composites. The fiber orientation of the composite structure is considered as an input for ANNs and DNNs to study its effect on flexural strength. The performance of 92.2% and 92.8% was achieved using ANN and DNN, respectively. Prasad et al. [138] used NN as a prediction model for flexural strength of coir polyester composites. There are other studies that used ANNs to model shear, flexural, and impact strength in composite materials ([139]–[144]).

Researchers also used ANNs for the prediction of the toughness of composite materials in the recent 20 years. Sharma and Kushvaha [145] studied the fracture toughness of silica-filled polymer composites by ANNs when carrying different loads. The performance of the trained ANNs was measured to be of R-value of 0.972 with respect to experimental results. Yang et al. [146] used CNN to predict composites' toughness. Jia-li et al. [147] used a Multilayer Perceptron (MLP) neural network to predict the toughness of wheat straw reinforced composites. The features for the NN are mold temperature, mold pressure, fiber content, and time. Studies that used ANNs show high performance in modeling the toughness of composite materials([148], [149]).

Bezazi et al. [150] studied the fatigue life of sandwich composites using Baysian NN. Ahmed et al. [151] used ANNs to study hot mix asphalt (HMA). The features of the ANN in this study are stiffness modulus, phase angle, shear stress amplitude, relaxation test coefficient, shear strain amplitude, air void percentage, and bulk density. The R-vale for the trained NN is more than 0.98. Other attempts to study the fatigue life of composites were done using ANNs([152]–[157]).

Based on the studies on using ANNs in the field of composite materials, this method presents promising capabilities for modeling the complex behavior of composite materials.

2.2 Objective

In a previous study by Naghashpour and Hoa [158], composite plates were divided into cells using the grids and for each cell 4 probes are required. This makes the method require lots of probes, wires, and contact points which is a limitation in the practicability of this method

(Figure 11). To have a new method without this limitation, fewer probes should be required to be capable of locating the defect. So, some probes should be removed by noting that the remaining probes should be around the area where the defects occur to be affected by them. By having these two key factors considered, this study aims to develop a method that can locate the defects inside a plate of composite by using measurements on the edges (Figure 12). By comparing Figure 11 and Figure 12, the saving in the number of probes for similar plate sizes is obvious.

To emphasize the difference between the previous method and the method in this study, a comprehensive view on cells and defects can help. In the previous method (Figure 11), the decision on whether there is a defect in a cell or not is based on the measurements on the corners of that cell, so for each cell its own measurements should be performed. On the other hand, for the method in this study (Figure 12), there are only fixed measurements for all the cells. It means by using unique measurements, the decision on being defective or not should be taken for all the cells on the plate rather than having specific measurements for each of them. This certainly does reduce the number of probes. However, it is not certain that the patterns of measurement values from probes on the edges will enable the determination of the existence of defects within the structure along with their locations. This degree of uncertainty (or certainty) may be addressed using the Machine Learning approach, which is described below.

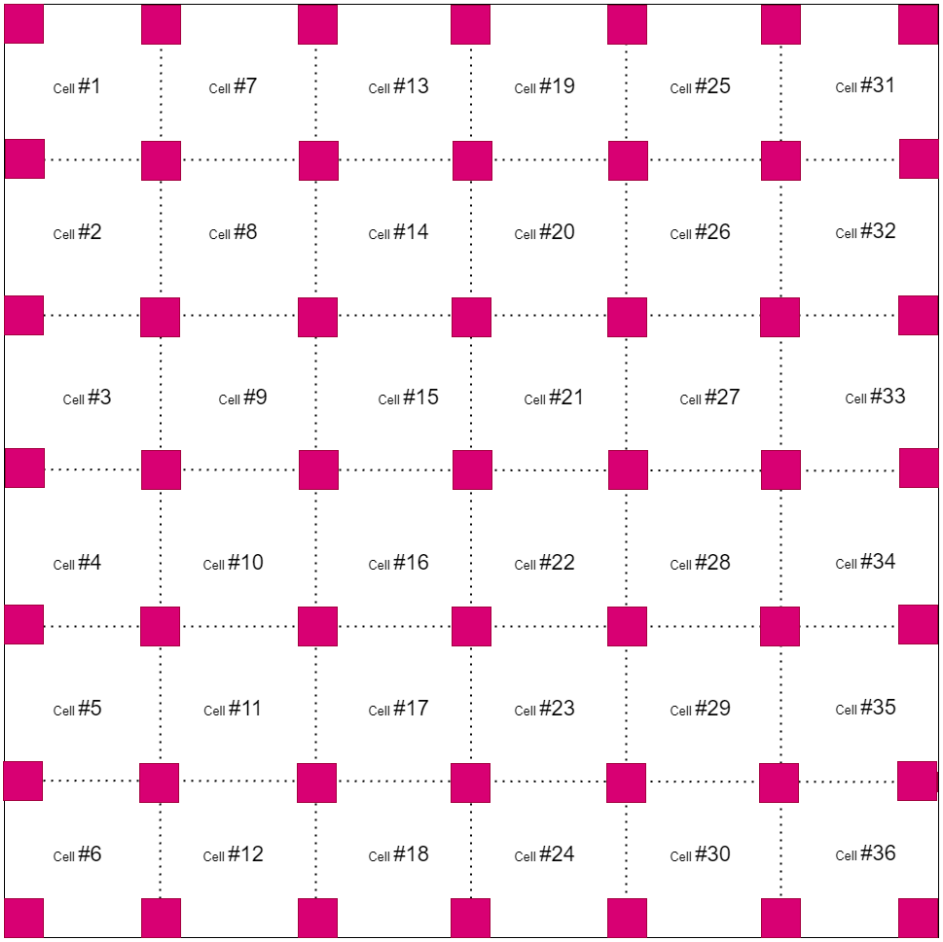

Figure 11: *Illustration of probes required in the method developed by Ali Naghashpour and Hoa.*[158]. *Purple squires represent probes.*

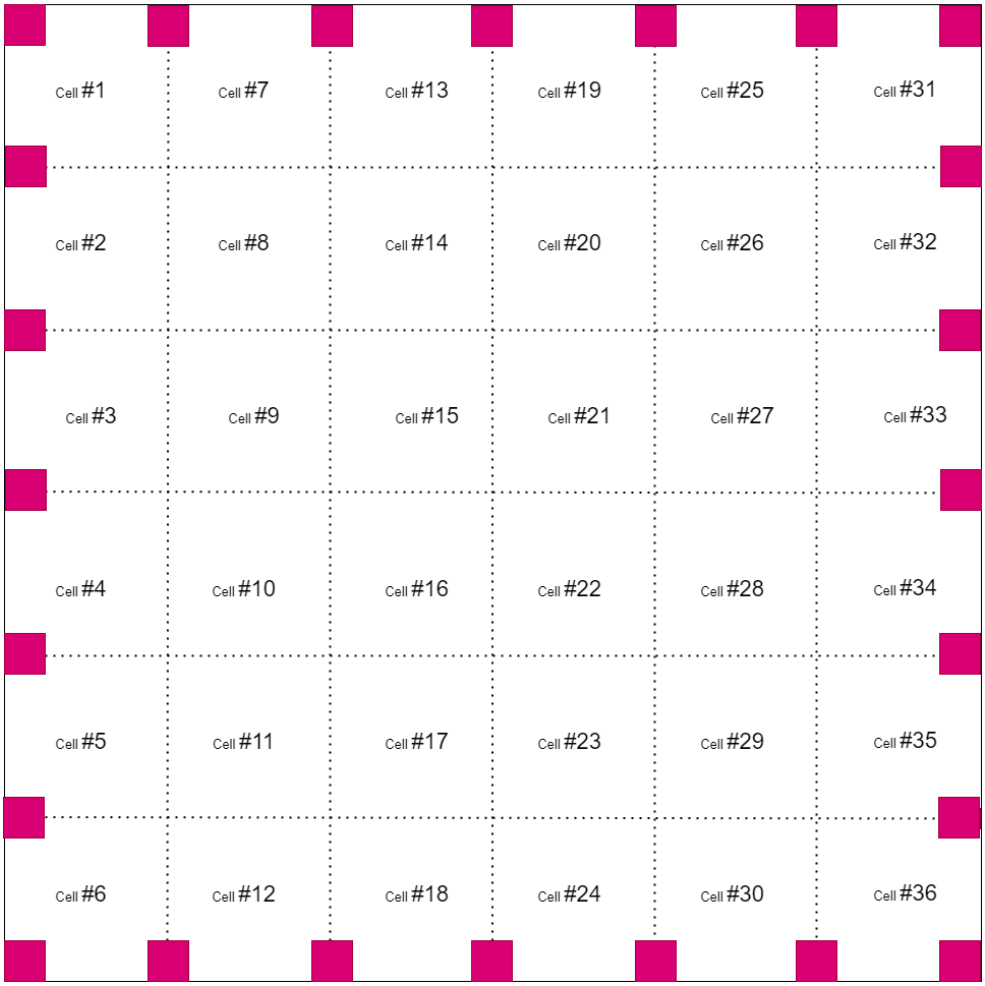

Figure 12: *Illustration of the number of probes required for this study to locate the location of the defect using probes on the edges. Purple squires represent probes.*

2.3 Rationale for selecting Machine Learning

By having the probes limited to the edges of the samples, the measurements may not be directly and independently related to each defect, as they were in the previous study [158]. There are two ways to tackle this problem. One way is to study the electrical behavior of composites with having CNTs embedded in their resin and develop a model that can precisely determine the complex electrical behavior of the structure. After that, by having a precise model for electrical behavior, it can be used to study the effects of defects on the electrical behavior and to detect the defects. As it is clear, this technique is time-consuming, costly, and may not be possible. Another way to do this with a smaller number of samples and with a reasonable cost is to try to relate the inputs (the measurements on the edges) to outputs (the

location of the defect) without modeling the exact and detailed way that they are related by using Machine Learning (ML). In other words, there are two approaches to tackle the problem:

1- Developing a physics-based model for the electrical behavior of nanocomposites + studying the effects of having a defect in this physics-based model
2- Trying to relate the measurements on the edges to the location of the defect without necessarily knowing how exactly they are related scientifically.

As the first approach requires numerous experiments and modeling, the second approach is picked for this study. To fulfill the second approach, ML methods are picked as they show promising capabilities in composite fields as mentioned in the previous section. Introduction to the method that is used, and steps that are taken are provided in the next sections.

2.4 Introduction to ML approaches and Method Selection

The advent of Artificial Intelligence and Machine Learning gives a lot of hope for the development of effective and efficient defect detection in composite structures.

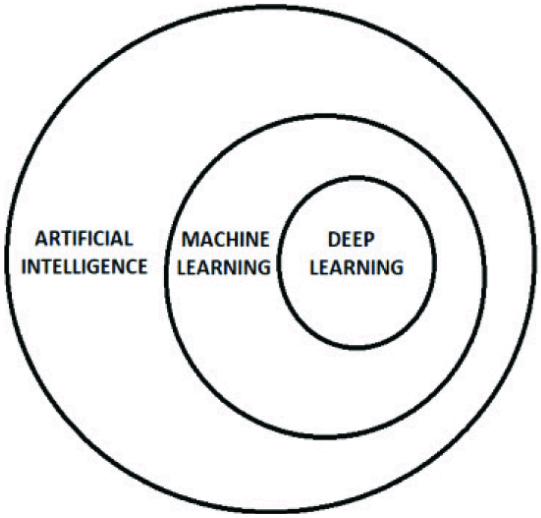

Figure 13: *Artificial Intelligence Subcategories [159]*

Machine Learning approaches can be classified to two categories: conventional ML and Deep learning. Conventional ML methods, like support vector machine (SVM), Decision Trees, K-means Clustering, are limited in the capability of processing data that are in their original form. These methods need a noticeable amount of understanding of the data and features[159], [160]. On the other hand, machine learning has a branch called deep learning. Deep learning is an advanced technique to machine learning that enables computers to

automatically extract, analyze, and comprehend the valuable information from the raw data. The technique of AI and Deep Learning may provide means for this detection[159]. Results from deep learning are far better than those from conventional methods for machine learning[161]. Deep neural networks employ a non-linear model with a number of hidden layers to enable the system to learn about the intricate connections between input and output. Deep learning has the benefit of not requiring manually retrieved or constructed features as conventiolan machine learning does. Automatic feature extraction from the raw data, processing, and decision-making are all done via deep learning[162], [163]. Deep learning techniques use non-linear models to turn the initial data into more abstract levels for decision-making, resulting in many abstractions of levels. Finding the solution to complicated and non-linear functions is made simpler as a result[164]. Deep learning relies on autonomous feature learning, which offers the benefits of modularity and transfer learning[159]. Based on the advantages of deep learning over conventional ML methods, for this study, Neural Network with multiple hidden layers (Deep Neural Network) is selected.

2.5 Special techniques to overcome the need for large amount of data

However, this technique requires a large amount of experimental data. This is troublesome for composites due to the exorbitant cost to generate these data. In this thesis, two techniques are used: One is to reduce the need for a large amount of data, and the other is to augment the data obtained from experiments. These are Transfer Learning (TL) and Data Augmentation (DA). Transfer Learning is a technique where the neural network is undergoing two levels of training. In the first level (level 1), the network is trained using a similar, and better-known problem where the data can be abundant. This problem is usually less complicated (or already solved) than the actual problem and is similar to the actual problem. It should be noted that the model for level 1 training may not exist for all phenomena or physical problems. Fortunately, for the detection of defects in composite structures using enhanced electrical conductivity due to the addition of carbon nanotubes, there are similarities to the circuit of the grid of resistors where the effect of the defect can be considered similar to increasing the electrical resistance in a particular cell. Once the training network has graduated from level 1, it is trained again using experimental data in level 2. The fact that the network was trained in level 1 allows it to provide better results in level 2. Since the number of experimental results may be limited, these data may be augmented using Data Augmentation (DA). In Data Augmentation, the limited

experimental data is augmented by Symmetry, Anti Symmetry, etc. A schematic of the procedure is shown in Figure 14.

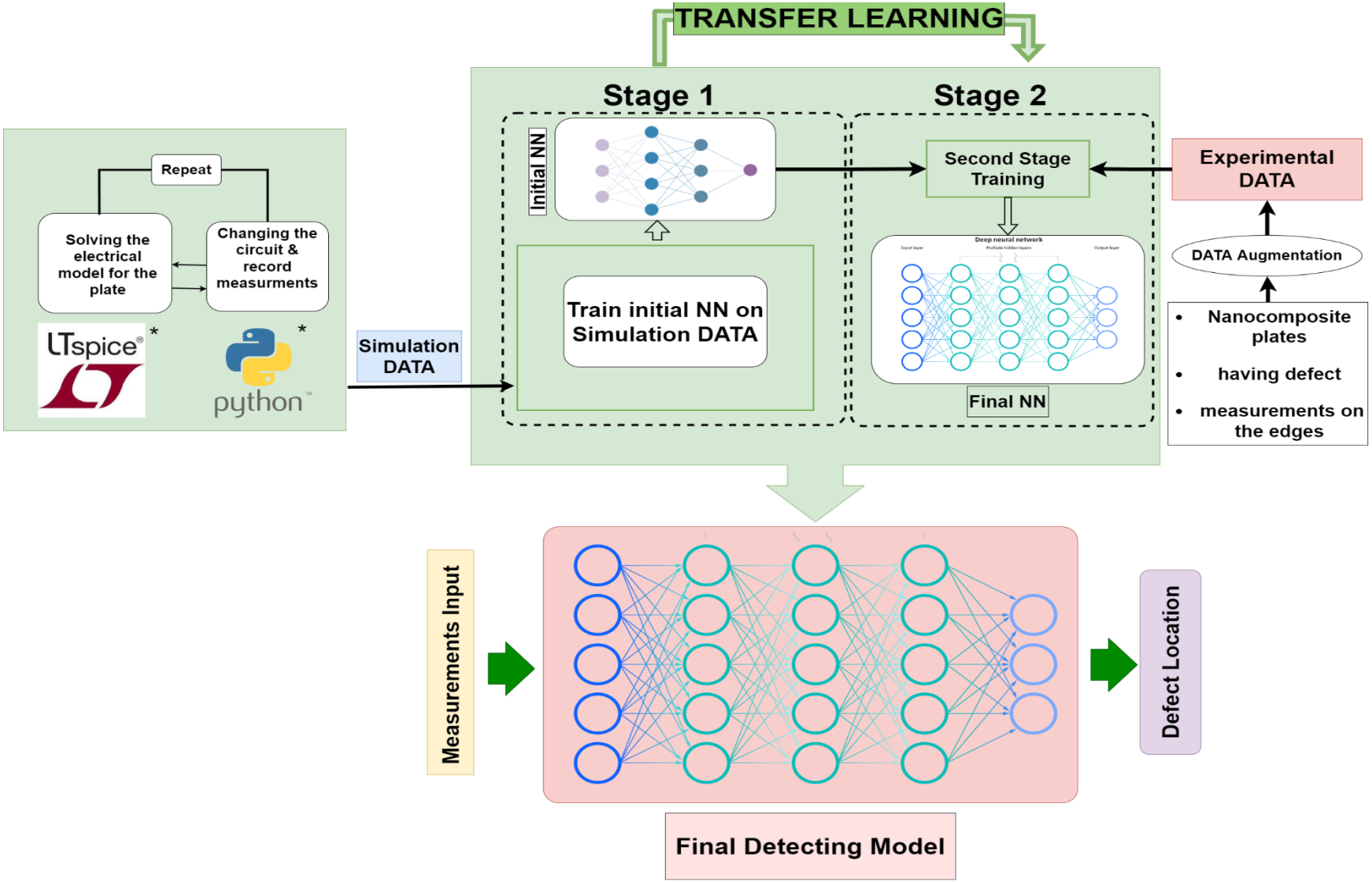

Figure 14: *The schematic of the procedure*

* Brief introduction of the tools used for data preparation is presented in chapter 4.

In Figure 14, the block on the left shows the procedure and software programs used to generate data from a similar, better-known problem. The electrical activity of the plate shown in Figure 15a may be modeled as a network of resistors shown in Figure 15b. This network as shown in Figure 15b is a grid of resistors. The existence of a hole in the middle of the plate in Figure 15a may be represented by increased values of resistance at corresponding position in Figure 15b. By using Kirchhoff law, the relation between the points on the edges of the plate may be written in terms of the resistances inside the plate[75]. LTspice is a simulation software that can model circuits [165]. Using this software electrical specifications between any points on the simulated circuit can be monitored. The software LTspice in Figure 14 is used to determine the equivalent resistances between points on the edges corresponding to values of resistances within the plate.

The simulation data is generated by modeling a grid of resistors in LTspice software. For generating each example of data, resistors creating the targeted cell were increased. The relative changes in equivalent resistances between every two opposite nodes on the edges of the grid of simulated resistors before and after increasing resistors' values were recorded as features.

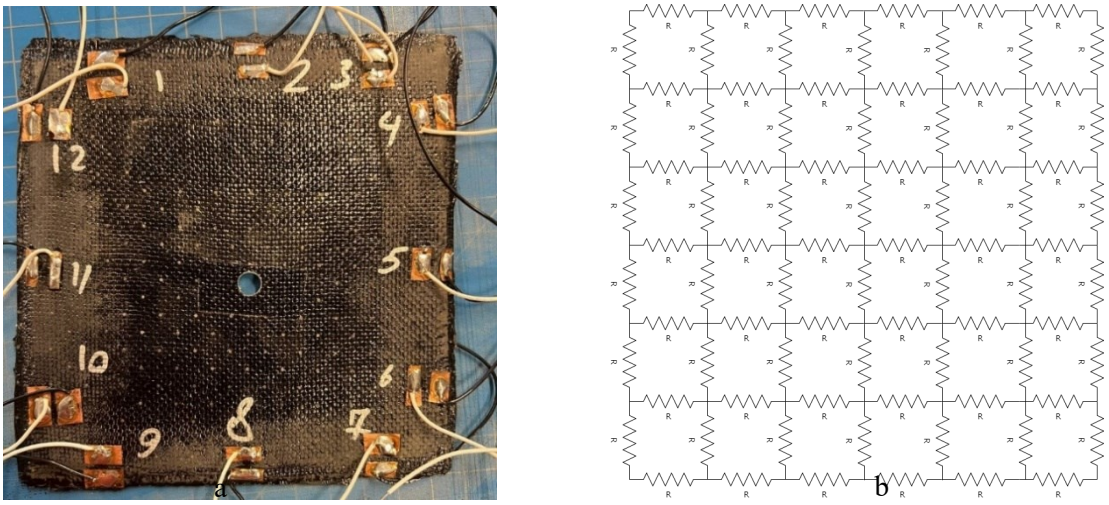

Figure 15: *a. Composite plate with probes, b. Model as network of resistors*

Sequential numbers were assigned to cells from left to right and from top to bottom. The number assigned to the cell with the increased resistors is recorded as the label. A Python code is also developed to automate model preparation in LTSpice and to record the data. The Python code provides the dataset in a reasonable amount of time relative to doing it manually. In the data preparation step, the features were normalized using standard deviation and mean.

The top row, right part in Figure 14 shows the data generation using experiments. Details of the experiments will be given in chapter 3. Also shown at the top row, right part of Figure

14 is the Data Augmentation (DA). The procedure for DA is described in more detail later in chapter 3.

The top row, middle block in Figure 14 shows the training portion of ANN. As mentioned before, there are 2 levels of training. In level 1, the training of the Neural Network is done using data generated from the simulation on the left. After level 1, the initially trained network is used as a base for the NN that is trained again using the augmented experimental data from the right in stage 2. Before the second training step, the last layer of the ANN from the previous stage is removed and new untrained layers were added on top. In the training step, the newly added layers were trained.

In the data preparation step, the data were normalized using mean and standard deviation. Each data set is divided into 3 subsets as the training set, development set, and test set. The initial and final ANNs are trained using the training set, optimized using the development set, and evaluated using the test set that comes from simulation and experimental data, respectively.

The last block at the bottom of Figure 14 shows the optimized ANN model after training in stages 1 and 2 as the final model. The inputs for this model are features that come from electrical measurements on the edges of the composite plate and the outputs are labels that represent the location of the defect.

CHAPTER 3: Materials, Sample preparation, and Experiments

This chapter explores the procedure and steps for making and testing samples. This step is an important step in the process of developing a real-time defect detection technique for composite plates.

Sample preparation consists of adding CNT to epoxy resin, cutting fibers, wetting the fibers, preparing probes on the edges of samples, and curing samples. Then samples are tested, the measurements are performed, and the data is summarized and labeled to be prepared for the next steps in training and testing the performance of the trained NN model.

Two sets of samples were made, first set consisted of samples with different CNT concentrations to find the best CNT concentration for getting the best response in the primary samples (to generate data for NN modeling). From the result of testing the first set of samples the concentration of CNT to prepare the primary samples was achieved.

In this chapter, the method, tools, and materials that are used to have the samples prepared and tested are reviewed.

3.1 Experiments

3.1.1 Materials

-CNT: single-walled CNT with the purity of 75% manufactured by TUBALL nanomodifier of materials (Figure 16)

-Epoxy resin: Hexion Epon 862, Epikure Curing Agent W (Figure 17)

-Glass Fiber: Plain woven fabric bought from FiberGlasst, item #224-A an areal weight of 7.4 oz/yard2.

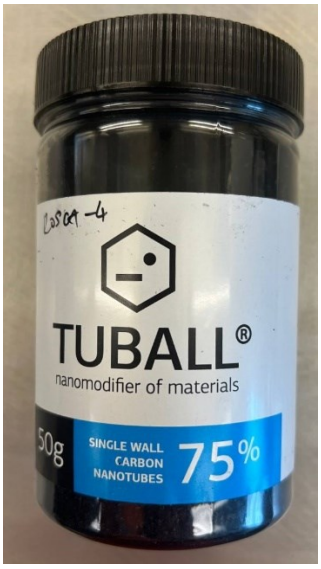

Figure 16: *CNT used to prepare samples*

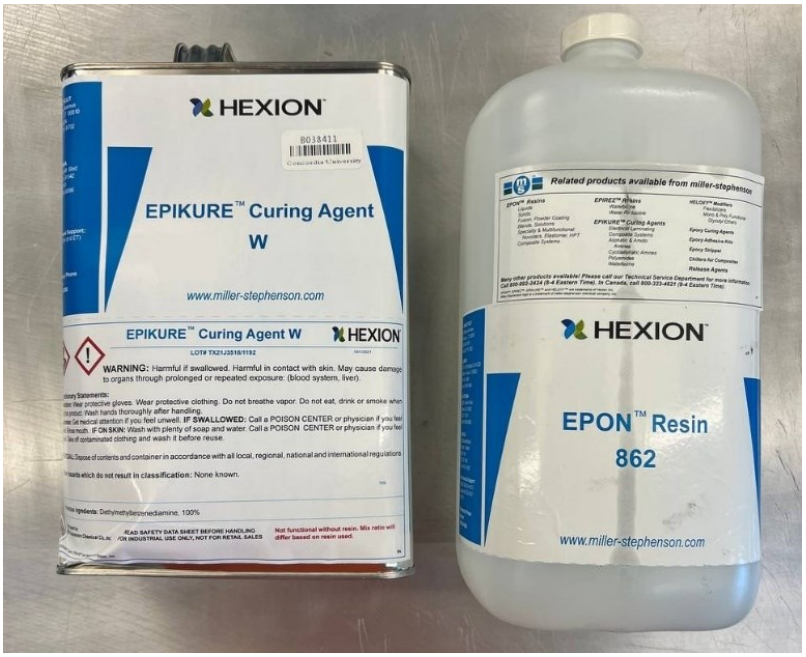

Figure 17: *Epoxy resin and Curing Agent used to prepare samples*

3.2 Determination of Optimum CNT Concentration

The technique of adding carbon nanotubes into epoxy to make the composite more conductive so that the occurrence of defects can be detected by measuring the change in resistance between probe points has two requirements for the amount of nanotubes. One is that

the amount of nanotubes should be large enough to make the resin matrix to be conductive. On the other hand, if the resin matrix is too conductive (too much nanotube), the material may not be sensitive to the occurrence of defects. The second scenario is similar to the case of a very conductive material such as copper. The occurrence of a small defect within a copper plate may not affect the resistance (or conductivity) between two probe points on the edge of the copper plate. This is because copper is very conductive, and there are many paths of conduction between the two probe points. The occurrence of a defect may disrupt the conductivity along one path, but there are many other paths available, which makes the occurrence of the defect ineffective in changing the resistance between the two probe points (Figure 18 a). If the paths of connection are not many a disruption in one path results in a more tangible change in the resistance between the two probe points (Figure 18 b).

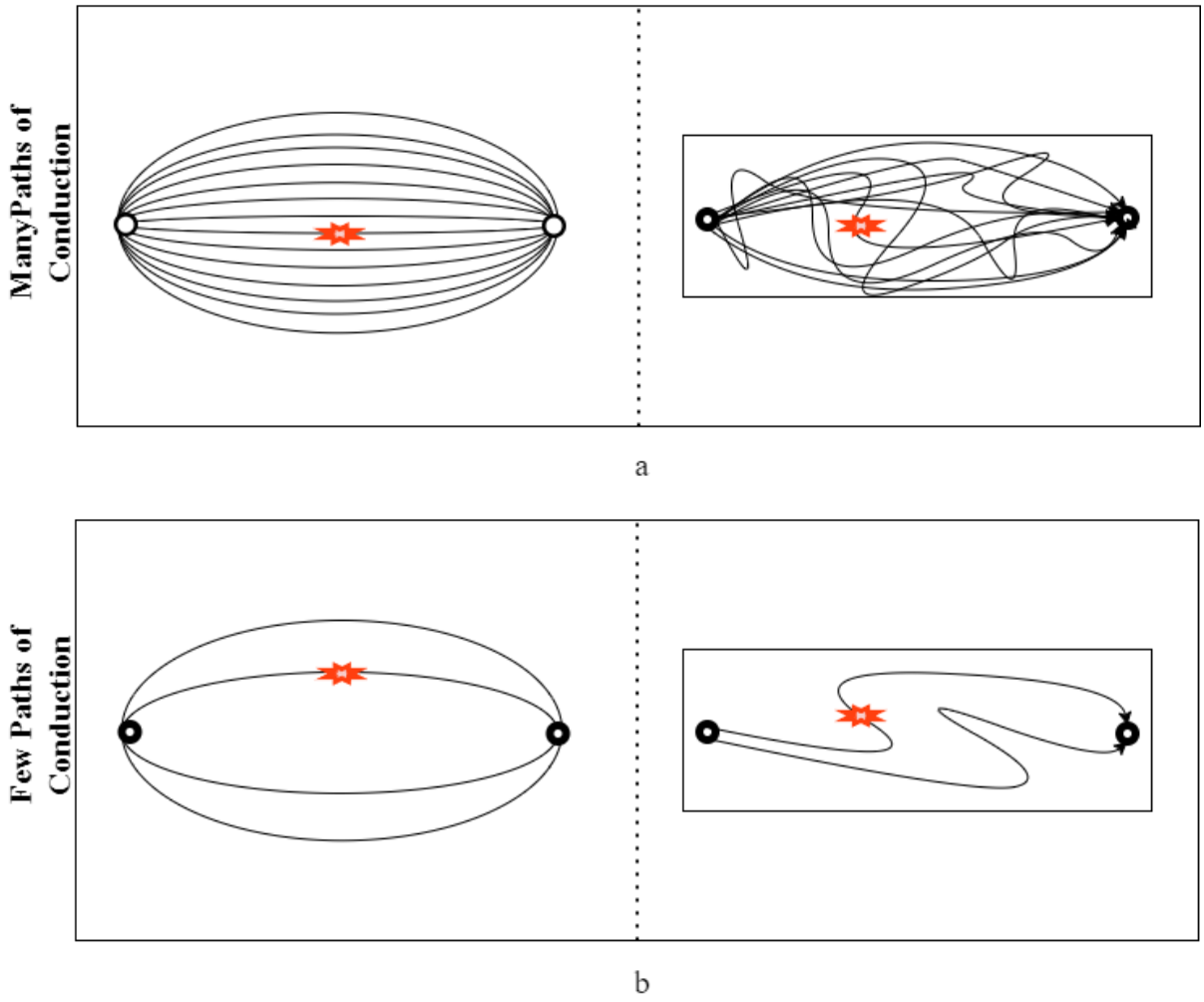

***Figure 18**: a. Many paths of conduction in a very conductive material. b. Few paths of conduction within a less conductive material*

As such, the amount of nanotubes should not be too much. The first and second requirements define a window for the amount of nanotubes to be used. In the following, two experiments were carried out. The first one is to determine the conductivity (resistivity) of the material, and the second one is to determine the sensitivity to the occurrence of the defect.

3.2.1 Effect of amount of nanotubes on resistivity

For the determination of the conductivity (resistivity), 8 samples of dimensions 6” by 6”. were made tested (Figure 21).

CNTs were dispersed into epoxy resin (Figure 19) by the required amount for the desired concentration using three-roll milling (EXAKT 80E; WXAKT Technologies, Inc.). The mixture of epoxy and CNT is then mixed with the curing agent (26.4 wt%) in the vacuum mixer for 3 minutes. The prepared resin was then used to wet 10 layers of plain weave glass fabric by hand layup. On the last layer of each sample films of copper in rectangular shape were co-cured in the autoclave. These copper films were used as probes to measure electrical properties. Probes are placed on the edges of samples in 6 pairs being opposite of each other (Figure 21). Two samples per each 4 different CNT concentration (0.05%,0.1%.0.25%,0.5%) are made. The average thickness of the samples is 2.17 mm.

Figure 19: *CNTs being dispersed in epoxy resin using three roll milling*

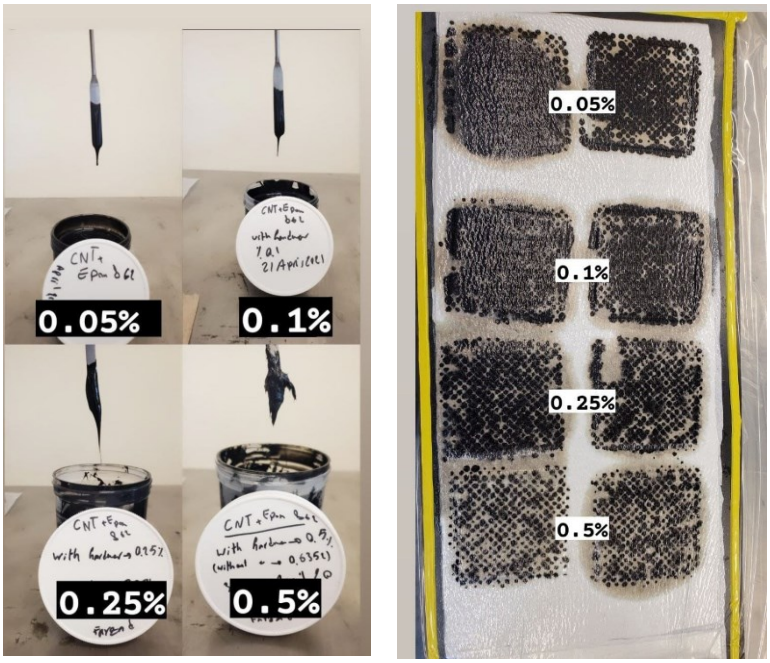

a b

Figure 20: *(a) Epoxy resin with different concentrations (Difference in viscosity is shown) (b) sample with different CNT concentrations under a vacuum bag.*

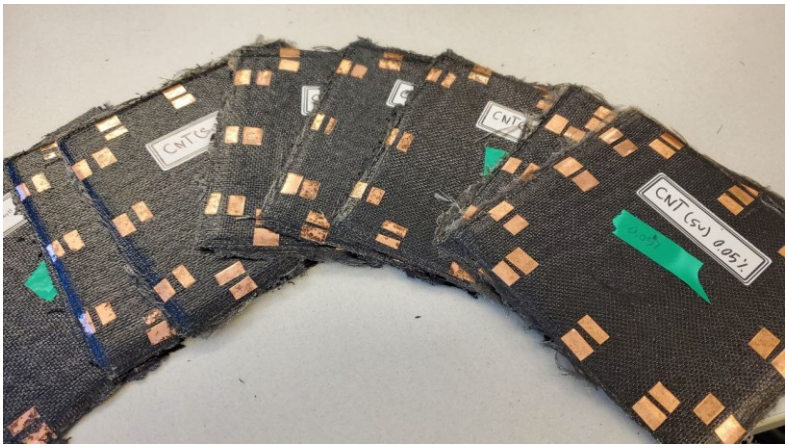

Figure 21: *Samples made with different concentrations of CNT*

To study the resistivity for different CNT concentrations, the Van der Pauw method [166] is used. This method is applicable to thin plates with small contact areas for probes [158], which is the case with our samples. To operate this method, the program that is developed in CONCOM is used [167]. The program controls the switches that control the current to the probes on the edges of the sample and measures the electrical voltages between the two other probes. The program solves the following equation based on the measurement.

$$e^{(-\pi.t.\sigma.R_A)} + e^{(-\pi.t.\sigma.R_B)} = 1 \quad (1)$$

Where t is the thickness of the sample, σ is conductivity and R_A, R_B are as follows:

$$R_A = \frac{1}{2}\left(\frac{V_{34}}{I_{12}} + \frac{V_{12}}{I_{34}}\right) \quad (2)$$

$$R_B = \frac{1}{2}\left(\frac{V_{41}}{I_{23}} + \frac{V_{23}}{I_{41}}\right) \quad (3)$$

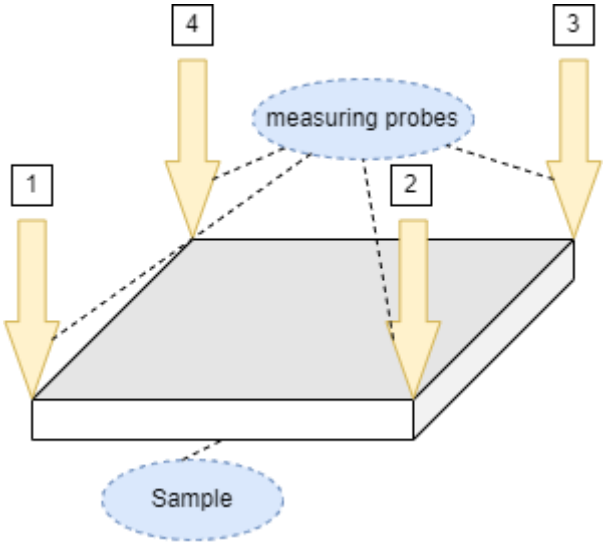

Figure 22: *Experimental setup for the Van-Pauw method*

V_{ij} represents the voltage difference between different probes on the edges of the samples (Figure 22). For conductivity and resistivity relation we have:

$$\rho = \frac{1}{\sigma} \tag{4}$$

ρ is resistivity and σ is conductivity.

The measurements were made using a current source and voltmeter. KEITHLEY 6220 Precision current source and KEITHLEY 2182A Nanovoltmeter are used for this purpose (Figure 23).

The resistivity is measured for each plate and the result is presented in Figure 25. Based on Figure 25, for concentrations more than 0.1w%, the resistivity is not decreasing that much as the concentration is increased. This means that although more CNTs are embedded into the resin, they do not contribute to conductivity. Also in the same figure, it is observed that there is a huge gap between the resistivity of plates with 0.05w% CNT and 0.1w% CNT which means the capacity of the network in 0.05w% resin is not sufficiently used to increase the conductivity. In other words, there are some unused capacities for CNTs to make conductive networks in samples with 0.05w% concentration.

3.2.2 Effect of amount of nanotubes on sensitivity to the occurrence of defects

To test the sensitivity for the detection of the occurrence of defects, the effects of having a hole in samples with different concentrations on resistances between opposite probes were measured before and after drilling a hole (with a diameter of 8.40 mm) in the middle of each sample. The relative resistance before and after having a hole is measured using a current source and voltmeter. KEITHLEY 6220 Precision current source and KEITHLEY 2182A Nanovoltmeter are used for this purpose (Figure 23). To measure the resistance between opposite probes, a constant current was injected between two outer probes, and the voltage difference is measured between inner probes. The value of voltage difference divided by the constant current is the equivalent resistance. An index for sensitivity (S) is defined by averaging the 6 resistances between every 2 opposite probes on the edge before and after having a hole in the middle (equations (5) and (6)).

$$R_{r,i} = \frac{R_{before\ defect} - R_{after\ defect}}{R_{before\ defect}} \times 100 \quad (5)$$

$$S = \frac{\sum_{i=1}^{6} R_{r,i}}{6} \quad (6)$$

As is shown in Figure 25 and Figure 26, the resistivity and sensitivity (S) are studied with respect to CNT concentration.

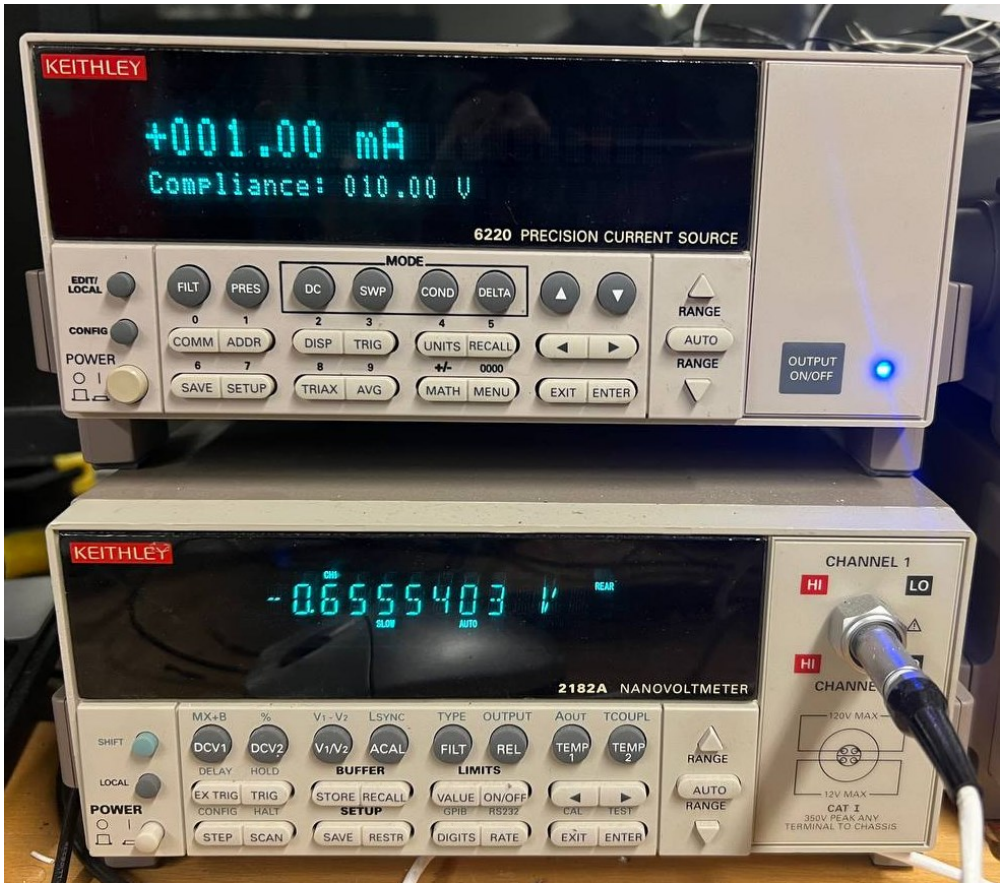

Figure 23: *The current source and voltmeter used*

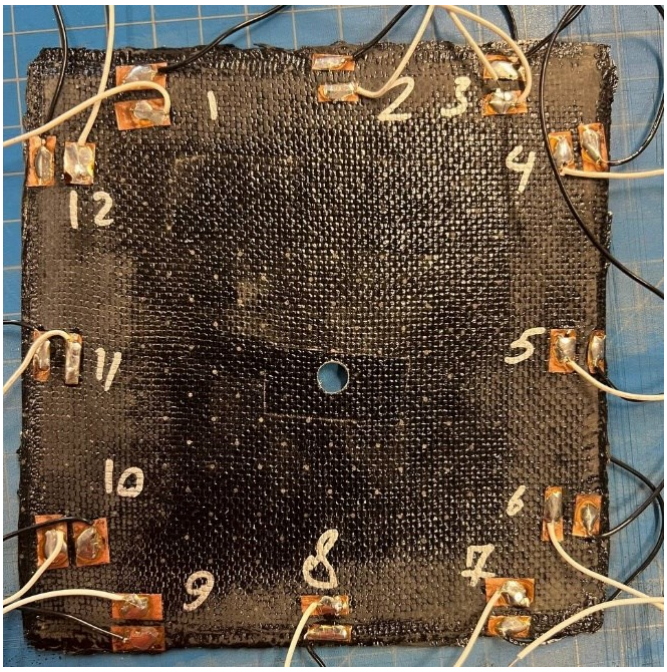

Figure 24: *Sample with a dilled hole to measure the measurable difference before and after the defect*

According to Figure 26, the sensitivity decreases while increasing CNT concentration. As a result, the least amount of CNT would be better for sensitivity. Although Sensitivity (S) for 0.05w% and 0.1w% CNT concentrations are not considerably different as mentioned in the previous section concentration less than 0.1w% is not acceptable. So, the optimum concentration of CNT is 0.1w%. The concentration of 0.1% of mass fraction for CNTs is picked to make samples for the generation of data for NN training. By choosing this concentration we minimized agglomeration of CNTs that may imply inconsistency in our results while keeping the sensitivity high.

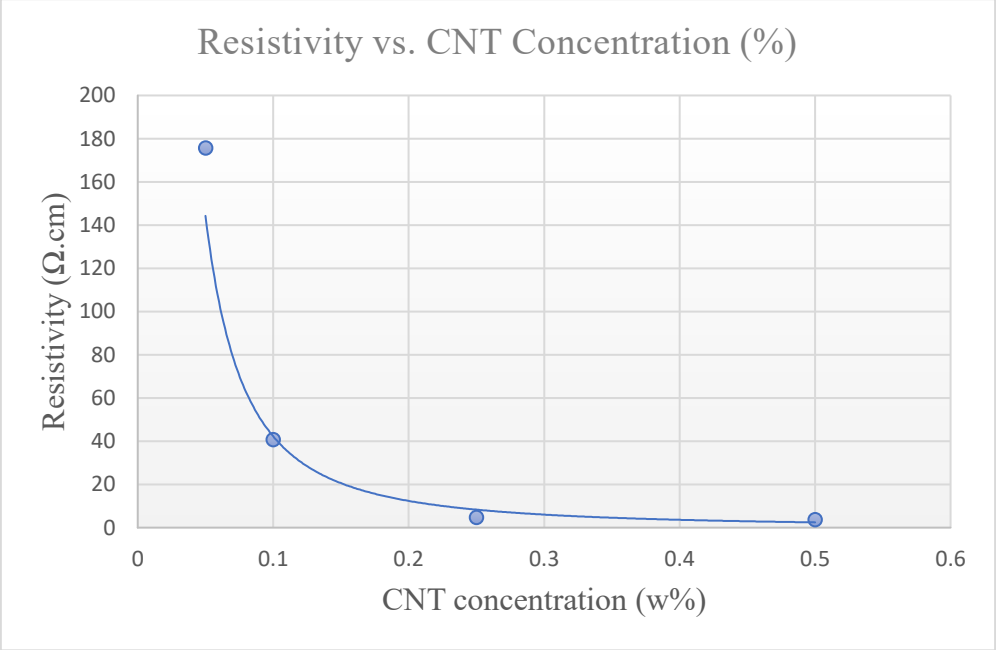

Figure 25: *Resistivity of samples vs. CNT concentration*

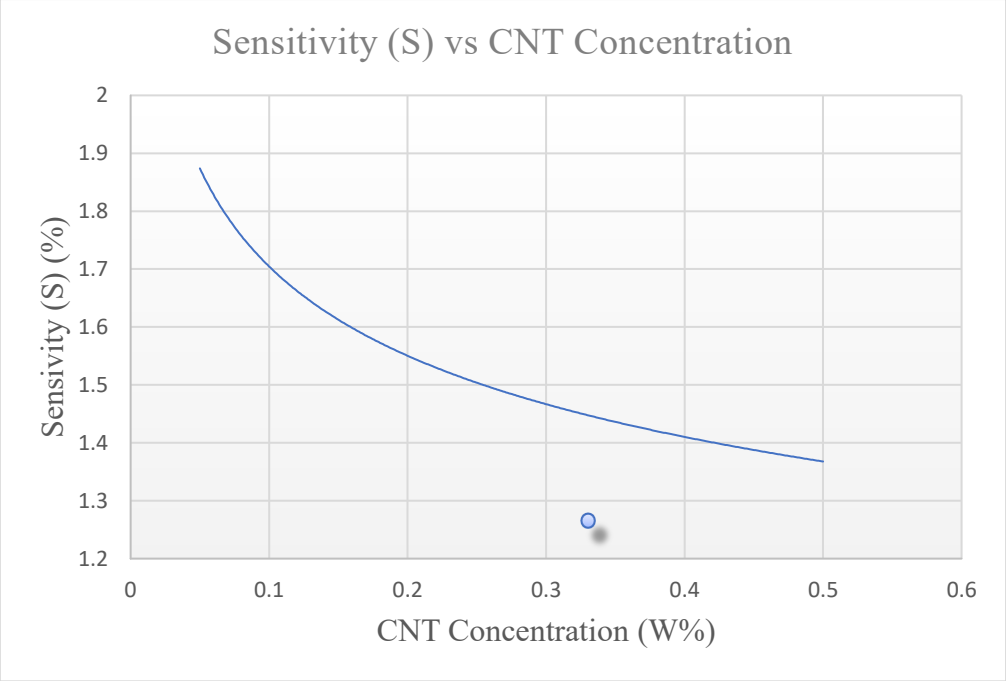

Figure 26: *Sensitivity (S) vs. CNT concentration*

Table 1*: Resistivity of samples with different CNT Concentration*

CNT Concentration (w%)	Resistivity (Ω.cm)	Average resistivity (Ω.cm)
0.5	3.6731	3.6677
0.5	3.6624	
0.25	4.4545	4.7063
0.25	4.9581	
0.1	39.2413	40.7410
0.1	42.2408	
0.05	175.121	175.6375
0.05	176.154	

3.3 Samples for Experimental Data Generation

To have 12”x12” plates made of CNT epoxy resin/glass fiber, glass woven fibers were cut into 12”x12” pieces. The samples are made using the same materials that are used for the previous set of samples (Figure 16 and Figure 17). To mix CNTs within epoxy resin, a three-roll milling method is used (same as the procedure for the first set of samples).

After preparing the resin with CNT, 10 layers of woven fiberglass were wetted by the prepared resin and stacked together. Before vacuuming, the copper film was cut into squares of 0.5” x 0.5” (for injecting electric current) and 0.25” x0.25” (for measuring voltages) and placed on the edges of the top layer. These copper films on the top are used as probes to inject current and read the voltage while testing. To avoid the probes to get dirty by epoxy resin, which makes the connecting wires unstable and erratic, they were covered by thermal resistant tape before placing them on the samples. These tapes were pulled off after curing to have the fresh and clean surface on copper probes ready for the wires to be connected. Using these tapes helped a lot to save time and removed the need for sanding them after curing. Sanding probes not only are time-consuming but would affect the quality of soldering and conductivity. The samples were vacuumed and co-cured with the copper films in the autoclave. The vacuumed layup is cured using the autoclave. For curing, the temperature is increased by the rate of 10 Deg F/min to 350 Deg F while the pressure of 50 psi is applied to the samples. The temperature is kept for three hours at 350 Deg F and then the sample is cooled to 140 Deg F at the rate of 5 Deg F/ min. After cooling, by venting the autoclave the pressure is taken off and the sample is cooled to room temperature.

The DSC test was done on the cured samples containing 0.1w% CNT. The result, as shown in Figure 27, proves that the samples are fully cured. Also, the heat flow curve shows that the glass transition temperature (T_g) is 147.92^o C.

The void content of the cured samples is checked and confirmed to be under 1%. As shown in Figure 28, the samples were cut out of the cured laminate, polished, and observed under a microscope. As shown the sizes of the voids are also small.

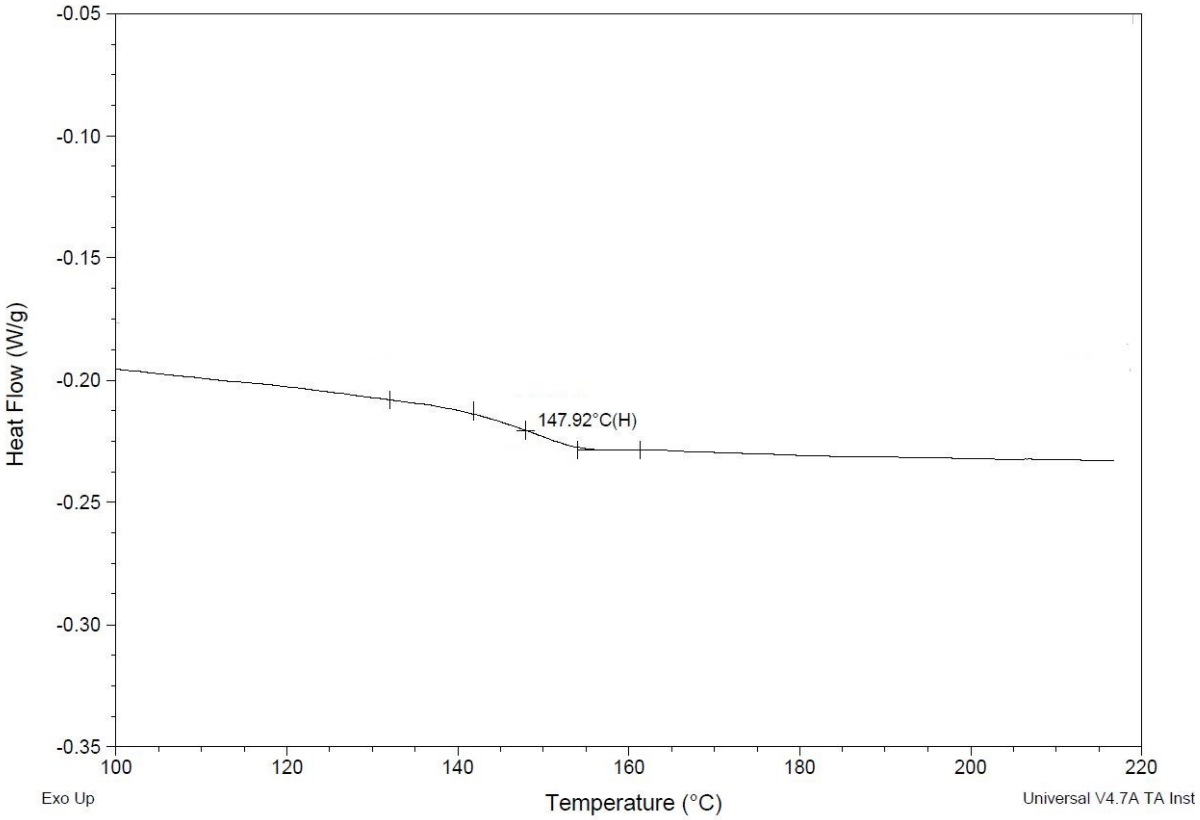

Figure 27: *DSC result of the cured sample.*

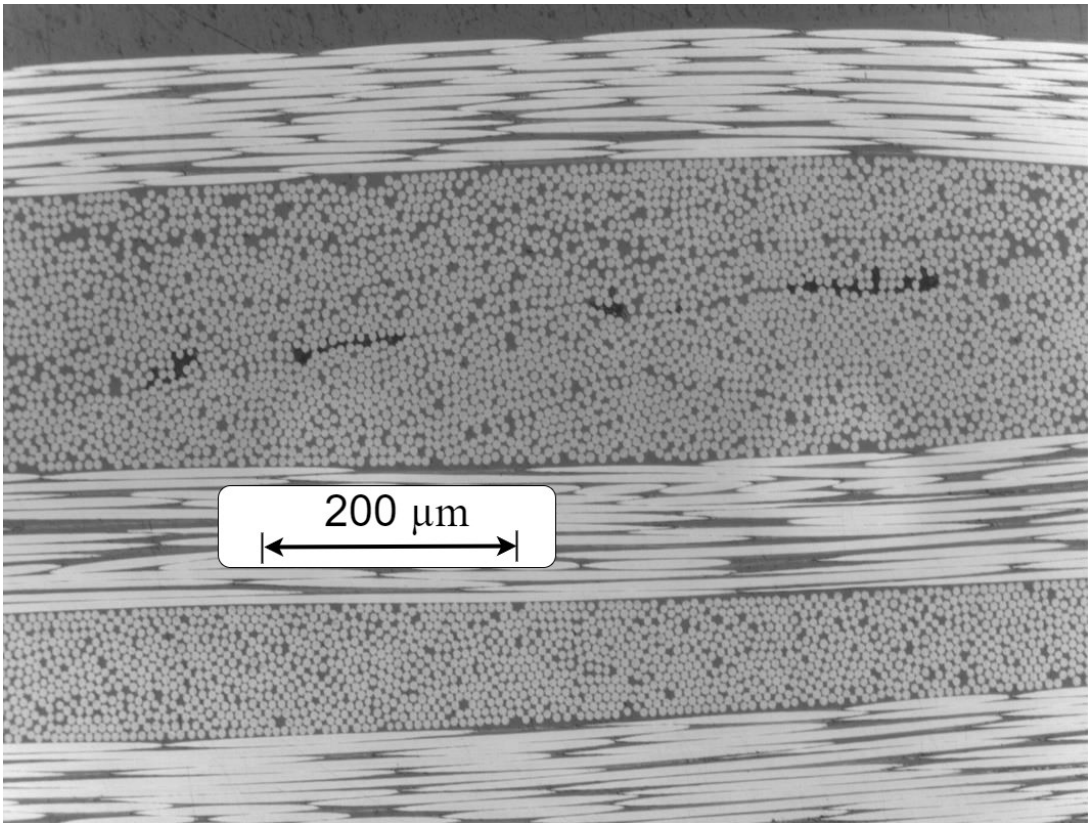

Figure 28: *Image of the cross-section of the cured layup under a microscope.*

After curing, the samples were trimmed. To test the samples, wires were attached to the probes on the plate using soldering.

The cured plate is shown in Figure 29. As illustrated in Figure 29 the plate is discretized into 36 cells (6 cells in each row and column). Each cell is 2” by 2”. There are two series of numbers on the plate, one in silver color and one in copper color. Figure 30 shows how the plate is numbered. Each node on the corner of the cells is numbered from top to bottom and from left to right. The cells are also numbered sequentially from top to bottom and from left to right. The numbers of each cell are in the middle of the cell with silver color. The copper-colored numbers on the edges specify the numbers attributed to each probe on the edges. The probes’ numbers are the numbers of the nodes that the probes are located on (Figure 30). These numbers are used during performing measurements to be sure that the equivalent resistances are measured between the correct probes. The number of the cells is used to record the label of each measurement that represents the location of the defect.

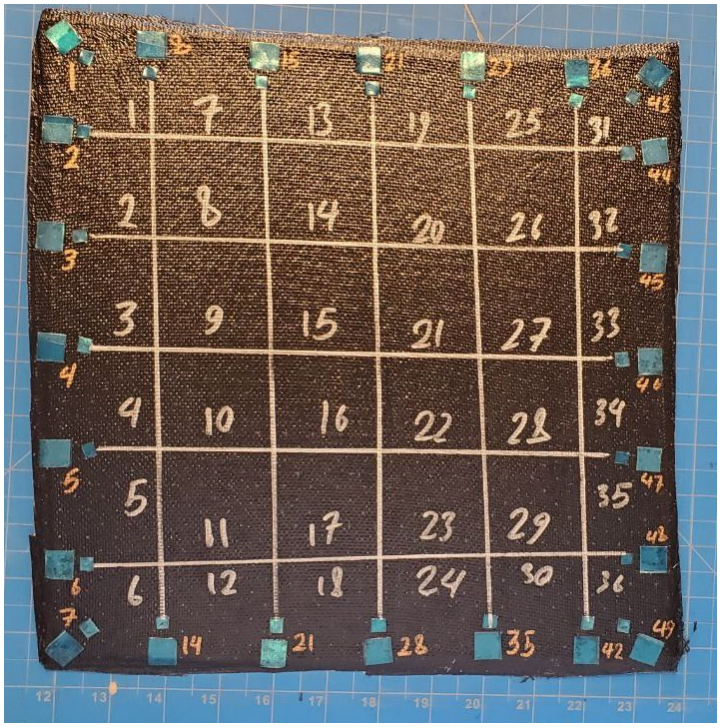

Figure 29: *A cured sample with node numbers on the edges and cell numbers in the middle of each cell*

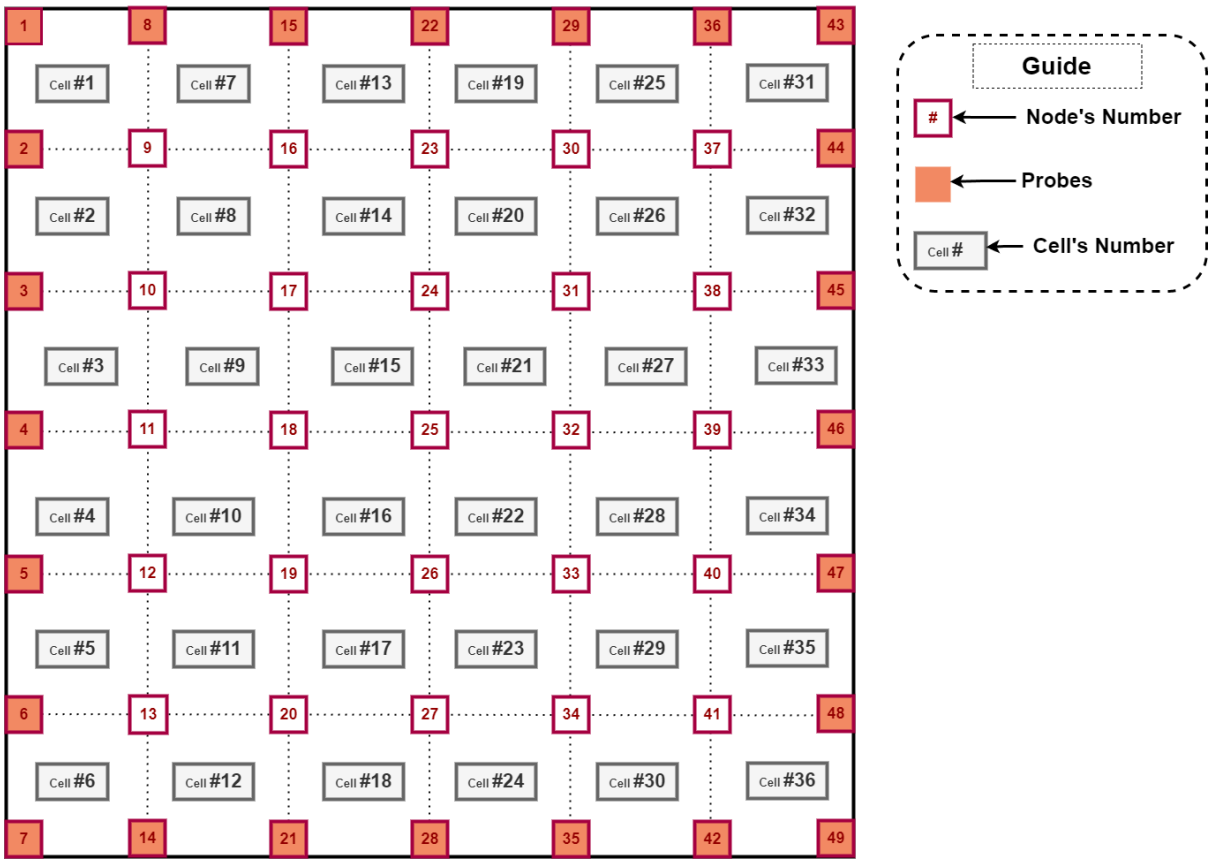

Figure 30: *Schematic of Numbering cells, Nodes, and Probes*

3.4 Electrical Resistance Testing

To generate data from testing manufactured samples, electrical resistances between every pair of opposite probes on the edges (for example between probe 1 and 43, or between probe 8 and 14) were measured.

3.5 Electrical Measurement Strategy

There are two available methods to measure the electrical resistance in plates:

1. Two-probe method
2. Four-probe method

In the two-probe method, two electrical probes are used to apply electrical voltage deference to force an electric current flow between these probes and then measure the electrical resistance between the probes. On the other hand, in the four-probe method, 2 pairs of probes

are being used. These four probes are used on a line to measure the electrical resistance between the inner pair. One pair is used to provide a constant electrical current. The other two inner probes are used to measure the drop in electrical voltage. The electrical resistance is calculated from the ratio of current applied and the voltage drop [158].

The benefit of using the four-probe method compared to the two-probe method is that in the four-probe method the contact resistance between probes and plates is eliminated while in the other one the contact resistance affects the outcome[158].

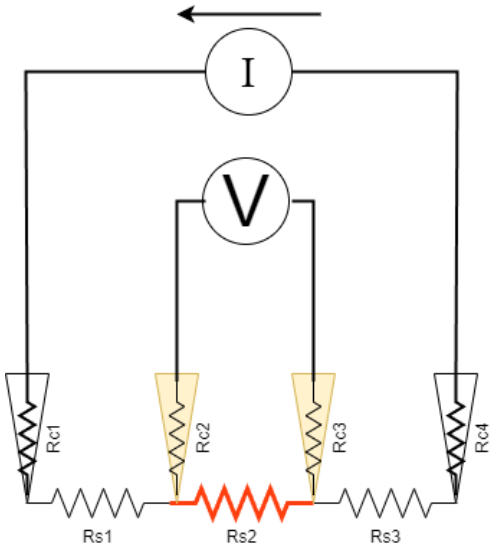

Figure 31: *Schematic diagram of a four-point probe circuit*

The four-probe method is used to eliminate the effect of contact resistances. This can be illustrated by writing the Kirchhoff equations. The target is to measure the resistance shown in red (in Figure 31 and Figure 32). This resistance is Rs2. As shown in Figure 31, there are contact resistances (illustrated by Rc1, Rc2, Rc3, and Rc4). By writing the Kirchhoff equation for the four-probe method (Figure 31), as shown in equation (7), the contact resistance is eliminated. In this equation, V is the electrical voltage difference measured by the voltmeter and I is the current injected by current source.

$$V = I \times R_{s2} \Rightarrow \frac{V}{I} = R_{s2} \tag{7}$$

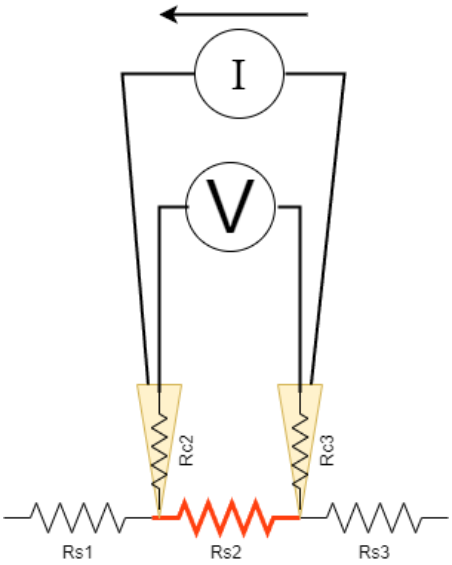

Figure 32: *Schematic diagram of a two-point probe circuit*

On the other hand, by writing the equation for the two-probe method (Figure 32), the contact resistances (R_{c2}, R_{c3}) cannot be eliminated. It is shown in equation (8).

$$V = I \times (R_{c2} + R_{s2} + R_{c3}) \Rightarrow \frac{V}{I} = R_{c2} + R_{s2} + R_{c3} \tag{8}$$

In this equation, V is the electrical voltage difference measured by the voltmeter and I is the current injected by the current source and R_{c2} and R_{c3} are contact resistances and R_{s2} is the resistance of the sample.

In our problem, the difference in electrical resistance before and after the defect is being used. As these differences are estimated to be small as compared to the contact resistances, the four-probe method is used for this study to eliminate any errors that may be related to contact resistances or the changes in contact resistances. So, the differences that are measured represent the effects of defects in the plate rather than changes in contact resistances. So, to measure the equivalent resistance between the probes on the plates, the 4-probe method is used. An illustration of applying this method for measurements is provided in Figure 33.

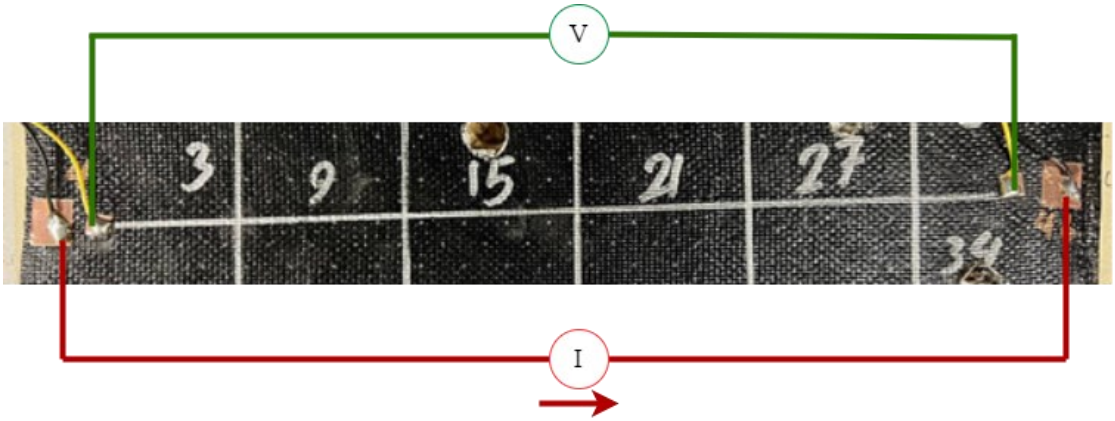

Figure 33: *A four-probe method applied for measurement on a sample plate*

As it is shown in Figure 34, 14 measurements needed to be done for each data point. These measurements are done between every two opposite probes on the edges. These measurements consist of 7 measurements between probes on the vertical edges and 7 measurements between probes on the horizontal edges. To perform all these measurements to generate the data points required for NN training, a data acquisition system is developed and used. The data acquisition system is described in the following section. By using the data acquisition system, all the measurements can be done without the need for switching the probes of the voltmeter and the current source between the probes on the plates. Developing the data acquisition system helped a lot in doing the measurements, to allow more quick and accurate measurements than doing them manually.

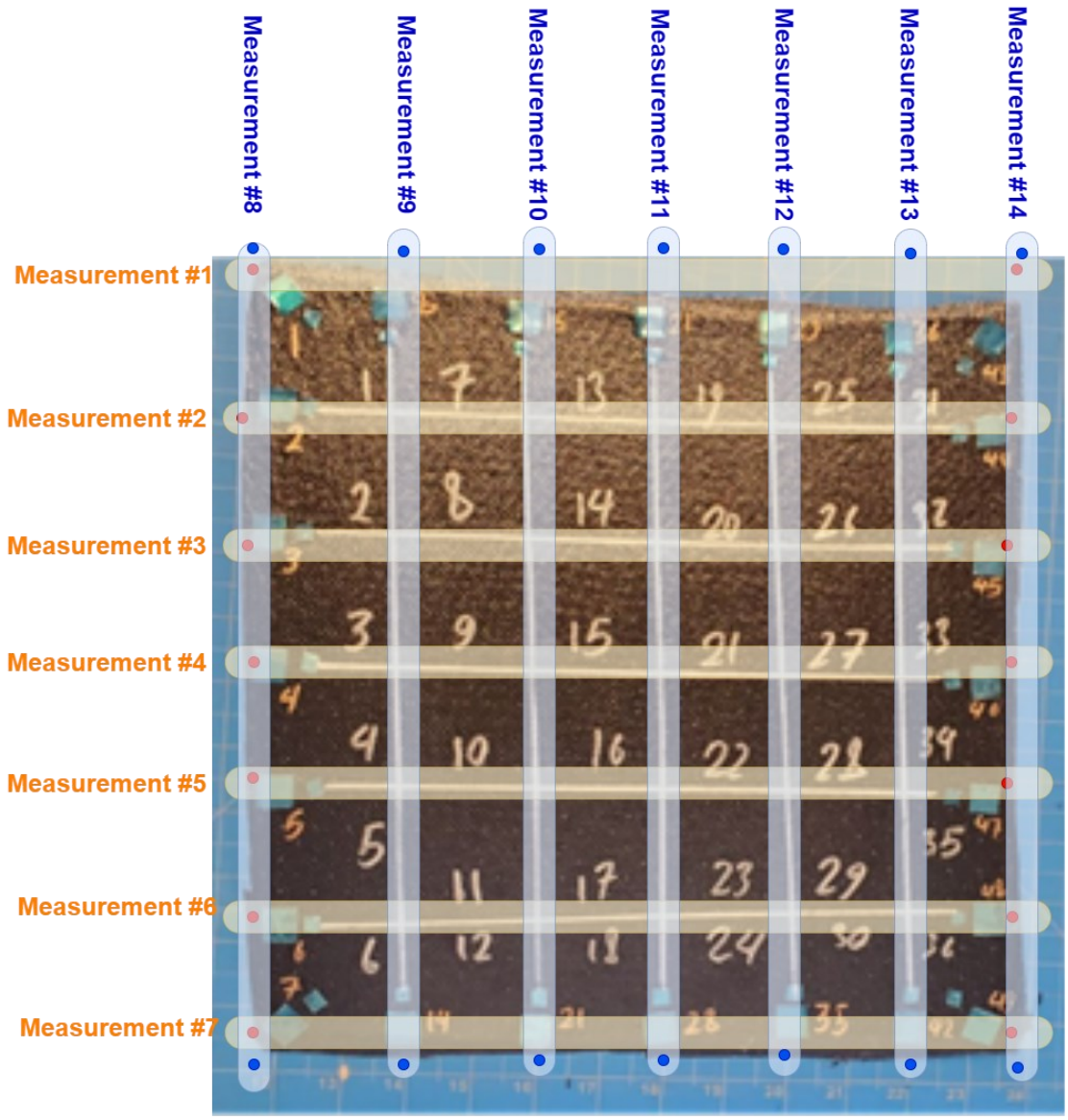

Figure 34: *Measurement on the sample.*

3.6 Data Acquisition System

As the measurements can be sensitive to the changes in connection and even length of the wires, a fixed method is needed that would be consistent both during testing a sample and through different samples. It is noteworthy that it should be fast, as for NN to be trained, sufficient data is needed.

To overcome these challenges, a data acquisition system is designed and developed. The data acquisition system is developed using an Arduino Mega board and multiple relays.

Arduino boards are microcontroller boards that can be programmed to perform tasks. These boards can be connected to personal computers and are popular for being easily programmed[168]. Arduino boards come with different numbers of pins that can be controlled. Based on the number of relays needed for our data acquisition system to be controlled, the Arduino Mega 2560 Rev3 board is used.

The Arduino Mega board is programmed to switch the current between the different probes and change the probes that the voltmeter is connected to accordingly. Using this Arduino system reduces the time needed to record data while sufficient consistency is achieved.

Arduino Mega is programmed using an open-source integrated development environment (IDE) developed by Arduino. Arduino software is also used to control switching from one to the other steps among 14-step-measurement cycles. The schematic diagram of the developed data acquisition system is presented in Figure 35.

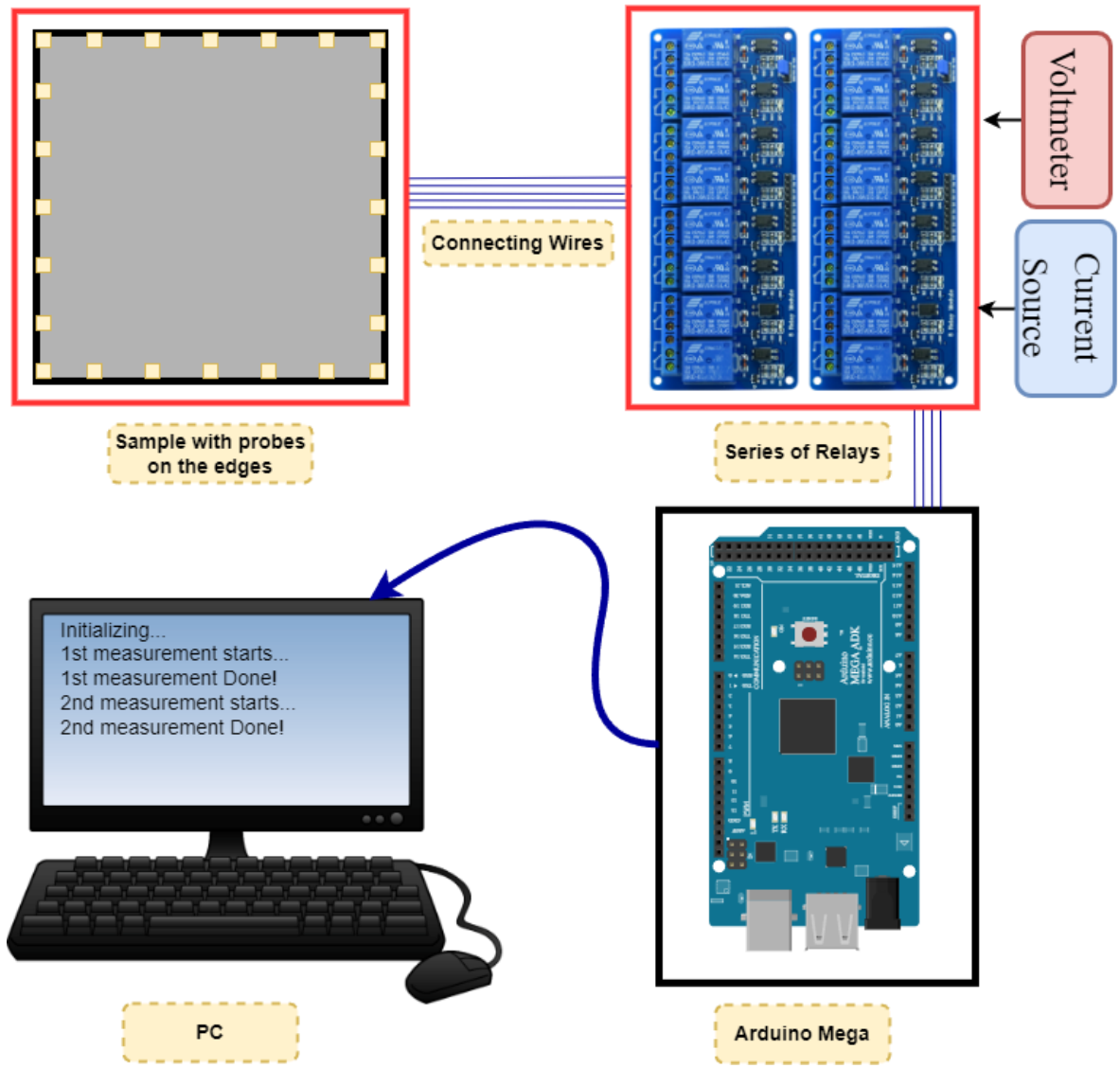

Figure 35: *Schematic diagram of the Data Acquisition System*

3.7 Measurements and Data Treatment

To generate experimental data set, for a data point, equivalent resistances between every pair of opposite probes before and after having a defect, which is generated in a randomly chosen cell, were measured. After performing measurements, there are 14 equivalent resistances for the sample before having any defects and 14 equivalent resistances for the sample after having a defect. The defect is generated by drilling a hole with the diameter of 11.5mm. The relative differences between the equivalent resistances before and after the defect

are recorded as features. The number assigned to the cell in which the defect is generated is recorded as the label.

As data points are the relative differences of the measurements before having a defect (reference state of the plate) and after a defect, one sample can be used to generate multiple data points. This is beneficial as a smaller number of samples is needed to generate data set for training NN. So, each plate is used to generate multiple data points. This can be done by changing the reference state of the sample after each defect. The assumption is that there was not any defect in the plate as the reference resistances of the plate were measured before generating a defect in a specific cell. In order to overcome the challenge of being compatible with this assumption while having plates with multiple defects, changing the reference point after each defect generation is used. The reference from which the relative changes are calculated is updated after having a new defect in the plate. For example, after having one defect at cell number 12 (which is picked randomly), the reference is changed to the resistance distribution of the plate with a defect in cell number 12. Then another defect is generated in cell 30 (which is picked randomly), the changes due to this new defect (in cell 30) are measured with respect to the new reference, which is with having a defect in cell 12. The formulas for recording the features are as follows:

$$R_r^i = \frac{R_{after\ i^{th} defect} - R_{after\ (i-1)^{th} defect}}{R_{after\ (i-1)^{th} defect}} \tag{9}$$

Or

$$R_r^i = \frac{R^i - R^{i-1}}{R^{i-1}} \tag{10}$$

$$\overline{R_r^i} = \frac{\sum_{n=1}^{14} R_r^{i,n}}{14} \tag{11}$$

$$\sigma_{R_r} = \sqrt{\frac{\sum_{n=1}^{14} (R_r^{i,n} - \overline{R_r})^2}{14}} \tag{12}$$

$$X_i^n = \frac{R_r^{i,n} - \overline{R_r}}{\sigma_{R_r}} \tag{13}$$

R_r^i is relative resistance after having i^{th} defect in one sample. X_i^n is the feature data point for i^{th} data point and n^{th} measurement ($n \in \{1,2,3,\dots,14\}$). $R_r^{i,n}$is the relative resistance change for n^{th} measurements after having i^{th} defect in a pate. $\overline{R_r^i}$ and σ_{R_r} are the mean and standard deviation of relative equivalent resistances after i^{th} defect, respectively.

Having a data acquisition system that is specifically designed for this task coupled with recording multiple data points from one plate helped a lot to reduce the number of samples needed and the amount of time needed. By using these methods 98 labeled data points (7 x 14) were recorded from testing 14 plate samples. Seven data points are generated by testing each plate. It is noteworthy that, as mentioned, each data point consists of 14 features (measurements on the probes on the edges) and a label (the defected cell number). Features will be the input and labels will be the output of the NN.

3.8 Data Augmentation

To be able to train a NN well enough, enough data points are required. As in our case, generating lots of data points is hard and expensive, generating new data points from existing data points is beneficial. To do so, data is "Augmented".

3.8.1 Introduction to Data Augmentation

"The term data augmentation refers to methods for constructing iterative optimization or sampling algorithms via the introduction of unobserved data or latent variables"[169]

The performance of deep learning models is fundamentally dependent on the size and diversity of the training set. Deep learning models (DL models) that are used for complex problems have many hidden layers. The more hidden layers in a model, the more parameters are needed to be optimized. The number of parameters in common-high performance models in computer vision like RESNET[1] (60M), and Inception-V3[2] (24M) is in the order of millions. So, much data is needed to train such large DL models. Often while dealing with complex problems, there are not sufficient labeled data available to train the models. In these cases, "Data Augmentation" can be used to enhance the data set in both aspects of being enough numbers and being diverse. The table below summarizes the performances of some models in different fields to show the effectiveness of data augmentation.[170]

[1] Residual Networks. RESNET was the winner of the ImageNet challenge in 2015. The invention of this model provides ways to train NN with more than 150 layers. [194]
[2] Inception V3 is a popular computer vision model. It provides an accuracy of greater than 78% on the ImageNet data set. This model is a result of the work of several researchers for years.[195]The model is based on a paper by Szegedy, et. al.[196]

Table 2: *Different models' performance with and without data augmentation*[170]

Application	Performance without Augmentation	Performance with Augmentation	Augmentation Method
Image Classification	57%	78.6%	Simple Image based
Image Classification	85.7%	85.7%	GAN based
NMT[3]	11 BLEU[4]	13.9 BLEU	Translation data augmentation
Text classification	79%	87%	Easy Data Augmentation

Data augmentation is effectively being used in training DL models for image classification. Some simple geometrical transformations are being used to augment the images. Some of these transformations are flipping, rotation, cropping, scaling, and… (Figure 36).

Figure 36: *Some of the simple image transformations used for image augmentation* [170]

[3] Neural Machine Translation is a machine translation method that uses NN to predict how much a set of words is in sequence.[197]
[4] bilingual evaluation understudy is an algorithm that provides a method to evaluate the performance of a machine-translated text from one language to another.[198]

3.8.2 Data Augmentation on Experimental Data Set

Although our problem and data set seem to not be similar to the common data sets that data augmentation is usually used on, the symmetry in the problem helps to apply the same method to get the benefits of data augmentation.

Imagine the case that we have a defect in cell number 8 (as it is depicted in Figure 37. The measurements are done and recorded on the edges of the plate. Now if we flip the whole plate with respect to the middle column (or similarly, look at it from the other side), it is like the defect is in cell 26. So, by just switching the elements in the vector X_i, without performing new measurements, data for the case as if we had a defect in cell #26 is achieved.

There are 3 axes of symmetry in the plate as below:

1- Horizontal axis

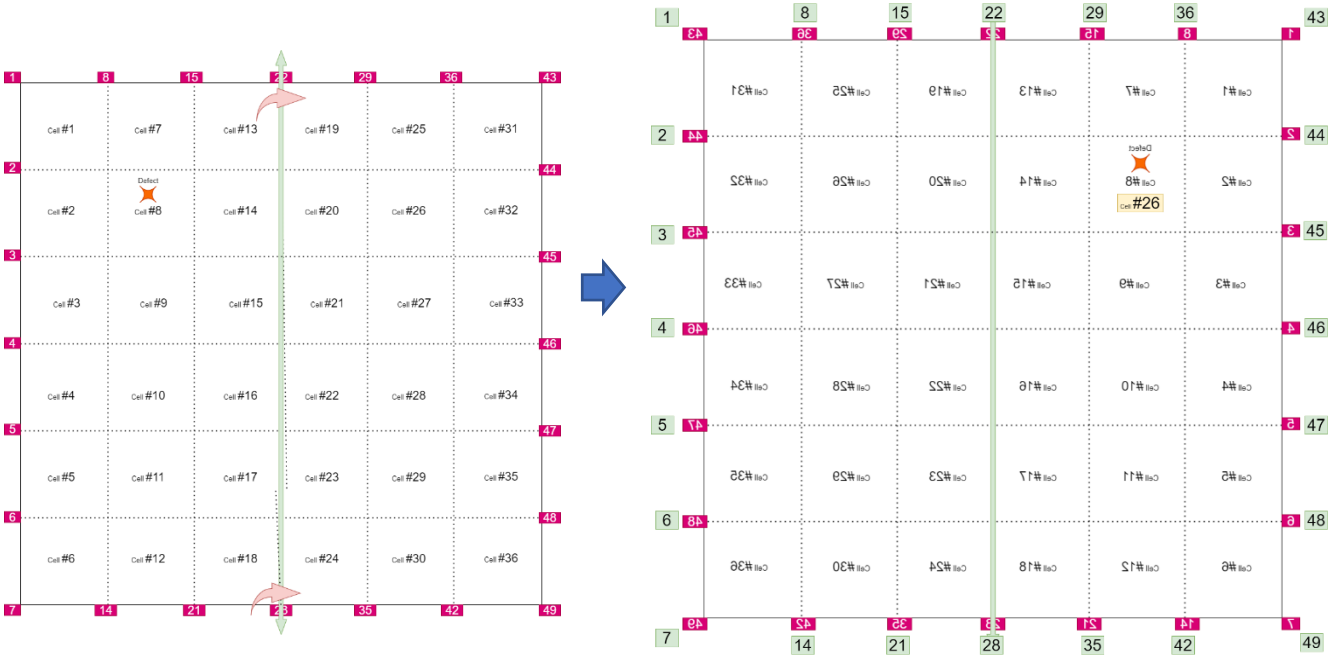

Figure 37: *presentation of data augmentation using horizontal flipping*

2- Vertical axis

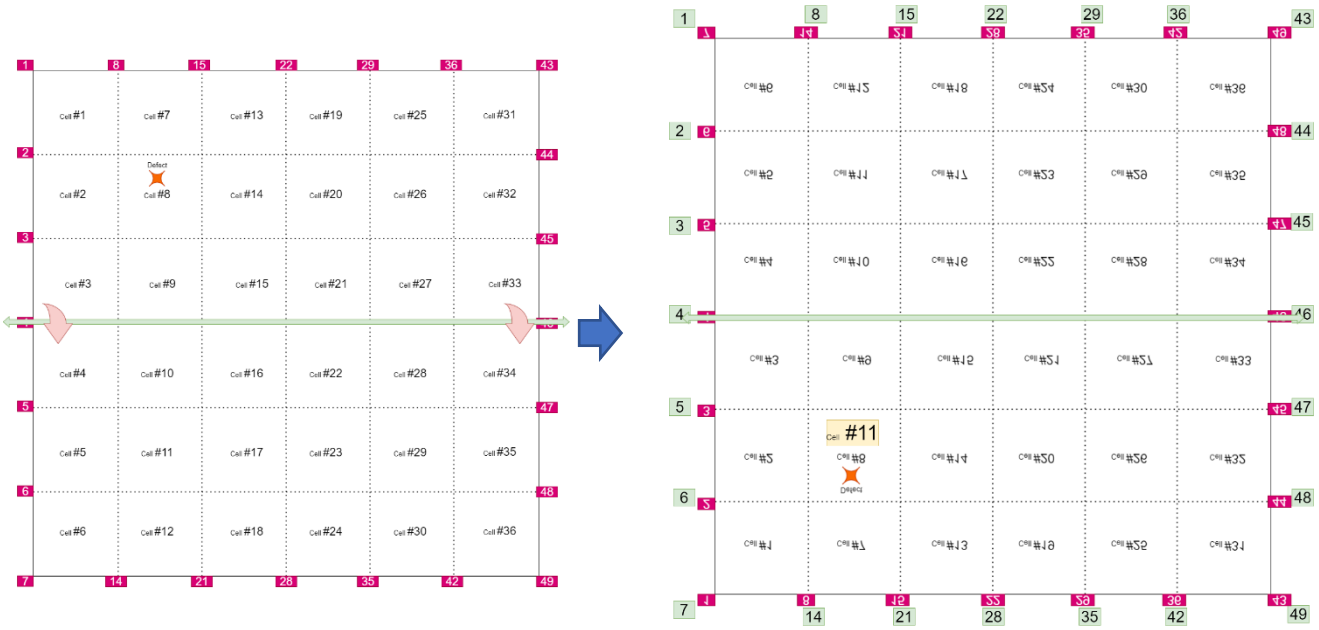

Figure 38: *presentation of data augmentation using horizontal flipping*

3- Diagonal axis

The same method is used at 45 degrees for the diagonal axis of flipping.

Each experimental data point in the original data set can be used to augment three new data points. So, the data set size is now 4 times bigger. There are 98 labeled data points from experiments.

$$Size(X_{original}^{1:98}) = 98 \tag{14}$$

$X^{1:98}$ means data examples from first till 98. Basically, there are 98 examples in the original data set (experimental data set).

$$X^{1:98} \xrightarrow{Horizontal\ flipping} X_H^{1:98} \tag{15}$$

$$X^{1:98} \xrightarrow{Vertical\ flipping} X_V^{1:98} \tag{16}$$

$$X^{1:98} \xrightarrow{Diagonal\ flipping} X_D^{1:98} \tag{17}$$

By doing these 3 flipping processes for the augmentation process, we have:

$$Size\ (X) = Size\left(X_{original}\right) + Size(X_H) + Size(X_V) + Size(X_D^{1:98}) \quad (18)$$
$$= 4 \times Size\ (X)$$
$$= 4\ \times 98 = 392$$

So, by using data augmentation without doing more experiments, the number of experimental data points is increased by a factor of four.

CHAPTER 4: Simulation and Data Preparation

4.1 Simulation

To generate data that is needed for the initial training of the NN in stage one of the transfer learning, a simulation for a similar problem is developed. This simulation models a grid of resistors. This simulation is used as there are similarities between the electrical behavior of the grid of resistors and composite plates[75].To do so LTspice software is used to model a 6-cell-by-6-cell grid of resistors. A python code is used to generate and record data from the electrical model. Introduction to LTspice and Python is provided below.

4.2 LTspice

LTspice is simulation software, schematic capture, and waveform viewer with enhancements and models for easing the simulation of analog circuits. Ltspice is a common software used for simulating electrical circuits in a range of research from simple phenomena like resistors to thermoelectric elements and sparks gap modeling ([171], [172]).

This software, in our problem, is used to model a circuit of resistors. The equivalent resistances between certain points are desired. LTspice is capable of calculating and providing the electrical attributes between any points in the modeled circuit. For data generation, certain points (nodes) are given to the software and the required attributes between them are recorded. The term “recording” is used in this chapter for the task of saving the values that are calculated and provided by LTspice software. This explanation is found to be necessary to avoid any confusion between “recording” values provided by LTspice and doing measurements in experimental testing that is mentioned in the previous chapter.

4.3 Python

Python is a high-level, general-purpose programming language that is interpreted. The use of considerable indentation in its design philosophy promotes code readability. Its language constructs and object-oriented approach are aimed at assisting programmers in writing clear, logical code for both small and large-scale projects [173].

4.4 Simulation of a Grid of resistors

In order to have a model to generate the data that is needed for the initial training of the NN, a circuit of a grid of resistors is developed. The rationale behind having similarities between such a circuit is that equivalent resistance for each cell in the continuous plate can be assumed to be similar to the effect of having 4 discrete resistors on the sides of the cells. The resistance of the resistors is considered to be proportional to the size of the cells. It is common in studying electrical elements to have them behave like known elements like resistors, capacitors, etc. So, it is possible to have the whole plate having similarities with the behavior of one resistor as, for this study, only the similarities in resistance behavior of the plate is considered. And that one resistor can be presented by equivalent resistors and this process is repeatable. This is the explanation of why the model shown in Figure 40 is considered to have similarities with the plate shown in Figure 39.

The equivalent electrical resistances between the points (nodes) on the edges of the grid (R_i) are calculated by injecting the current (I0) from the selected points and then recording the voltage difference between the same nodes (V0) in LTspice software. The actual plate, the schematic figure, and the resistor model in LTspice are shown in Figure 39 and Figure 40, respectively.

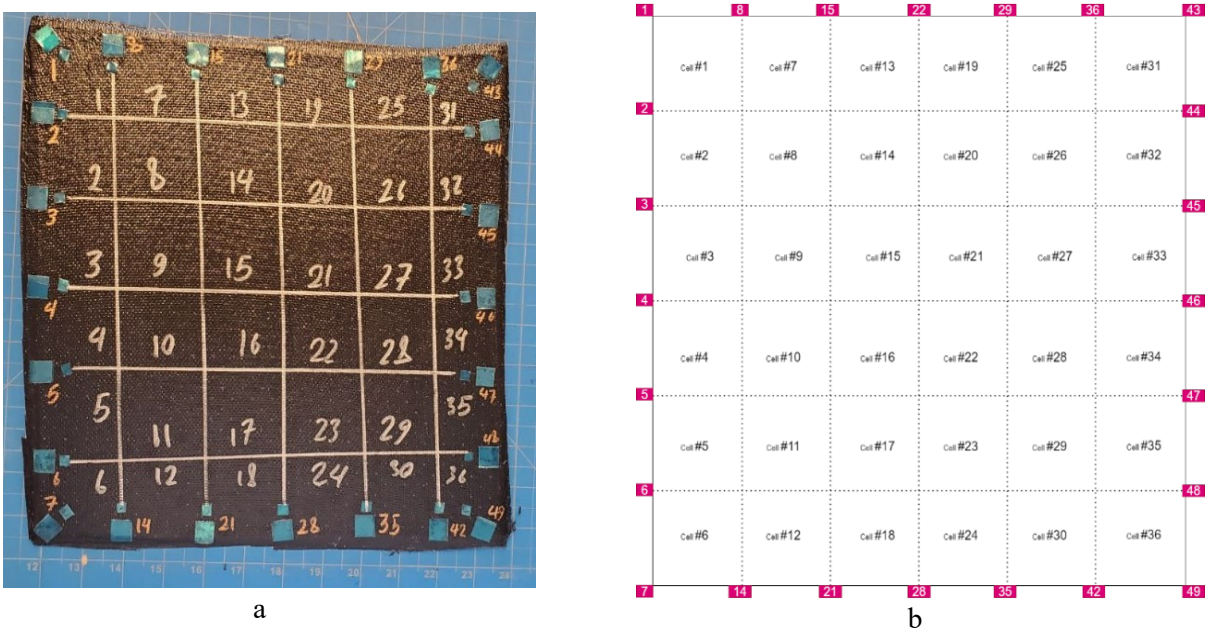

a b

Figure 39: *(a) The actual glass fiber reinforced Epoxy with CNTs*
(b) The schematic of the plate indicating cell numbers and probes and their assigned numbers

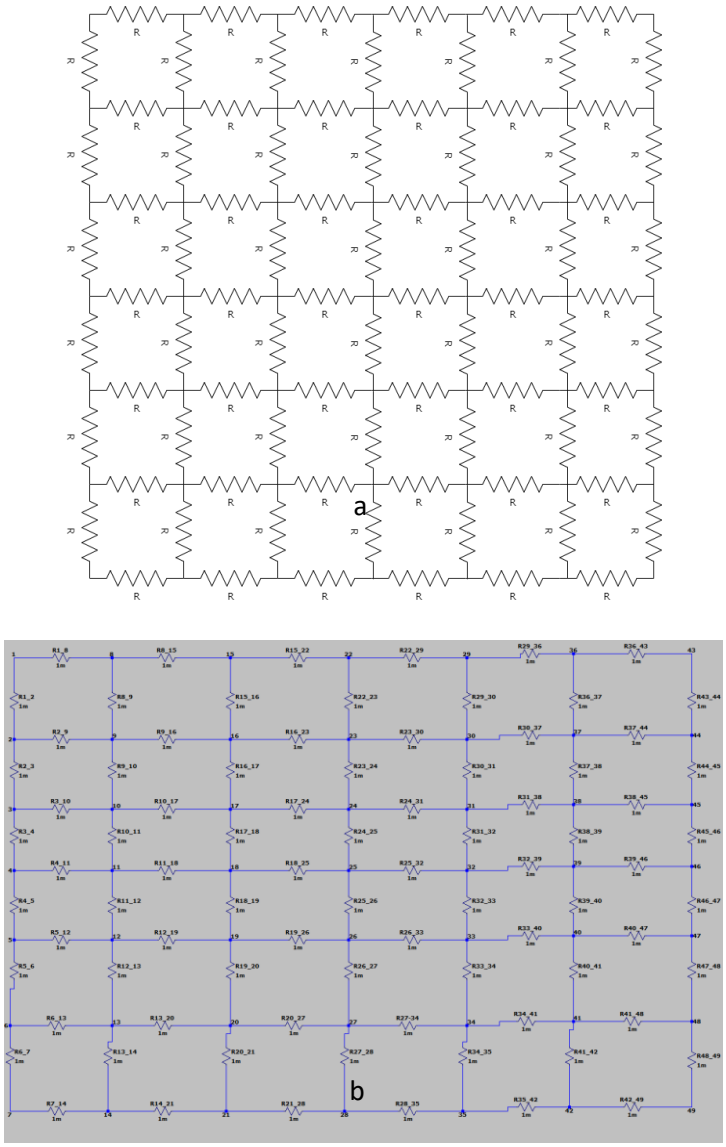

Figure 40:*(a) A schematic of the circuit of a 6 by 6 grid of resistors used to model the composite plate (b) The circuit that is shown in Fig3 (a) modeled in LTspice software*

Calculating the equivalent resistances in 7 vertical lines of resistors and 7 horizontal lines of resistors requires 14 times running of the electrical model and recording the electrical voltages between different nodes on the edge of the model (Figure 41). To do so a python code was developed to run the circuit model in LTspice and record the data for each run.

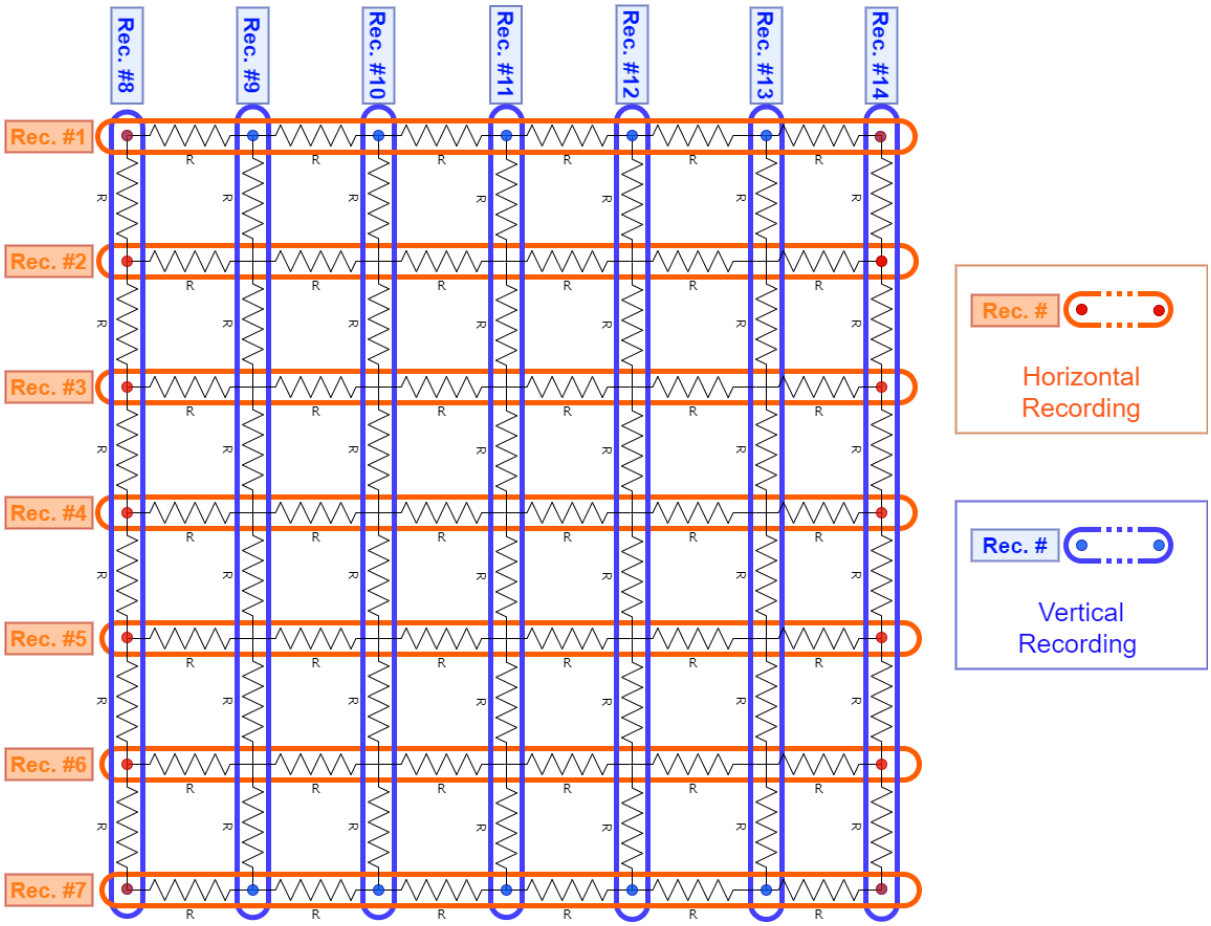

Figure 41: *Illustration of recording electrical voltages between 14 opposite pairs of nodes.*

A grid of discrete resistors is formed in LTspice. The resistors were assigned values between 1 to 10 Ohms with random distribution. The reason for having the values assigned randomly is based on the assumption that more similarities to the actual problem (plate of nanocomposite) can be achieved with this randomness. This assumption is rooted in the fact that the nano composite plates have a random distribution of CNTs. This randomness in CNT distribution makes randomness in the paths of conductivity which results in variation in conductivity (resistivity) in different locations on a plate. It is noteworthy that changing the range of initial values for resistors in the model would not change the values of the data points that will be used in training the NN. The reason is that the normalized values of relative difference will be used for data points. In other words, multiplying a number to this range would not change the normalized resistance values that are used.

To represent a defected cell in the plate, the resistors making that targeted cell are increased in value. After trying and checking the results with the experiments in order to make a more

realistic model, the four resistors were increased by four different random values between 30 and 40 Ohms. The process is depicted in Figure 42.

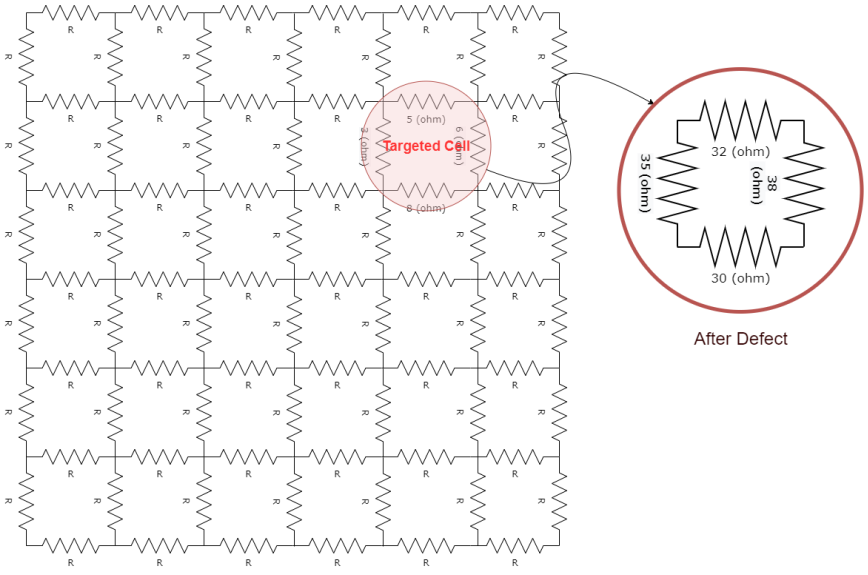

Figure 42: *One cell is targeted at each run of LTspice model and the values for resistors making that cell increase from initial values (random between 1Ω-10Ω) to random values between 30-40 Ω*

The flowchart of the python code is depicted in Figure 43. To be able to change the grid and record required values a ".text" file as the input for LTSpice software is needed. This file is generated by having a grid of resistors modeled in LTSpice. The ".text" file was then changed and imported to LTspive using the python code.

First, values for the resistors were randomly generated between 1-10 ohms. These values were replaced in the ".text" input file. This action is repeated in the "Loop for initializing grid of resistors" (Figure 43). A new input file is generated for each distribution of resistors. The counter for this loop is "i" which controls the iteration for 100 times of repetition (100 is chosen as a large round number).

Then in the second loop, defects are addressed. In "Loop for having defects in cells" (Figure 43) four random values for each targeted cell's sides are generated. These values (R_{d1}, R_{d2}, R_{d3}, R_{d4}) are between $R_{D,min}$= 30 ohms and $R_{D,max}$ = 40 ohms. These values are allocated in the input file for the j^{th} cell as defective. Counter j is for the loop to 36 as there are 36 cells in each plate.

In the last loop, the voltage recordings and equivalent resistance determinations are performed. As there are voltage recordings needed between 14 opposite nodes (7 in horizontal, 7 in vertical) that are on the boundaries of the grid of resistors, k (the counter for this loop) goes to 14. For each recording, an electrical current of 1A is injected between the k^{th} pair of probes, and the voltage needed to be recorded between them. The input file with the instruction is sent to LTSpice software and the circuit was solved by LTspice and the values are recorded. The recorded voltage is saved as equivalent resistances for all 14 pairs of opposite nodes (equation (19)).

$$R_{eq}^{k} = \frac{V^k}{I^k} = \frac{V^k}{1\ A} = V^k \tag{19}$$

By using this python code, 3600 unique labeled data points are generated. The number of labeled data generated can be calculated using counters of the loops in python code as in equation (20). As mentioned, $Max(i) = 100$ (a random large number) and $Max(j) = 36$ (number of cells).

$$Number\ of\ labled\ data = Max(i) \times\ Max(j) = 100 \times 36 = 3600 \tag{20}$$

4.5 Data Preparation

To have the features for simulation data points, the relative differences in values of equivalent resistances before and after increasing resistance values of the targeted cells were calculated.

$$R_r = \frac{R_{after\ defect} - R_{initial}}{R_{initial}} \tag{21}$$

After having the relative changes in equivalent resistances, the data was normalized using standard deviation and mean:

$$\overline{R_r} = \frac{\sum_{i=1}^{14} R_r^i}{14} \tag{22}$$

$$\sigma_{R_r} = \sqrt{\frac{\sum_{i=1}^{14}(R_r^i - \overline{R_r})^2}{14}} \tag{23}$$

$$X_i = \frac{R_r^i - \overline{R_r}}{\sigma_{R_r}} \tag{24}$$

In which $\overline{R_r}$ and σ_{R_r} are the mean and standard deviation of equivalent resistances, respectively. X_i is the ith feature of the data point.

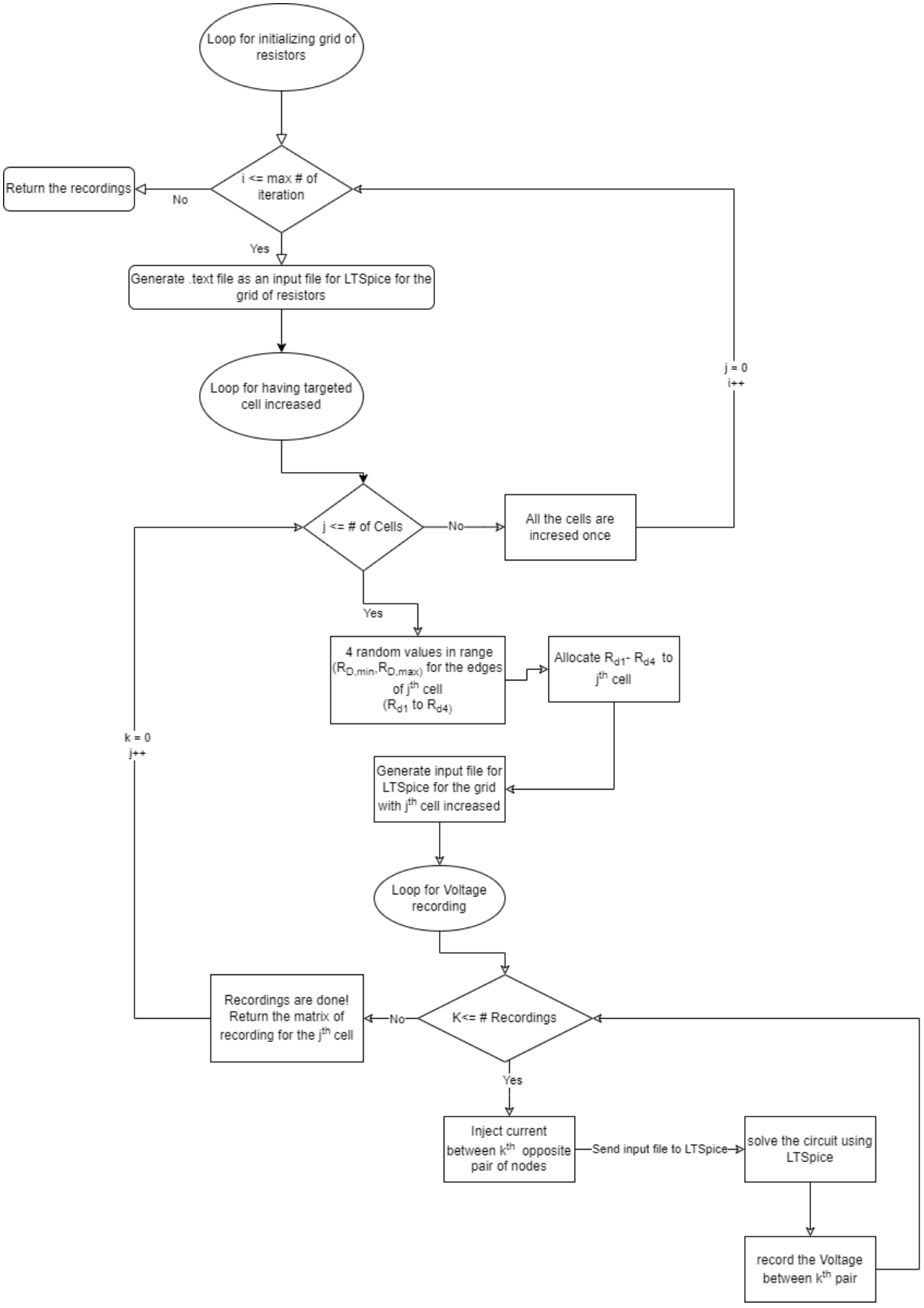

Figure 43: *Flowchart for the python code*

By running the Python script which solves the circuit model with random initialization and random cell as damaged one each time, 3600 unique data points were generated. Each of these data points consists of two main vectors: X and y

$$X^m = \begin{Bmatrix} X_1 \\ X_2 \\ \cdots \\ X_i \\ \cdots \\ X_{14} \end{Bmatrix} \tag{25}$$

$$y \in \{1,2,3,\dots,36\} \tag{26}$$

X^m is the feature vector, m indicates the number of data points, $m \in \{1,2,3,\dots,3600\}$. y is the number associated with the cell which targeted to be increased.

In order to have y be a vector that is compatible with future calculations, vector Y is defined as follows:

$$Y^m = \begin{Bmatrix} 1: if\ (y^m = 1); else: 0 \\ 1: if\ (y^m = 2); else: 0 \\ \cdots \\ 1: if\ (y^m = i); else: 0 \\ \cdots \\ 1: if\ (y^m = 36); else: 0 \end{Bmatrix} \tag{27}$$

$$m \in \{1,2,3,\dots,3600\} \tag{28}$$

So now features and labels for data points are generated as X^m and Y^m, respectively. The data set for initial training in stage 1 of transfer learning is summarized in equations (29) and (30).

$$X^m \in R^{1\times 14} \tag{29}$$

$$Y^m \in R^{1\times 36} \tag{30}$$

CHAPTER 5: ANN Training, Optimizing, Testing, and Results

In this chapter, the focus is on the development of NN models. The NN model development consists of two stages: Stage1. Initial training based on simulation data. Stage 2. Final training on experimental data. To develop NN models, data points in the training set (examples for training the NN) are fed to NN and the parameters of the NN (weight and biases) will be updated based on the difference between the current prediction and the actual value for each data points. The NNs are optimized and evaluated. Also, in this chapter, the study of precision and sample size is done and presented.

5.1 Introduction to ML and Tools that are Used for ANN Model

5.2 Development

To predict the cell with the defect, y^m, we had a feature vector of 14 elements to analyze. To develop a model to predict y^m from X^m, Neural Network (NN) from Machine Learning (ML) as a branch of Artificial Intelligence (AI) is used.

5.2.1 What is ML?

"Machine learning (ML) is the study of computer algorithms that can improve automatically through experience and by the use of data [174]." It is a branch of the more general topic of Artificial Intelligence (AI).

Machine learning algorithms build models using sample data, known as training data, to make predictions or decisions without being explicitly programmed to do so.

Without being explicitly programmed, machine learning programs may complete tasks. It entails computers learning from data in order to do specific jobs. It is possible to write algorithms that tell the machine how to perform all steps required to solve the problem at hand for basic jobs; no learning is required on the computer's behalf. It can be difficult for a human to manually build the algorithms required for increasingly complicated tasks. In practice,

assisting the computer in developing its own algorithm rather than having human programmers explain each required step can prove to be more productive.[175]

5.2.2 Training Deep NN model

To train a deep neural network model, a relatively large data set is needed. To tackle this challenge transfer learning is used to use the simulation model data set to "transfer" the knowledge of ideal modeling to our training process.

All the codes for developing and training NN are prepared in Python language and run using Google colaborator. "Colaboratory, or "Colab" for short, is a product from Google Research. Colab allows anybody to write and execute arbitrary python code through the browser and is especially well suited to machine learning, data analysis, and education. More technically, Colab is a hosted Jupyter notebook service that requires no setup to use, while providing free access to computing resources including GPUs [176]."

A lot of research works have been done using Google Colab. It is especially useful to develop a deep neural network. Examples are in the fields of emotion recognition based on videos[175], detecting skin cancer [177], and so on. Even a paper studies the performance of Google Colab on accelerating deep learning applications. The results reveal that, given the same resources, the performance achieved using this cloud service is similar to the performance achieved using dedicated testbeds[178]. TensorFlow, Google's large-scale machine learning toolkit, simplifies often-complex computations by modeling them as graphs and efficiently mapping parts of the graphs to cluster machines or single-machine processors [179].

To build robust ML models, one of the easy ways is to use TensorFlow. "TensorFlow is an end-to-end open-source platform for machine learning. It has a comprehensive, flexible ecosystem of tools, libraries, and community resources that lets researchers push the state-of-the-art in ML, and developers easily build and deploy ML-powered applications [180]."

To develop the models in the TensorFlow platform, the Keras library is popular. "Keras is an open-source software library that provides a Python interface for artificial neural networks. Keras acts as an interface for the TensorFlow library [181]." Keras includes many implementations of standard neural-network building blocks like layers, objectives, activation functions, optimizers, and a slew of other tools to make working with picture and text data easier while also reducing the amount of coding required to write deep neural network code [181].

5.3 Transfer Learning

Transfer learning is the process of learning a new activity more effectively by applying what has already been learned about a related one. The creation of algorithms that promote transfer learning is a subject of constant attention in the machine-learning field, despite the fact that the majority of machine learning algorithms are created to handle particular tasks [182].

TL is a machine-learning strategy that aims to provide a faster and better answer while requiring less work to gather the required training data and rebuild the model [183]. Recent neurophysiological studies have demonstrated the efficacy of the TL for improving classification performance by using/learning data/information from other individuals [184]–[187], in addition to its great progress in the domains of document, speech, and image classification [188]–[190].

5.3.1 Definition

The definition would be as follows in terms of domains and tasks:

"Given a source domain DS and learning task TS, and a target domain DT and learning task TT, TL aims to help improve the learning of the target predictive function f(•) in DT using the knowledge in DS and TS, where DS ≠ DT, or TS ≠ TT."[191]

5.3.1.1 Notation:

"A domain D consists of two components: a feature space $\mathcal{X}$ and a marginal probability distribution P(X), in which X = {x1, …, xn} ∈ $\mathcal{X}$. Given a specific domain, D = {$\mathcal{X}$, P(X)}, a task consists of two components: a label space $\mathcal{Y}$ and an objective predictive function f(•), denoted by T={$\mathcal{Y}$, f(•)}, which can be learned from the training data pairs {xi, yi}, where xi ∈ $\mathcal{X}$ and yi ∈ $\mathcal{Y}$. The f(•) can be used to predict the label of a new instance x, which can be rewritten by the probabilistic form of conditional probability distribution P(Y|X). A task can then be defined as T= {$\mathcal{Y}$, P(Y|X)}".[191]

From running the LTspice model which simulates a grid of resistors that is used to model the electric behavior of a nanocomposite plate a data set is gathered to perform the initial training of the model.

By running the Python code, which manages the LTspice model to generate unique examples, 3600 data points from the simulation were generated. From these 3600 data points,

2880, 360, and 360 were randomly chosen as training, development, and test set, respectively (equations (31)-(36)). The training set is used to train NN, the development set is used to optimize NN's parameters, and the test set is used to check the final performance of the optimized NN on unseen data examples. The data set for initial training is as follows:

$$X^{train}_{initial\ trainng} \in R^{2880 \times 14} \quad (31)$$

$$Y^{train}_{initial\ trainng} \in R^{2880 \times 36} \quad (32)$$

$$X^{Dev.}_{initial\ trainng} \in R^{360 \times 14} \quad (33)$$

$$Y^{Dev.}_{initial\ trainng} \in R^{360 \times 36} \quad (34)$$

$$X^{test}_{initial\ trainng} \in R^{360 \times 14} \quad (35)$$

$$Y^{test}_{initial\ trainng} \in R^{360 \times 36} \quad (36)$$

Different dimension of NN was trained using the training set and checked the performance on the development set to optimize the best number of neurons for each layer. The dimensions of the input layer and output layers are fixed as there are 14 inputs (features) for each example and 36 classes for output (36 possible values for labels). So, the input layer (first layer) has 14 neurons, and the output layer (the last layer) has 36 neurons. The summary of different NN and the performance on the development set is shown in Table 3. Accuracy is used as the metric for evaluating the performances of the models (equation (37)). It is noteworthy that as the datasets are kept almost balanced, this matric is appropriate for evaluating the performances. A balanced dataset is a dataset with the same number of examples for all the classes (in our case, cells).

$$Performance = \frac{Number\ of\ correct\ predictions\ in\ the\ dataset}{total\ data\ points\ in\ the\ dataset} \quad (37)$$

Table 3: *Optimizing initial NN on the Dev. Set data example of simulation*

NN Structure (Number of neurons in layers)	**Performance of Model on Dev. set**
14-40-36	**89.44%**
14-50-50-36	**95.83%**
14-50-40-36	**96.94 %**
14-45-40-36	**98.89 %**

Dimensions of NNs are presented as a series of numbers under the "NN structure in Table 3. The Series of numbers are the number of neurons for each layer. For example, 14-45-40-36 represents a NN that has 14 neurons in the first layer, 45 neurons in the second layer, 40 neurons in the third layer, and 36 neurons in the fourth layer.

The model with the highest performance is selected as optimized initial NN (14-45-40-36). The optimized initial model dimension is shown in Figure 44. By running the training using Keras in the Colab platform and optimizing the parameters, the performance of the trained model on 360 test set data points from the simulation is 98.61% (Table 4). This high performance of NN on the simulation data comes from the fact that the data points are gathered using a simplified and ideal simulation of the grid of resistors. In other words, there are not any unknown phenomena considered in simulation data so the NN can perfectly find the pattern in data to get high accuracy as a means for measuring the performance of the NN modeling the simulation data. This highly accurate model is then used as the base for the training in the next stage which is to model the actual electrical behavior of the plates using experimental data.

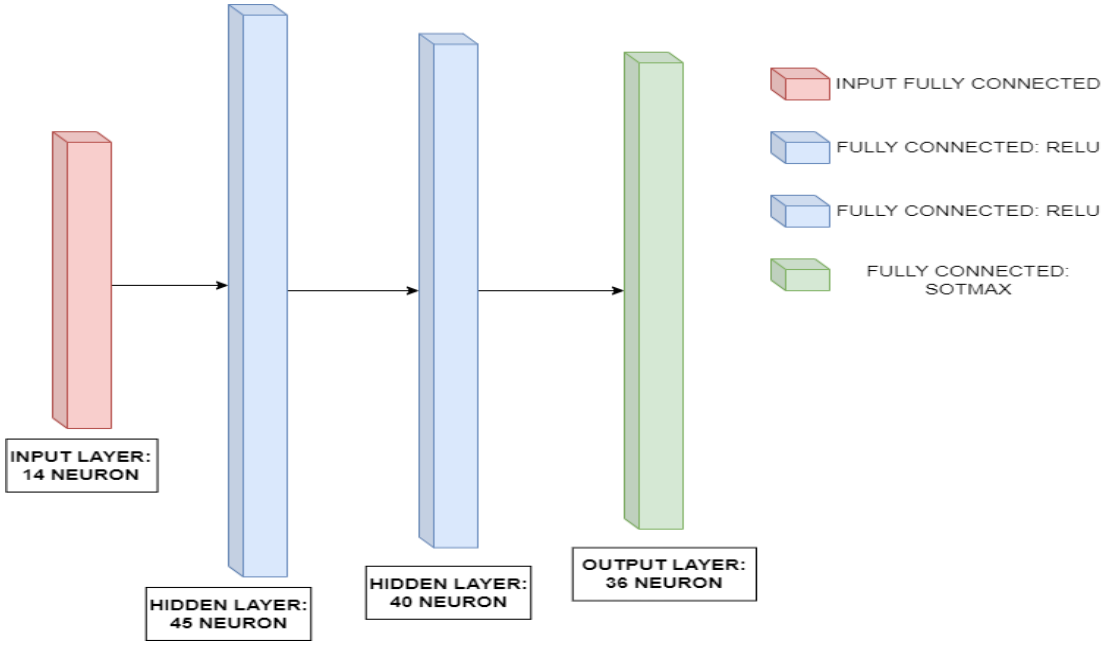

Figure 44: *Initial NN that is trained on simulation data*

As illustrated in Figure 44, the activation functions for the hidden layers (middle layers) are ReLU (Rectified Linear Unit). This is a common activation function for NNs that is proven to be an appropriate choice to speed up the convergence of the NN during training [192]. For the last layer (output layer) the activation function is Softmax. Softmax is a well-known activation function for the last layer of the NN that is capable of providing the prediction of the NN as probabilities of possible outcomes[193].

Table 4: *Performance of initial NN model on the simulation model*

No. Test set	No. Correct predictions	No. Wrong predictions	Performance
360	355	5	**98.61%**

After training the initial Neural Network, experimental data is used to perform the final training on the Neural Network. To do so, the top layer (36-softmax layer) in the initial NN is removed (Figure 45). The first two layers were frozen which means the values for their neuron were considered fixed (will not be updated during the second round of training). The experimental data is also grouped into training, development, and test sets as shown in equations (38)-(43). The training set, development set, and test set of experimental data contain 282, 40, and 70 data points, respectively.

$$X_{Final\ trainng}^{train} \in R^{282 \times 14} \quad (38)$$

$$Y_{Final\ trainng}^{train} \in R^{282 \times 36} \quad (39)$$

$$X_{Final\ trainng}^{Dev.} \in R^{40 \times 14} \quad (40)$$

$$Y_{Final\ trainng}^{Dev.} \in R^{40 \times 36} \quad (41)$$

$$X_{Final\ trainng}^{test} \in R^{70 \times 14} \quad (42)$$

$$Y_{Final\ trainng}^{test} \in R^{70 \times 36} \quad (43)$$

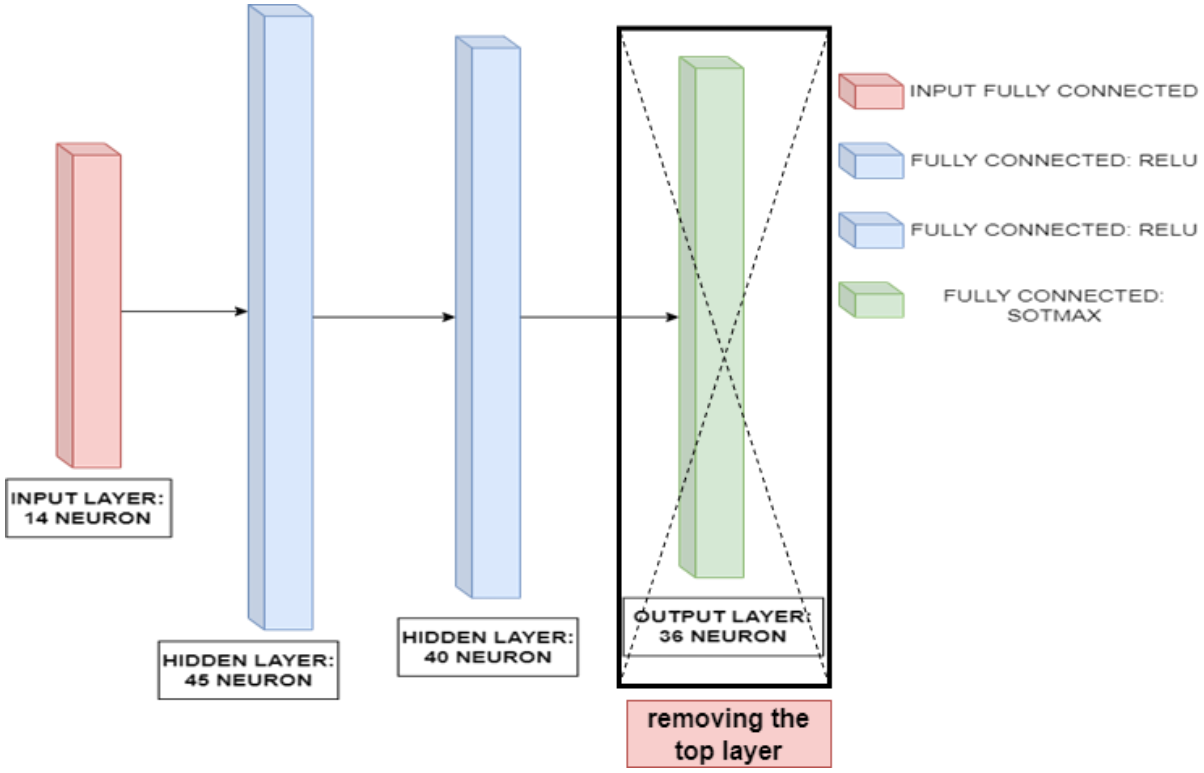

Figure 45: *Removing the top layer of the initial NN structure.*

Then three new, randomly initiated, layers were added to the top of the previous network. To optimize the final NN, different structures (number of neurons in different layers) were tested on the development set. The summary of the accuracies of different NN structures is presented in Table 5. Based on these results, the structure with the number of neurons in different layers as 14-45-40-36-36-36 is picked as the highest performance on the development

set. This NN model is shown in Figure 46. The performance of the final NN model on the test set is 78.57% as summarized in Table 6.

Table 5: *the performance of final NN on the experimental development set of data*

NN Structure (Number of neurons in layers)	**Performance of Model on Dev. set**
14-45-40-45-40-36	**72.50%**
14-45-40-50-45-36	**75.00 %**
14-45-40-30-25-36	**67.50%**
14-45-40-36-36-36	**82.5%**

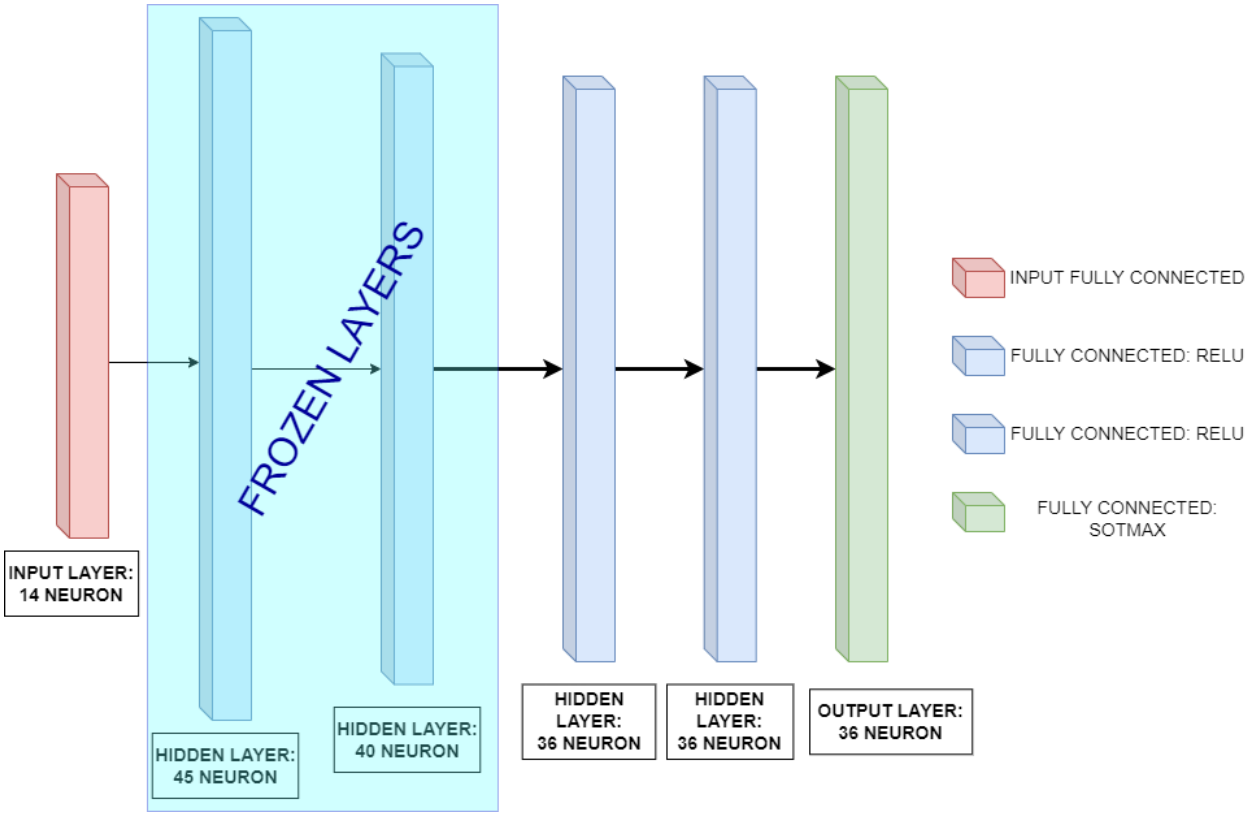

Figure 46: *Adding 3 new layers on the top and training the parameter based on experimental data*

Table 6: *Performance of final NN model on the test set from the experimental data*

No. Test set	No. Correct predictions	No. Wrong predictions	Performance
70	55	15	**78.57%**

5.4 Precision Study

The presented model is able to locate the defect on a composite plate in one of 36 cells which each has the size of 2” by 2”. To study the performance of the NN model for detecting defects in different cell sizes, new NNs were trained on data points with different cell sizes. The cell size in which a defect is located is defined as the precision. If the defect is detected using the NN in a 2” by 2” cell, the precision of the model is 2” by 2”. To study the precision of the NN models in defect detection, the original data (the data with 36 possible cells) is manipulated to have fewer possible cells by grouping different numbers of cells into one new cell. This procedure is used to go from 36 possible cells to 9, 4, and 2 possible classes.

The process of doing so is shown in the following figures. In Figure 47 the original cell class distribution is shown. By grouping each 4 of the original cell classes into one new cell, the plate with 9 possible cell classes is achieved. So, by doing this on data with the precision of 2” by 2”, data with a precision of 4” by 4” is achieved. In other words, as an example, all Y data points representing the cells associated with numbers 1, 2, 7, and 8 would be changed to cell number 1 of the new distribution. This process is shown in Figure 48. It is noteworthy that the features (X vector for the examples) are not changed and only the labels (values for Y) are changed.

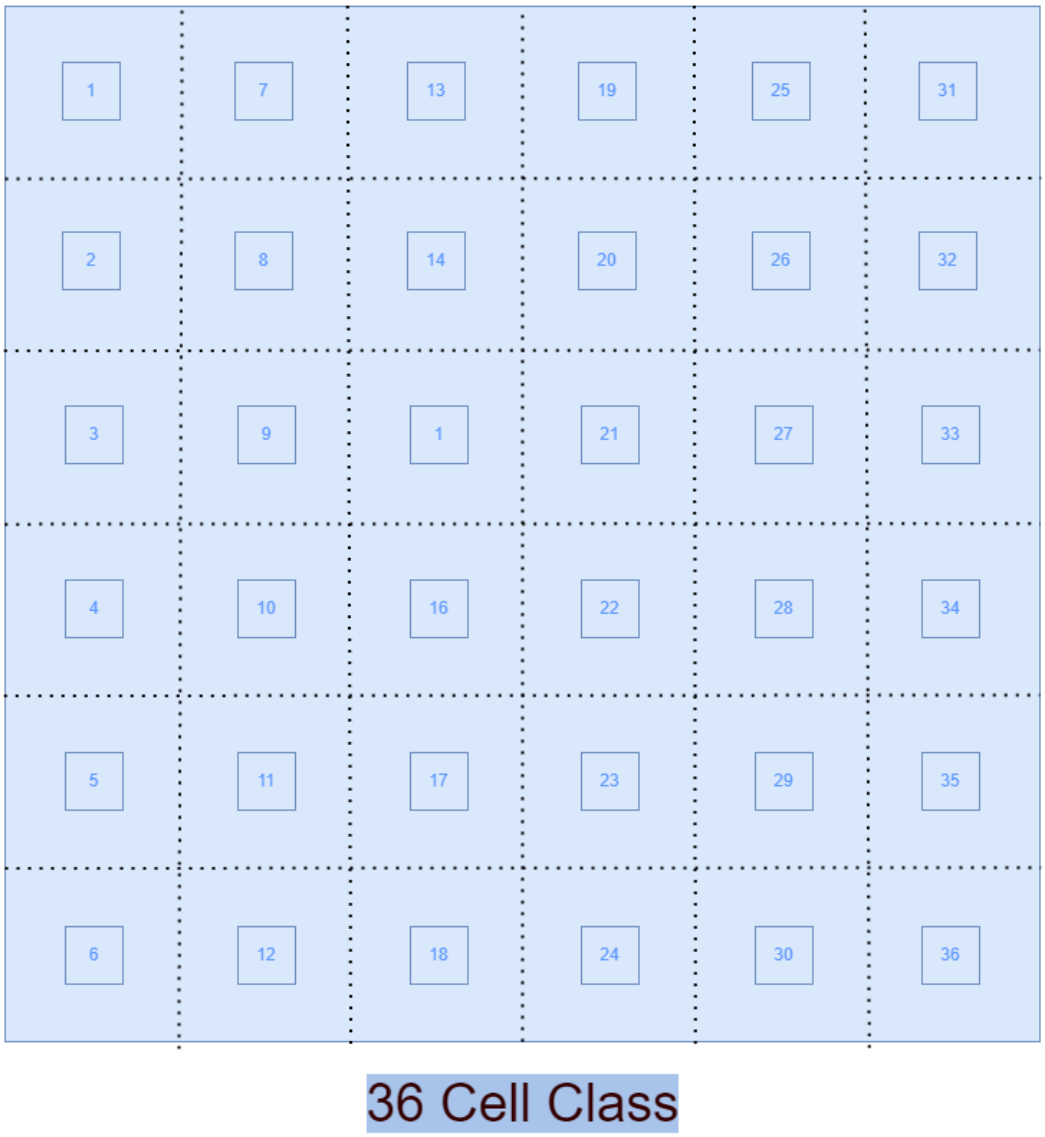

Figure 47: *The original cell classes distribution. A sample with 36 possible cell classes*

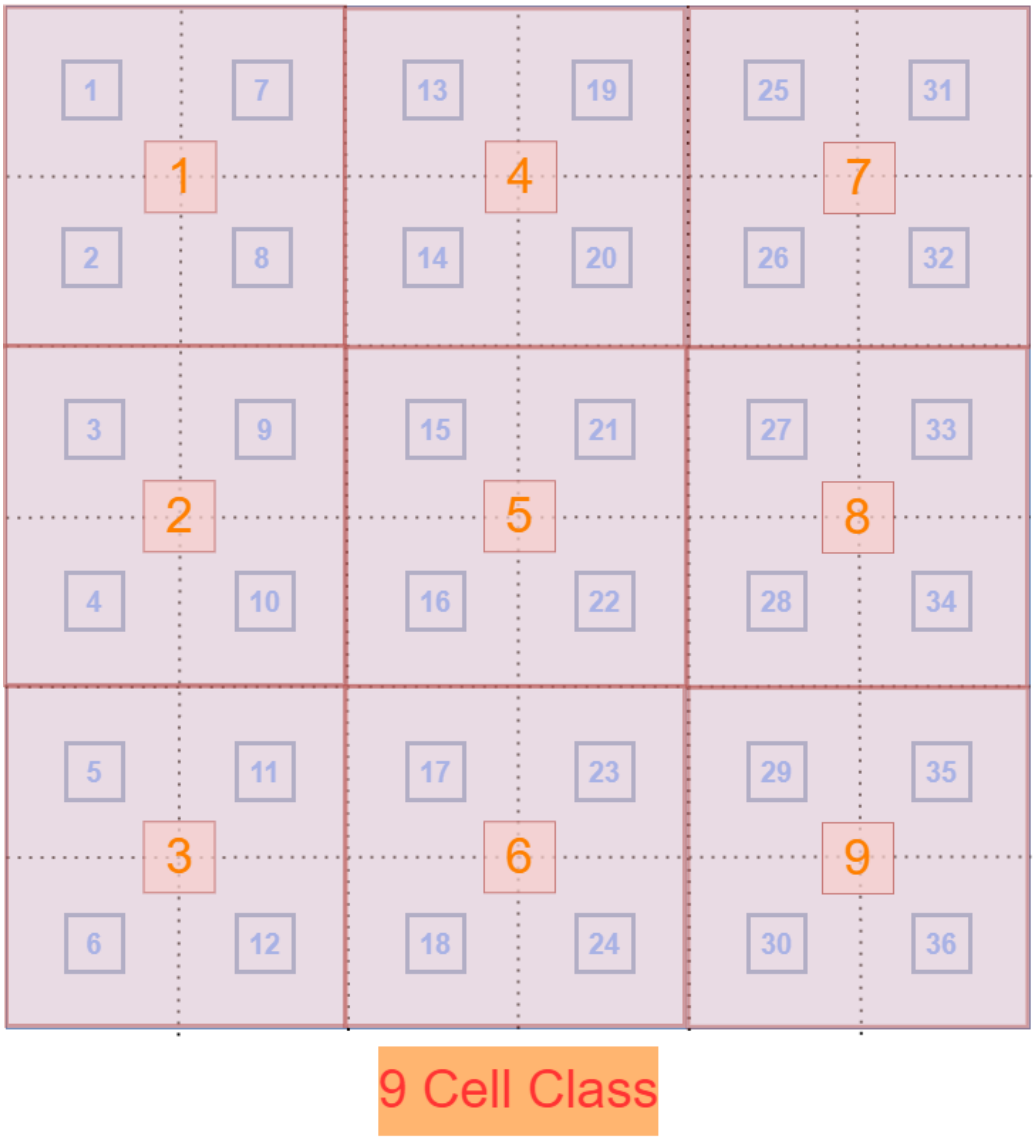

Figure 48: *The distribution of plate with 9 cell classes by grouping 4 cells of 36 cell class distribution into one new cell*

This process of manipulating the original data to generate data with different precision is repeated for other precision of 6" by 6" (4 possible cell classes), and 12" by 6" (2 possible cell classes). The process is shown in Figure 49 and Figure 50. Also, by doing these changes in the labels of the existing data points and keeping the features unchanged, the data for different precisions is achieved without the need to do new simulations and experiments. In the final step, these new data points are used to develop new NN models to locate the defects with different precisions. The steps for having the models trained and tested are the same as the original NN with the precision of 2" by 2" (36 possible cell classes). The performance of these NN trained and tested on data with different precision is presented in Table 7.

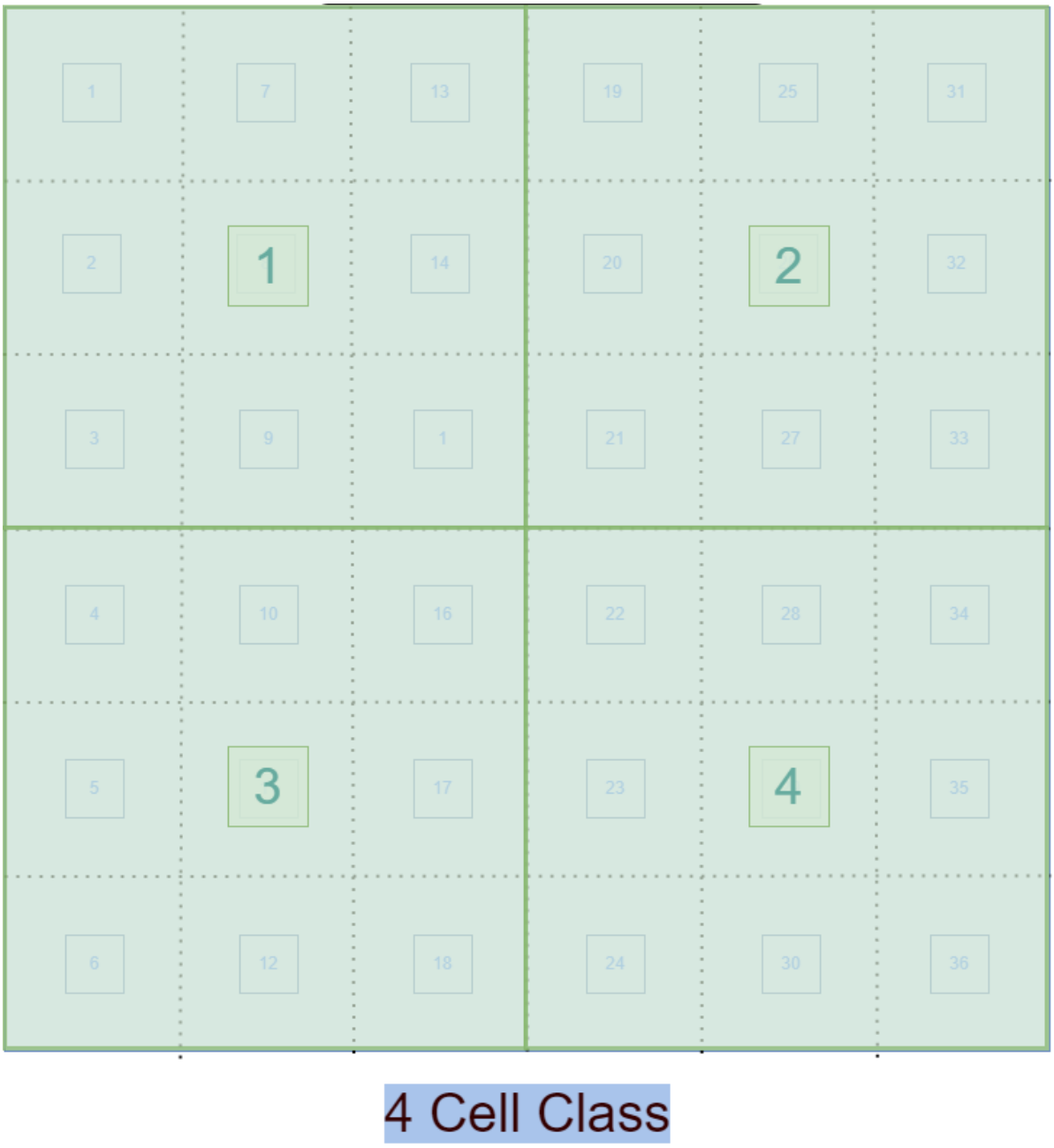

Figure 49: *The 4 possible cell classes from 36 possible cell class distributions.*

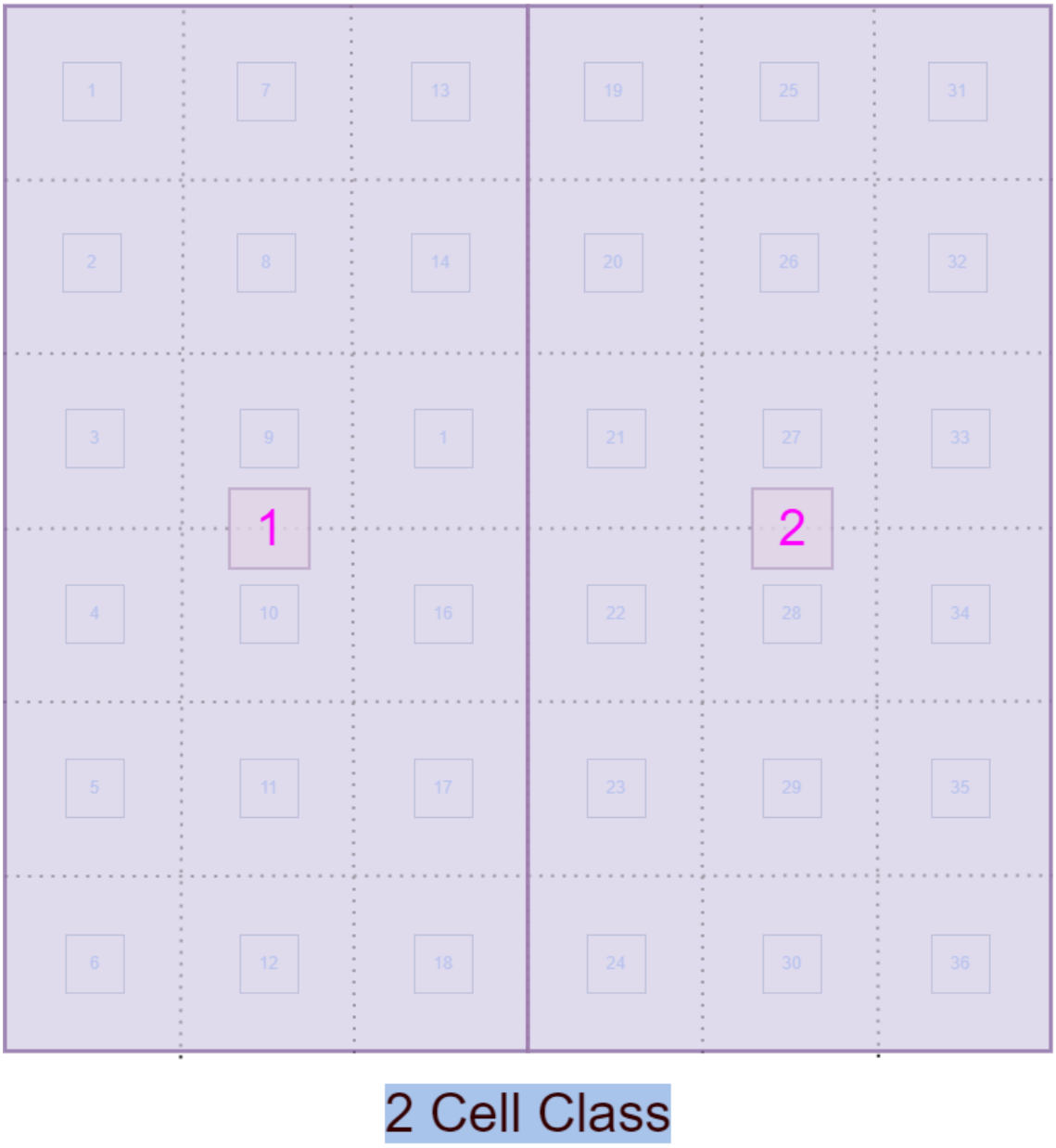

Figure 50: *The 2 possible cell classes from 36 possible cell class distributions.*

Table 7: *The performance of the developed NN model on different precision data distribution*

Precision (Inch by Inch)	precision area (inch^2)	Random classifier accuracy (%)	Accuracy (%)	Gained Accuracy (%)
2"x2"	4	2.78	78.57	75.79
4"x4"	16	11.11	84.29	73.18
6"x6"	36	25	80.00	55
6"x12"	72	50	90.00	40

The performance of the trained NN models is measured based on two parameters: accuracy and gained accuracy. “Random classifier accuracy” in Table 7 explains the performance of a model which randomly predicts the location of the defect in our example. As an example, if the possible answer for each given output is within 36 classes, the accuracy of a random classifier is 1/36=2.78%. Comparing random classifier accuracy to absolute accuracy defines how well our model is performing. The difference between the absolute accuracy and random classifier accuracy is called gained accuracy (equation (44)). Gained accuracy defines how much the trained model is boosting the performance in comparison to a random classifier. The trends of accuracy and gained accuracy for different precision are presented in Figure 51 and Figure 52, respectively.

$$Accuracy_{Gained} = Accuracy_{model} - Accuracy_{random\ classifier} \tag{44}$$

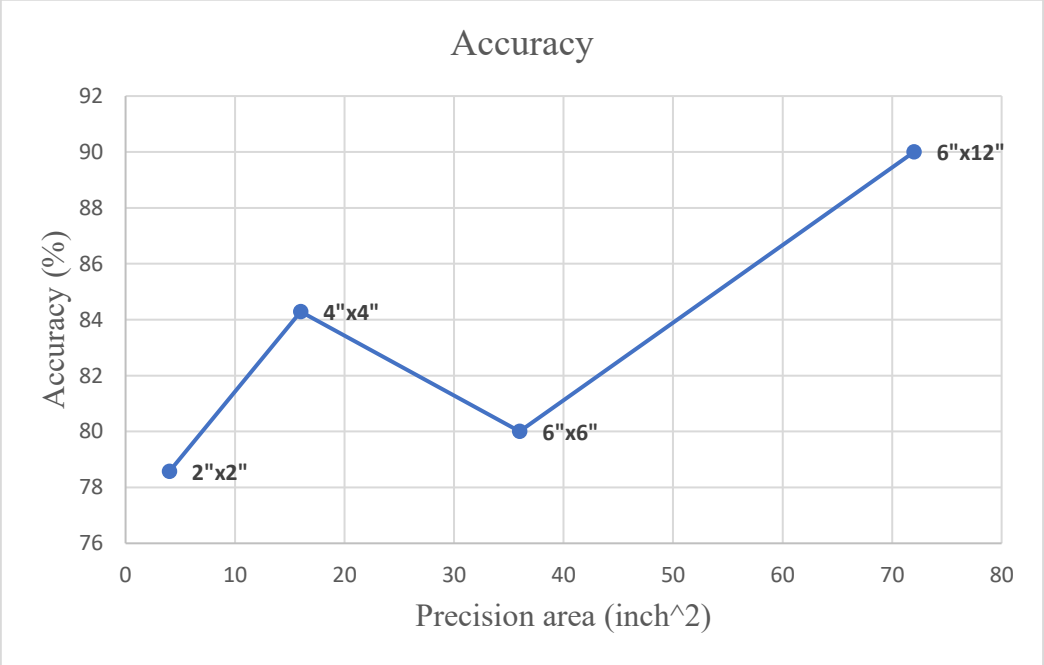

Figure 51: *Change of accuracy with respect to changes in the precision area*

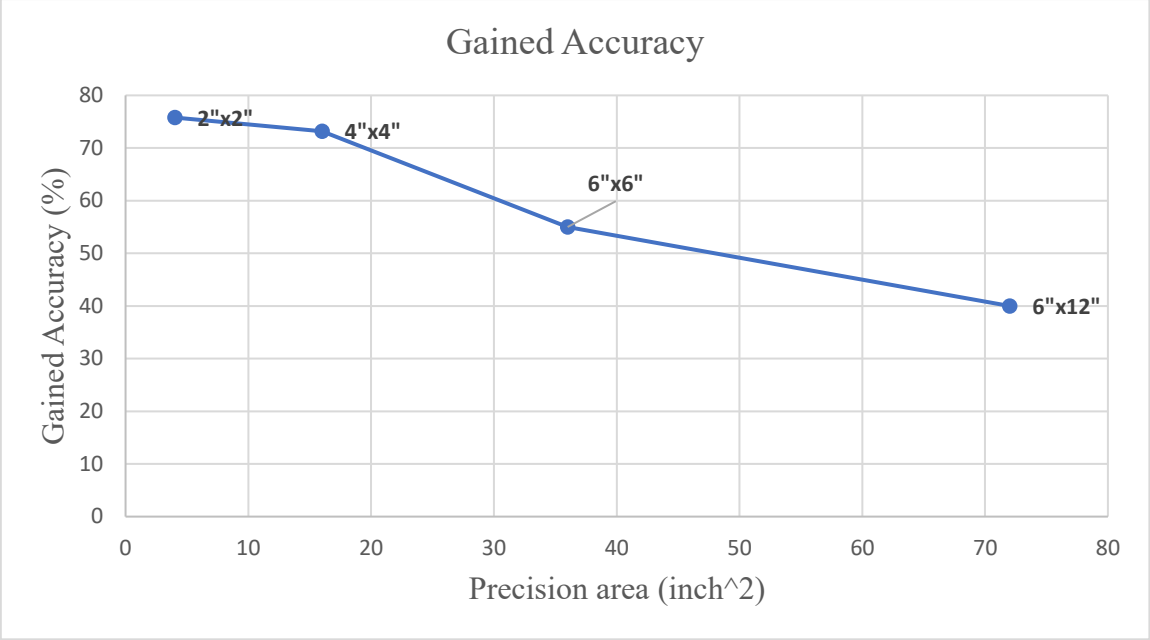

Figure 52: *Change of gained accuracy with respect to changes in the precision area*

5.5 Study of Sample Size

After training different NNs for different precisions, in this section, the study focuses on the study of the performance of these NNs for different sample sizes. As it is discussed in chapter 3, the nanocomposite plates were manufactured in the size of 12” by 12”. But in the data preparation step, before the training process, the data is normalized based on the average and standard deviation of the measurements. So, from the NN model’s perspective, there is not any input representing the sample size. To study the effect of the size of the sample on the performance of the NN models for different sample sizes, new samples were manufactured in sizes of 9” by 9” and 15” by 15”. So, with the original 12” by 12” samples, three sizes of samples were manufactured for studying the effect of the size of the sample. Figure 53 shows these three different sizes of samples in a picture.

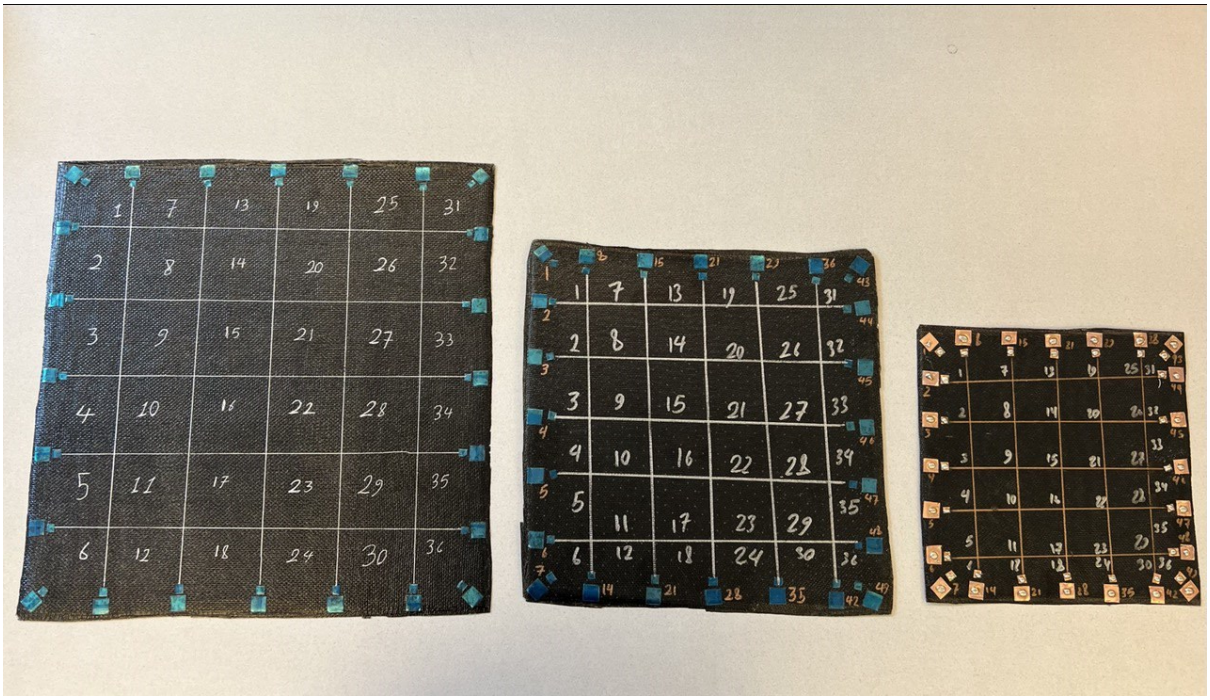

Figure 53:*Samples are manufactured in different sizes: 15"by15" on the left, 12" by 12" in the middle and 9" by 9" on the right side of the picture.*

The samples of new sizes (15" by 15" and 9" by 9") are tested to generate data. The new data is recorded and prepared using the same method mentioned for measurements and data preparation of samples with the size of 12" by 12". The data is then fed to the trained NN for different precisions and the performances are recorded. The summary of the results for samples with sizes of 9" by 9" and 15" by 15" is presented in Table 8 and Table 9, respectively. It is noteworthy that the result for samples with the size of 12" by12" is already presented in the previous section.

Table 8:*The result of the performance of NNs on the data from testing samples with the size of 9" by 9"*

Precision (Inch by Inch)	**precision area (inch^2)**	**Random classifier accuracy (%)**	**Accuracy (%)**	**Gained Accuracy**
1.5" x 1.5"	2.25	2.78	82.61	79.83
3" x 3"	9	11.11	85.87	74.76
4.5" x 4.5"	20.25	25.00	84.78	59.78
4.5" x 9"	40.5	50.00	93.48	43.48

Table 9: *The result of the performance of NNs on the data from testing samples with the size of 15" by 15"*

Precision (Inch by Inch)	precision area (inch^2)	Random classifier accuracy (%)	Accuracy (%)	Gained Accuracy
2.5" x 2.5"	6.25	2.78	72.83	70.05
5" x 5"	25	11.11	80.43	69.32
7.5" x 7.5"	56.25	25.00	81.52	56.52
7.5" x 15"	112.5	50.00	93.48	43.48

To develop a bigger picture representative of the performance of the developed NNs on different sample sizes and precisions, the performances of NNs are presented in two separate figures (Figure 54 and Figure 55). These figures study the changes in the performance of the NNs with changes in precision and sample sizes. The test data set size for samples in sizes of 15" by 15" and 9" by 9" are 92 data points for each sample size. Figure 54 summarizes the performance based on absolute accuracy while Figure 55 compares the gained accuracy.

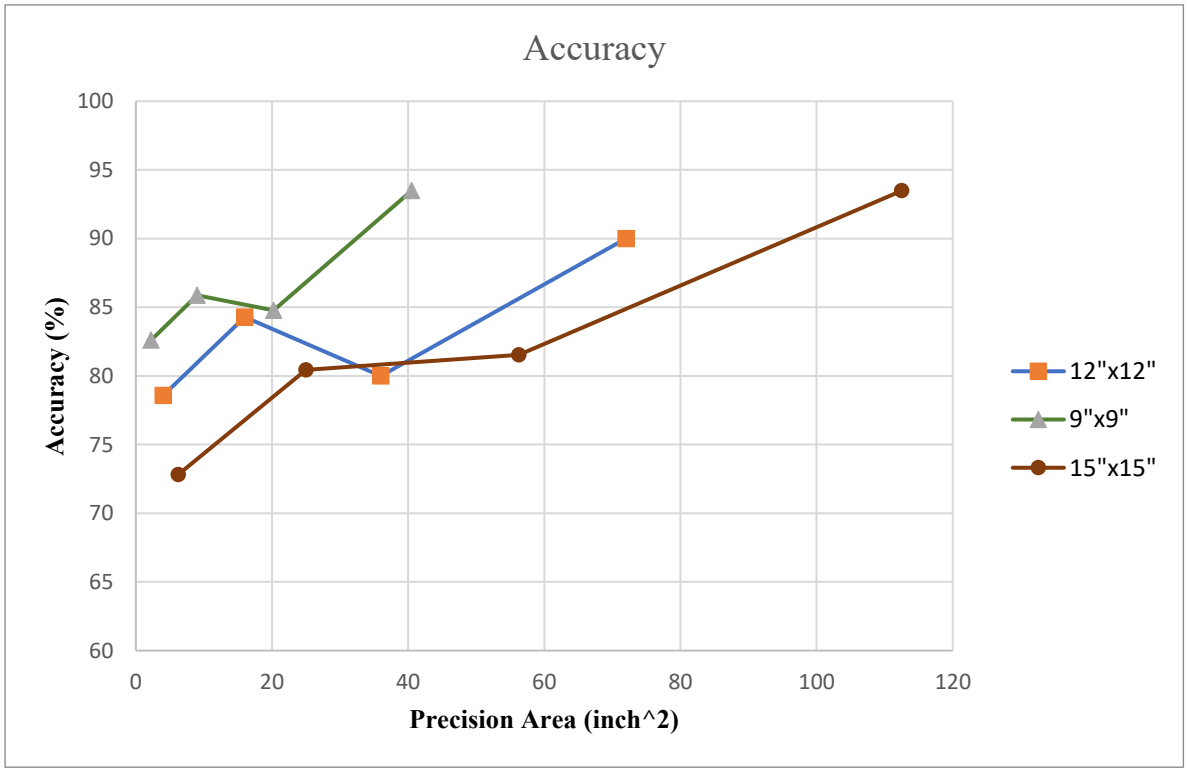

Figure 54: *Changes in the accuracy of the developed NN with respect to precision and sample size.*

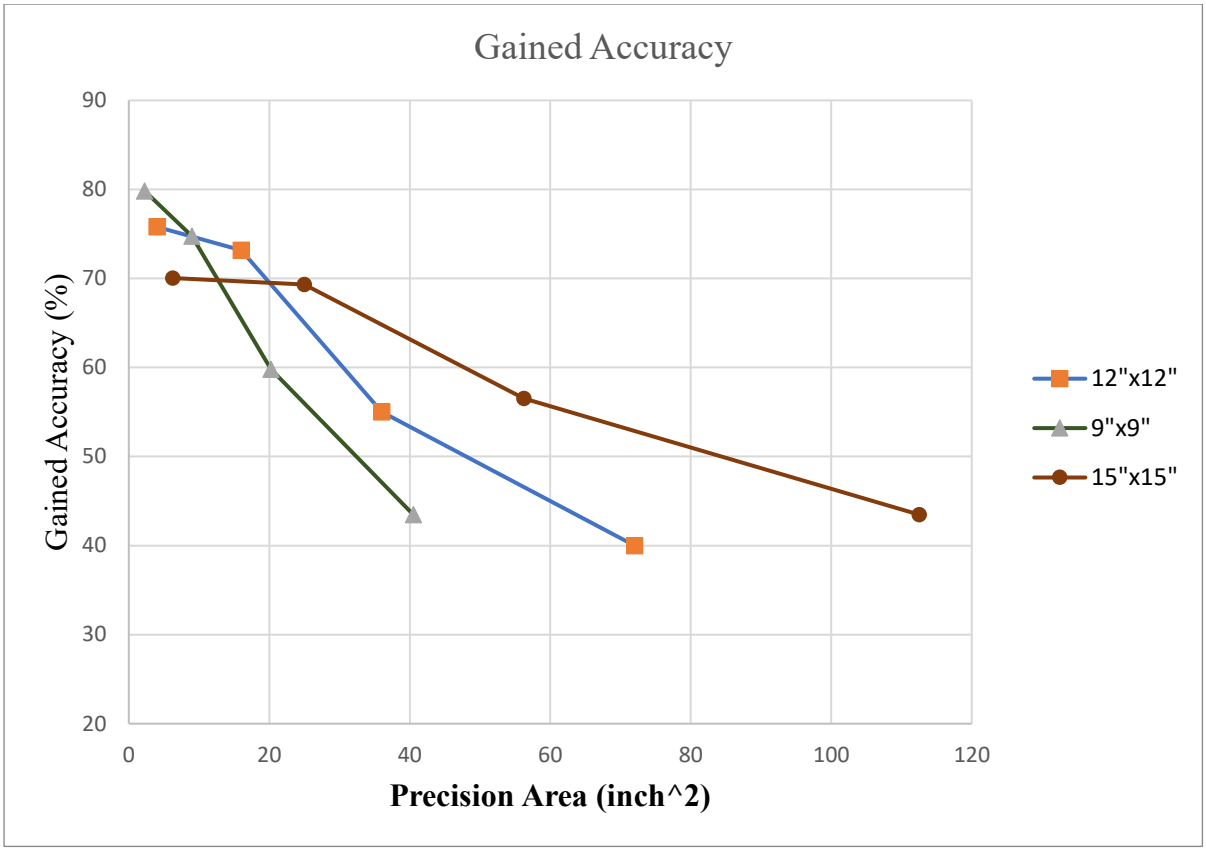

Figure 55: *Changes in gained accuracy of the developed NN with respect to precision and sample size.*

CHAPTER 6: Results, Conclusion, and Future Works

6.1 Results and Discussion

As described in the previous chapters, ANN models were developed to detect the location of a defect in nanocomposite plates. Also, the performance of the trained NNs studied in different precision and on different sample sizes. NN models were trained on two separate stages. In the first stage, NNs were trained, optimized, and tested based on data points from electrical stimulation. These data points were generated using LTSpice software which is controlled using a Python script. The first step is used to transfer the knowledge from a electrical model of the grid of resistors to the actual problem. Before the final training, the top layer of the initial NN is removed and the rest of it is kept fixed (layers were frozen). Then in the second stage, new layers were added to the basic NN (initial NN), and training, optimization, and testing is performed using augmented data from the experiments. Data is prepared for different precisions. The labels of the original data is changed to match the number of cell classes in each precision. These steps are repeated on the data prepared for different precisions. The NN models that are trained for different precisions are tested using the experimental data from samples of different sizes. The performance of the NN models with respect to the sample size and precision is presented in Figure 56 and Figure 57. Absolute and gained accuracy is depicted in Figure 56 and Figure 57, respectively.

As it is shown in Figure 56, the absolute accuracy of the NN models is generally increasing as the precision area increases. This phenomenon is because of the fact that as the precision area increases the number of possible cell classes for the defect to be detected in is decreased. So the possible classes are decreased and, understandably, the performance increases as the problem is less complicated. In other words, as it is harder to find the location of the defects among 36 possible cells than 9 possible cells, it will be harder for the NNs to find the patterns with the same amount of data. This fact is also understandable as the performance of a random classifier increases as the possible classes decreases.

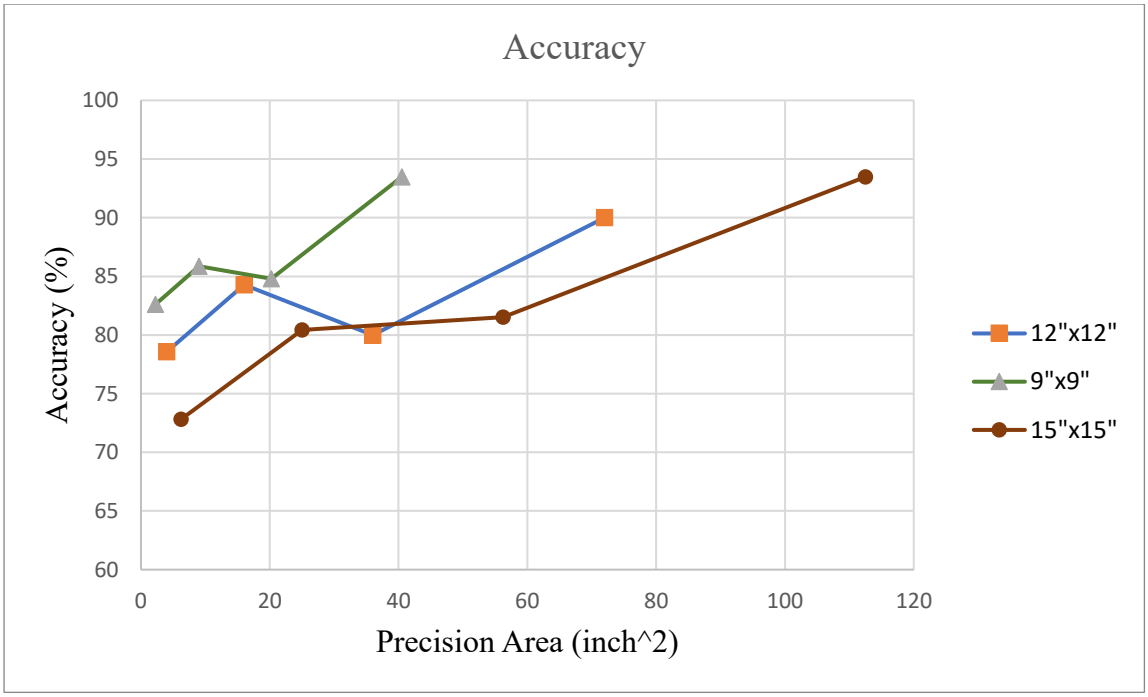

Figure 56: *Changes in the accuracy of the developed NN with respect to precision and sample size.*

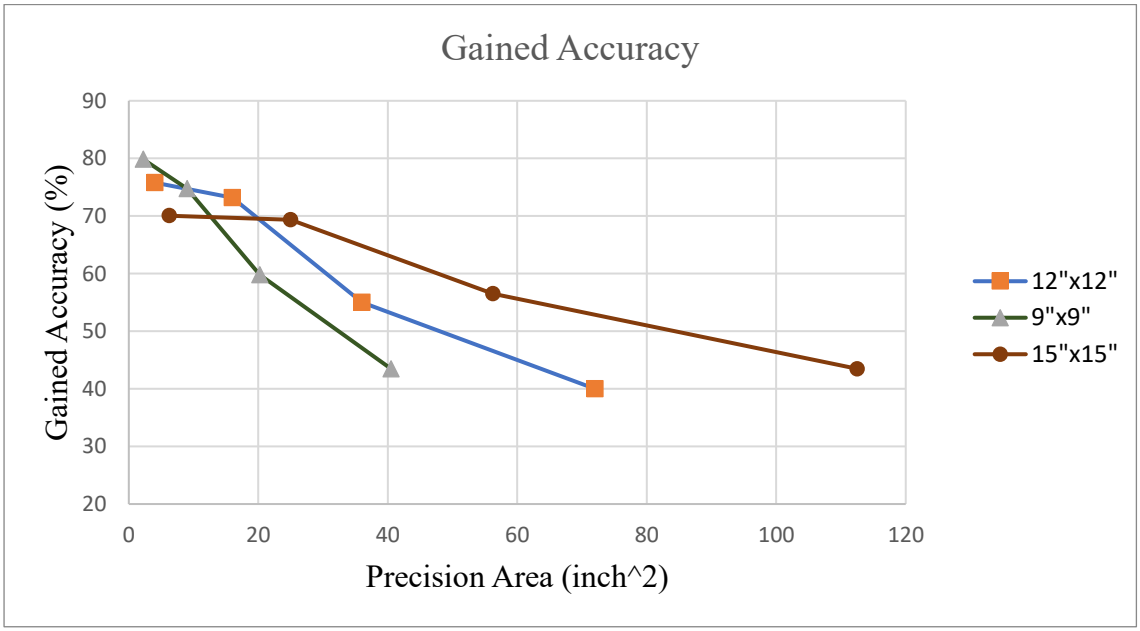

Figure 57: *Changes in gained accuracy of the developed NN with respect to precision and sample size.*

The average performance of a random classifier can be calculated using the following formula.

$$\bar{P}_{random\ classifier} = \frac{1}{N} * 100 \tag{45}$$

N is the number of possible classes that the output can be among them. For example, the average accuracy of a random classifier in a classifying problem that has two possible outcomes (like tail and head in throwing a coin) is 50%. In Figure 58 the graph shows this equation for various possible class numbers.

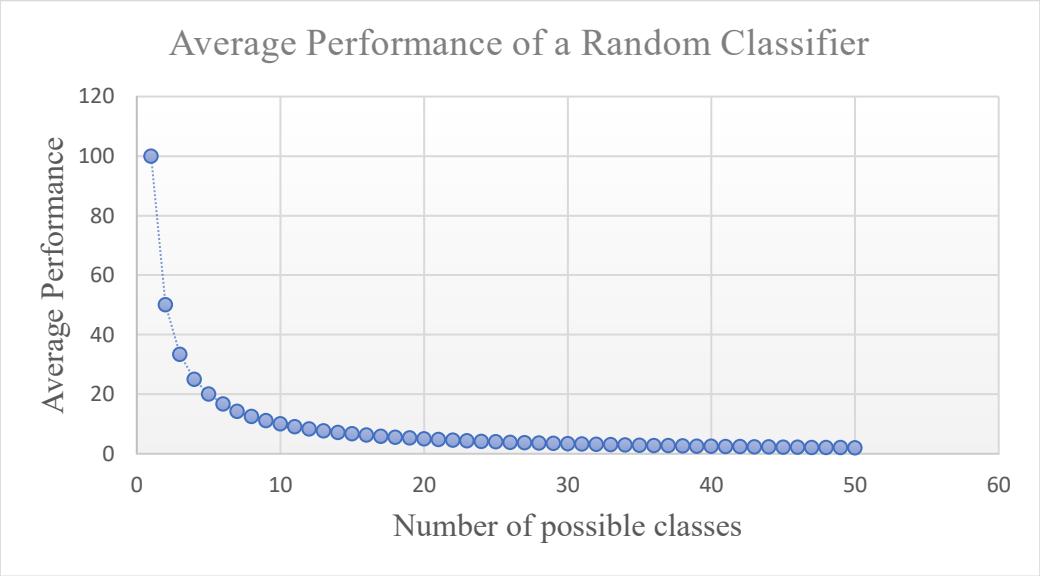

Figure 58: *The average performance of a random classifier with respect to the number of possible classes*

Figure 58 also explains the reason that the gained performance of the NNs decreases as the number of possible cell classes decreases or the precision increases in each sample size. As the precision area increases (while the sample size is constant) the number of possible cells for the defect to be located among them decreases. So, the random classifier performance is increased and as the gained performance is the absolute performance minus the average random classifier performance, the gained performance is decreased.

It is also observable that the performances (accuracies) of the NN models are higher in smaller sample sizes. This is due to the fact that the signals representing defects in the samples are stronger when the samples are smaller as the measurement probes, which are located on the edges, are closer to each other compared to the larger samples. Also, in larger samples the number of conductive paths is higher than in smaller samples, so the sensitivity is higher in smaller samples.

The only discontinuity in the results is the decrease in accuracy when changing the possible cell classes (precision) from 9 to 4 for sample sizes of 12” by 12” and 9” by 9”. This is due to the way discretization is done. As the discretization is done as shown in Figure 48 and Figure 49 for 9 possible and 4 possible cell classes, respectively, all 4 original cells in the middle (15, 16, 21, 22) are grouped together in one new cell for the case of 9 possible cell classes while in 4 possible cell classes, these are grouped into four different new cell classes. Also, as these cells are the most critical locations for the models to detect (as they are far from the probes), the way they are grouped in one cell or in four different ones is important. In 9 possible cell class precision, as these critical cells are grouped in one cell, the performance is high as the difference between them is not important. But in 4 possible cell class precision, these critical cells are grouped in 4 different cells, so it is harder for models to distinguish the location of the defect while happening in the middle of the samples. The difference in the way the discretization can cause this discontinuity in the graph of accuracy is shown in Figure 59 and Figure 60.

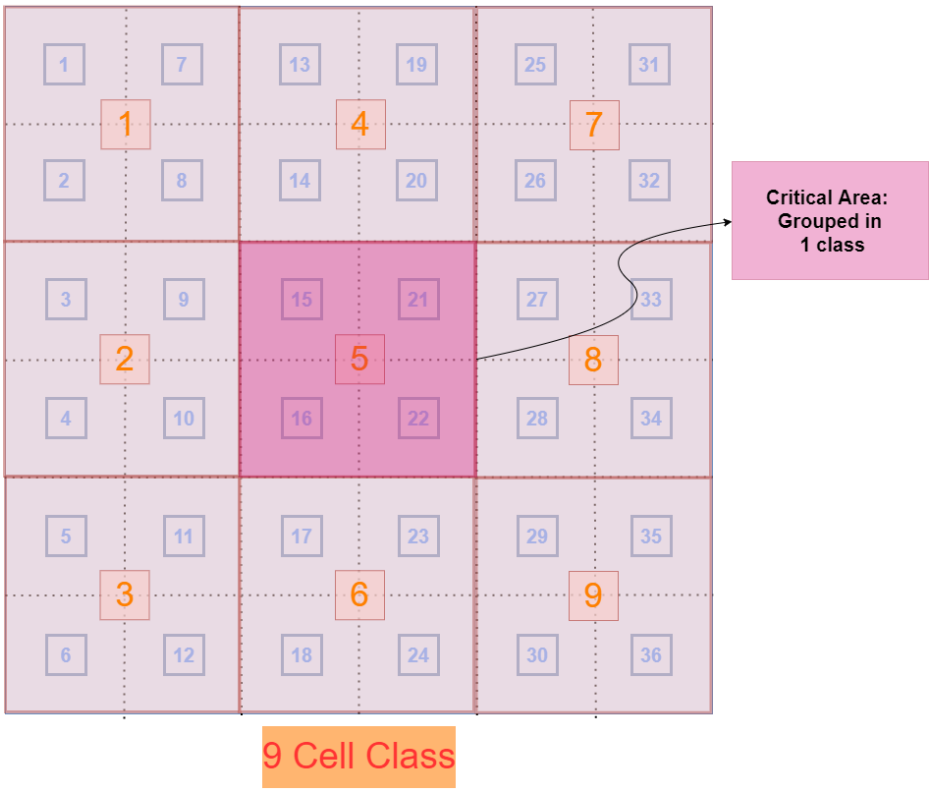

Figure 59: *The way all 4 cells in the middle (in 36 cell precision) are grouped into one cell in 9 cell class precision*

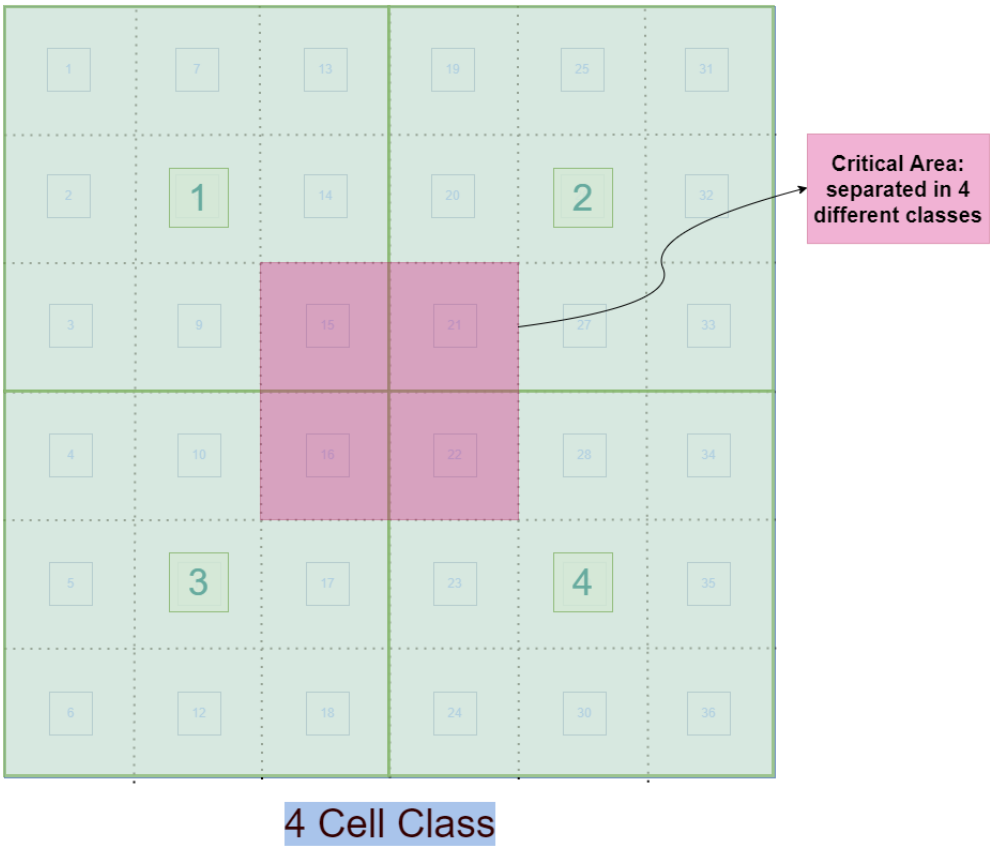

Figure 60: *The way every 4 cells in the middle (in 36 cell precision) are grouped into different cells in 4 cell class precision*

6.2 Conclusion

This study aims to increase the practicality of using electrical properties to perform health monitoring on a composite plate. The problem with the previous method in this area was that lots of probes and wires are needed. The reason is that the grid size that was used was small (3 inches) and on each corner of the cells there where a probe [158].In this study, a method is developed using ML and Transfer Learning that is capable of detecting defects on composite plates with reasonable productivity in a range of precision (as mentioned in chapter 5) while the number of probes is restricted. In this method, probes are needed only to be on the edges of a composite plate. A good performance of detecting defects on 9” by 9”, 12” by 12”, and 15” by 15” plates with different precisions is achieved by having only 24 probes on the edges of the samples. The highest precision for sample sizes of 9” by 9”, 12” by 12” and 15” by 15” are 1.5”, 2”, and 2.5”, respectively. The precision for previous work is 3”. Also, the method from previous work uses 49 probes and wires for this less precision. This reduction in the

number of probes and wires, while increasing the precision, makes this method more practical and easier for aerospace applications in different sections based on the accuracy and precision that are required.

6.3 Contributions

Beside reducing the number of required probes for defect detection of a composite plate, by performing a detailed study of the effects of the size of the samples and precision on the performance of the NN models for defect detection, an intuition is provided in the case of choosing the proper model for different applications. Also, it is proven that using the Transfer Learning method for developing NN models in the field of composite is a huge benefit as it eliminates the need for having a lot of data points that are very expensive to generate in the field of composite. The use of Augmenting Data in defect detection is another contribution of this work. By using the symmetries in the geometry of the problem more data points are generated without performing extra experiments. This increases the applicability of NN models in the field of composite.

6.4 Future Works

Recently, there is a huge and ongoing advancement in the field of Artificial Intelligence and Deep Learning. There are some complex problems in the field of composite materials that by using conventional methods, sufficient performance is not yet achieved. As this study proved the capacity of using NNs in tackling problems in composites, using AI approaches in the following fields is recommended:

- For imposing defects in composite plates, the method of drilling holes is used. In future works, more diverse methods can be used.
- For modeling and testing samples, direct current is used. The reason is that the electrical response is tried to be as simple as possible to limit the parameters needed to address in modeling. But as this study provide a solid application of NNs in detecting defects, using alternating current (AC) is recommended for future works as more details in the electrical behavior of composites can be modeled.

- Using other Deep learning algorithms (like Recurrent Neural Network) in studying the fatigue life of composites can be recommended as detection of the defects using electrical behavior and NN models are proven to be possible.

References

[1] Z. CH., "Composite Materials," in *Mechanical engineers' handbook, volume 1: Materials and engineering mechanics*, 4th ed., M. Kutz, Ed. Hoboken, NJ: John Wiley & Sons, 2015, pp. 401–438.

[2] A. G. Koniuszewska and J. W. Kaczmar, "Application of polymer based composite materials in transportation," *Prog. Rubber Plast. Recycl. Technol.*, vol. 32, no. 1, pp. 1–24, 2016.

[3] Jollivet T, P. C, and L. F., "Damage of Composite Material," in *5th Fatigue design conference*, M. Afzali and Lefebcvre F, Eds. Senlis, 2013, pp. 746–758.

[4] M. Senthilkumar, T. G. Sreekanth, and S. Manikanta Reddy, "Nondestructive health monitoring techniques for composite materials: A review," *Polym. Polym. Compos.*, vol. 29, no. 5, pp. 528–540, 2021.

[5] T. Peng, Y. Liu, A. Saxena, and K. Goebel, "In-situ fatigue life prognosis for composite laminates based on stiffness degradation," *Compos. Struct.*, vol. 132, pp. 155–165, 2015.

[6] T. P. Masango, O. Philander, and V. Msomi, "The continuous monitoring of the health of composite structure," *J. Eng.*, vol. 2018, 2018.

[7] J. Sun, D. Chen, C. Li, and H. Yan, "Integration of scheduled structural health monitoring with airline maintenance program based on risk analysis," *Proc. Inst. Mech. Eng. Part O J. Risk Reliab.*, vol. 232, no. 1, pp. 92–104, 2018.

[8] Y. J. Yan, L. Cheng, Z. Y. Wu, and L. H. Yam, "Development in vibration-based structural damage detection technique," *Mech. Syst. Signal Process.*, vol. 21, no. 5, pp. 2198–2211, 2007.

[9] S. W. Doebling, C. R. Farrar, M. B. Prime, and D. W. Shevitz, "Damage identification and health monitoring of structural and mechanical systems from changes in their vibration characteristics: a literature review," 1996.

[10] W. J. Staszewski, S. Mahzan, and R. Traynor, "Health monitoring of aerospace composite structures–Active and passive approach," *Compos. Sci. Technol.*, vol. 69, no. 11–12, pp. 1678–1685, 2009.

[11] S. Gopalakrishnan, M. Ruzzene, and S. Hanagud, *Computational techniques for structural health monitoring*. Springer, 2011.

[12] F. Frigui, J.-P. Faye, C. Martin, O. Dalverny, F. Pérès, and S. Judenherc, "Global methodology for damage detection and localization in civil engineering structures," *Eng. Struct.*, vol. 171, pp. 686–695, 2018.

[13] T.-W. Chou, *Microstructural Design of Fiber Composites*. Cambridge: Cambridge University Press, 1992. doi: DOI: 10.1017/CBO9780511600272.

[14] V. Giurgiutiu, *Structural health monitoring of aerospace composites*. Cambridge: Academic Press, 2016.

[15] S. Takeda, Y. Aoki, T. Ishikawa, N. Takeda, and H. Kikukawa, “Structural health monitoring of composite wing structure during durability test,” *Compos. Struct.*, vol. 79, no. 1, pp. 133–139, 2007, doi: 10.1016/j.compstruct.2005.11.057.

[16] D. Balageas, C.-P. Fritzen, and A. Güemes, *Structural health monitoring*, vol. 90. John Wiley & Sons, 2010.

[17] G. Y. Baaklini, “Nondestructive evaluation, structural health monitoring and optical diagnostics at NASA Glenn: A summary,” *Emerg. Technol. Non-Destructive Test. V*, pp. 3–5, 2012.

[18] V. Giurgiutiu and C. Soutis, “Enhanced composites integrity through structural health monitoring,” *Appl. Compos. Mater.*, vol. 19, no. 5, pp. 813–829, 2012.

[19] S. Sugimoto, T. Aoki, Y. Iwahori, and T. Ishikawa, “Nondestructive Evaluation of Composites Using Micro-Focused X-Ray CT Scanner,” in *AIP Conference Proceedings*, 2005, vol. 760, no. 1, pp. 1081–1086.

[20] W. Boyes, *Instrumentation reference book*. Butterworth-Heinemann, 2009.

[21] G. Birkelbach, I. J. Aldave, I. López, and W. Grill, “Integral ultrasonic structural health and load monitoring on a fiber reinforced polymer-based composite helicopter tail boom,” in *Health Monitoring of Structural and Biological Systems 2012*, 2012, vol. 8348, pp. 258–262.

[22] P. Rizzo, A. Marzani, and J. Bruck, “Ultrasonic guided waves for nondestructive evaluation/structural health monitoring of trusses,” *Meas. Sci. Technol.*, vol. 21, no. 4, 2010.

[23] J. Veilleux, S. E. Kruger, K.-T. Wu, and A. Blouin, “Multi-element, high-temperature integrated ultrasonic transducers for structural health monitoring,” in *Smart Sensor Phenomena, Technology, Networks, and Systems Integration 2013*, 2013, vol. 8693.

[24] Y. Sun, Y. Zhang, C. Qian, and Z. Zhang, “Near-field ultrasonic phased array deflection focusing based CFRP wing box structural health monitoring,” *Int. J. Distrib. Sens. Networks*, vol. 9, no. 11, 2013.

[25] T. D’orazio, M. Leo, A. Distante, C. Guaragnella, V. Pianese, and G. Cavaccini, “Automatic ultrasonic inspection for internal defect detection in composite materials,” *NDT e Int.*, vol. 41, no. 2, pp. 145–154, 2008.

[26] T. Segreto, R. Teti, and V. Lopresto, “Non-destructive testing of low-velocity impacted composite material laminates through ultrasonic inspection methods,” *Charact. some Compos. Mater.*, pp. 45–66, 2018.

[27] R. P. Finotti, F. de Souza Barbosa, A. A. Cury, and C. Gentile, “A novel natural frequency-based technique to detect structural changes using computational intelligence,” *Procedia Eng.*, vol. 199, pp. 3314–3319, 2017.

[28] R. Y. Liang, J. Hu, and F. Choy, “Theoretical study of crack-induced eigenfrequency changes on beam structures,” *J. Eng. Mech.*, vol. 118, no. 2, pp. 384–396, 1992.

[29] D. Maity and R. R. Tripathy, “Damage assessment of structures from changes in natural frequencies using genetic algorithm,” *Struct. Eng. Mech. An Int. J.*, vol. 19, no. 1, pp. 21–42, 2005.

[30] Z. Zhang *et al.*, “Vibration-based assessment of delaminations in FRP composite plates,” *Compos. Part B Eng.*, vol. 144, pp. 254–266, 2018.

[31] H.-Y. Kim, “Vibration-based damage identification using reconstructed FRFs in composite structures,” *J. Sound Vib.*, vol. 259, no. 5, pp. 1131–1146, 2003.

[32] C. Mahieddine and L. Rachid, “Comparative study of direct and inverse problems of cracked beams,” in *MATEC web of conferences*, 2018, vol. 149, p. 2015.

[33] A. Malekjafarian, P. J. McGetrick, and E. J. OBrien, “A review of indirect bridge monitoring using passing vehicles,” *Shock Vib.*, vol. 2015, 2015.

[34] K. Roy and S. Ray-Chaudhuri, “Fundamental mode shape and its derivatives in structural damage localization,” *J. Sound Vib.*, vol. 332, no. 21, pp. 5584–5593, 2013.

[35] J. J. Lee, J. W. Lee, J. H. Yi, C. B. Yun, and H. Y. Jung, “Neural networks-based damage detection for bridges considering errors in baseline finite element models,” *J. Sound Vib.*, vol. 280, no. 3, pp. 555–578, 2005, doi: https://doi.org/10.1016/j.jsv.2004.01.003.

[36] M. A. Perez, L. Gil, and S. Oller, “Impact damage identification in composite laminates using vibration testing,” *Compos. Struct.*, vol. 108, pp. 267–276, 2014.

[37] K.-H. Ip and P.-C. Tse, “Locating damage in circular cylindrical composite shells based on frequency sensitivities and mode shapes,” *Eur. J. Mech.*, vol. 21, no. 4, pp. 615–628, 2002.

[38] H. Hu, B.-T. Wang, C.-H. Lee, and J.-S. Su, “Damage detection of surface cracks in composite laminates using modal analysis and strain energy method,” *Compos. Struct.*, vol. 74, no. 4, pp. 399–405, 2006.

[39] T. M. Whalen, “The behavior of higher order mode shape derivatives in damaged, beam-like structures,” *J. Sound Vib.*, vol. 309, no. 3–5, pp. 426–464, 2008.

[40] O. S. Salawn, “Damage location using vibration mode shapes,” in *Proceedings of 12th IMAC*, 1994, pp. 933–938.

[41] F. Just-Agosto, B. Shafiq, and D. Serrano, “Development of a damage detection scheme applicable to sandwich composites,” *J. Sandw. Struct. Mater.*, vol. 9, no. 4, pp. 343–363, 2007.

[42] H. Li, C. He, J. Ji, H. Wang, and C. Hao, “Crack damage detection in beam-like structures using RBF neural networks with experimental validation,” *Int. J. Innov. Comput. Inf. Control*, vol. 1, no. 4, pp. 625–634, 2005.

[43] C. P. Ratcliffe, “A frequency and curvature based experimental method for locating damage in structures,” *J. Vib. Acoust.*, vol. 122, no. 3, pp. 324–329, 2000.

[44] M. Wevers and M. Surgeon, “Acoustic emission and composites,” in *Comprehensive composite materials, volume 5:test methods, nondestructive evaluation, and smart materials*, L. Carlsson, Ed. Amsterdam: Elsevier Science Ltd, Oxford, UK, 2000, pp. 345–357.

[45] Z. Kral, W. Horn, and J. Steck, “Crack propagation analysis using acoustic emission sensors for structural health monitoring systems,” *Sci. World J.*, vol. 2013, 2013.

[46] P. Rizzo and F. L. di Scalea, “Acoustic emission monitoring of carbon-fiber-reinforced-polymer bridge stay cables in large-scale testing,” *Exp. Mech.*, vol. 41, no. 3, pp. 282–290, 2001.

[47] M. Nishino, Y. Harada, T. Suzuki, and H. Niino, “Acoustic damage detection in laser-cut CFRP composite materials,” in *Laser Applications in Microelectronic and Optoelectronic Manufacturing (Lamom) Xvii*, 2012, vol. 8243.

[48] D. G. Aggelis, N.-M. Barkoula, T. E. Matikas, and A. S. Paipetis, “Acoustic structural health monitoring of composite materials: Damage identification and evaluation in cross ply laminates using acoustic emission and ultrasonics,” *Compos. Sci. Technol.*, vol. 72, no. 10, pp. 1127–1133, 2012.

[49] R. Austin, P. Ziehl, and D. FORSYTH, “Development and validation of Acoustic Emission structural health monitoring for aerospace structures,” *Struct. Heal. Monit. 2013*, vol. 1,2, pp. 2123–2129, 2013.

[50] S. Masmoudi, A. El Mahi, and R. El Guerjouma, “Mechanical behaviour and health monitoring by acoustic emission of sandwich composite integrated by piezoelectric implant,” *Compos. Part B Eng.*, vol. 67, pp. 76–83, 2014.

[51] R. De Oliveira and A. T. Marques, “Health monitoring of FRP using acoustic emission and artificial neural networks,” *Comput. Struct.*, vol. 86, no. 3–5, pp. 367–373, 2008.

[52] M. Haggui, A. El Mahi, Z. Jendli, A. Akrout, and M. Haddar, “Static and fatigue characterization of flax fiber reinforced thermoplastic composites by acoustic emission,” *Appl. Acoust.*, vol. 147, pp. 100–110, 2019.

[53] J. P. McCrory *et al.*, “Damage classification in carbon fibre composites using acoustic emission: A comparison of three techniques,” *Compos. Part B Eng.*, vol. 68, pp. 424–430, 2015.

[54] M. Saeedifar, M. A. Najafabadi, D. Zarouchas, H. H. Toudeshky, and M. Jalalvand, “Barely visible impact damage assessment in laminated composites using acoustic emission,” *Compos. Part B Eng.*, vol. 152, pp. 180–192, 2018.

[55] S. Sengupta, A. K. Datta, and P. Topdar, “Structural damage localisation by acoustic emission technique: A state of the art review,” *Lat. Am. J. Solids Struct.*, vol. 12, pp. 1565–1582, 2015.

[56] G. P. McCombe, J. Rouse, R. S. Trask, P. J. Withers, and I. P. Bond, “X-ray damage characterisation in self-healing fibre reinforced polymers,” *Compos. Part A Appl. Sci. Manuf.*, vol. 43, no. 4, pp. 613–620, 2012, doi: 10.1016/j.compositesa.2011.12.020.

[57] R. Usamentiaga, P. Venegas, J. Guerediaga, L. Vega, J. Molleda, and F. G. Bulnes, “Infrared thermography for temperature measurement and non-destructive testing,” *Sensors*, vol. 14, no. 7, pp. 12305–12348, 2014.

[58] B. Wiecek, “Review on thermal image processing for passive and active thermography,” in *2005 IEEE Engineering in Medicine and Biology 27th Annual Conference*, 2006, pp. 686–689.

[59] S. M. Shepard, “Introduction to active thermography for non-destructive evaluation,” *Anti-Corrosion Methods Mater.*, pp. 236–239, 1997.

[60] X. P. V Maldague, “Overview of nondestructive evaluation (NDE) using infrared thermography,” in *Nondestructive evaluation of materials by infrared thermography*, Springer, 1993, pp. 1–22.

[61] L. Cheng and G. Y. Tian, “Comparison of nondestructive testing methods on detection of delaminations in composites,” *J. sensors*, vol. 2012, 2012.

[62] W. Harizi, S. Chaki, G. Bourse, and M. Ourak, “Mechanical damage assessment of Glass Fiber-Reinforced Polymer composites using passive infrared thermography,” *Compos. Part B Eng.*, vol. 59, pp. 74–79, 2014.

[63] J. Montesano, H. Bougherara, and Z. Fawaz, “Application of infrared thermography for the characterization of damage in braided carbon fiber reinforced polymer matrix composites,” *Compos. Part B Eng.*, vol. 60, pp. 137–143, 2014.

[64] S. Boccardi, G. M. Carlomagno, C. Meola, G. Simeoli, and P. Russo, “Infrared thermography to evaluate thermoplastic composites under bending load,” *Compos. Struct.*, vol. 134, pp. 900–904, 2015.

[65] T. Lisle, C. Bouvet, N. Hongkarnjanakul, M.-L. Pastor, S. Rivallant, and P. Margueres, “Measure of fracture toughness of compressive fiber failure in composite structures using infrared thermography,” *Compos. Sci. Technol.*, vol. 112, pp. 22–33, 2015.

[66] J.-W. Kim, H.-S. Kim, and D.-G. Lee, “Measurement of tensile strength and infrared thermography on unidirectional GFRP,” *Mater. Res. Bull.*, vol. 58, pp. 35–38, 2014.

[67] T. D’Orazio, C. Guaragnella, M. Leo, and P. Spagnolo, “Defect detection in aircraft composites by using a neural approach in the analysis of thermographic images,” *NDT E Int.*, vol. 38, no. 8, pp. 665–673, 2005.

[68] K. Srinivas, A. O. Siddiqui, and J. Lahiri, “Thermographic inspection of composite materials,” in *Proc. National Seminar on Non-Destructive Evaluation*, 2006, vol. 12, pp. 7–9.

[69] J. M. Menendez, P. Munoz, J. M. Pintado, and A. Guemes, “Damage detection in composite materials by FBGs,” in *Second European Workshop on Optical Fibre Sensors*, 2004, vol. 5502, pp. 451–454.

[70] H. Zhao, Q. Wang, Y. Qiu, J. Chen, Y. Wang, and Z. Fan, “Strain transfer of surface-bonded fiber Bragg grating sensors for airship envelope structural health monitoring,” *J. Zhejiang Univ. Sci. A*, vol. 13, no. 7, pp. 538–545, 2012.

[71] Y. Shimada and A. Nishimura, “Development of optical fiber Bragg grating sensors for structural health monitoring,” *J. Laser Micro Nanoeng.*, vol. 8, pp. 110–114, 2013.

[72] J. J. Bai, J. X. Li, J. Zhang, X. Y. Zhang, L. Wang, and Y. Wu, “Smart Structural Health Monitoring Based on Detecting Picometer-scale Wavelength Shift of Fiber Bragg Grating,” in *Key Engineering Materials*, 2013, vol. 562–565, pp. 1346–1352.

[73] E. Kirkby, R. De Oliveira, V. Michaud, and J. A. Månson, “Impact localisation with FBG for a self-healing carbon fibre composite structure,” *Compos. Struct.*, vol. 94, no. 1, pp. 8–14, 2011.

[74] Y. Y. Hung, “Shearography: a new optical method for strain measurement and nondestructive testing,” *Opt. Eng.*, vol. 21, no. 3, pp. 391–395, 1982.

[75] A. Naghashpour, “In-situ damage and strain monitoring of large polymer composite structures using carbon nanotube networks,” Concordia University, 2014.

[76] A. J. Jefferson, V. Arumugam, and H. N. Dhakal, *Repair of polymer composites: methodology, techniques, and challenges*. Woodhead Publishing, 2018.

[77] W. Steinchen, L. X. Yang, G. and Kupfer, P. Mäckel, and F. Vössing, “Strain analysis by means of digital shearography: potential, limitations and demonstration,” *J. Strain Anal. Eng. Des.*, vol. 33, no. 2, pp. 171–182, 1998.

[78] X. Wang, S. Wang, and D. D. L. Chung, “Sensing damage in carbon fiber and its polymer-matrix and carbon-matrix composites by electrical resistance measurement,” *J. Mater. Sci.*, vol. 34, no. 11, pp. 2703–2713, 1999.

[79] D.-C. Seo and J.-J. Lee, “Damage detection of CFRP laminates using electrical resistance measurement and neural network,” *Compos. Struct.*, vol. 47, no. 1–4, pp. 525–530, 1999.

[80] R. Schueler, S. P. Joshi, and K. Schulte, “Damage detection in CFRP by electrical conductivity mapping,” *Compos. Sci. Technol.*, vol. 61, no. 6, pp. 921–930, 2001.

[81] M. Kupke, K. Schulte, and R. Schüler, “Non-destructive testing of FRP by dc and ac electrical methods,” *Compos. Sci. Technol.*, vol. 61, no. 6, pp. 837–847, 2001.

[82] A. S. Kaddour, F. A. R. Al-Salehi, S. T. S. Al-Hassani, and M. J. Hinton, “Electrical resistance measurement technique for detecting failure in CFRP materials at high strain rates,” *Compos. Sci. Technol.*, vol. 51, no. 3, pp. 377–385, 1994.

[83] A. Todoroki, “The effect of number of electrodes and diagnostic tool for monitoring the delamination of CFRP laminates by changes in electrical resistance,” *Compos. Sci. Technol.*, vol. 61, no. 13, pp. 1871–1880, 2001.

[84] S. Wang and D. D. L. Chung, “Mechanical damage in carbon fiber polymer-matrix composite, studied by electrical resistance measurement,” *Compos. interfaces*, vol. 9, no. 1, pp. 51–60, 2002.

[85] A. Todoroki, Y. Mizutani, Y. Suzuki, and D. Haruyama, “Fatigue damage detection of CFRP using the electrical resistance change method,” *Int. J. Aeronaut. Sp. Sci.*, vol. 14, no. 4, pp. 350–355, 2013.

[86] L. Hou and S. A. Hayes, “A resistance-based damage location sensor for carbon-fibre composites,” *Smart Mater. Struct.*, vol. 11, no. 6, pp. 966–969, 2002.

[87] S. Hayes and F. Jones, “Electrical damage detection system for a self-healing polymeric composite,” U.S. Patent Application 11/577,968, Dec. 03, 2009

[88] B. P. Rice, “Sensing system for monitoring the structural health of composite structures,” U.S. Patent No. 7,921,727, Apr. 12, 2011

[89] T. W. Ebbesen, H. J. Lezec, H. Hiura, J. W. Bennett, H. F. Ghaemi, and T. Thio, “Electrical conductivity of individual carbon nanotubes,” *Nature*, vol. 382, no. 6586, pp. 54–56, 1996, doi: 10.1038/382054a0.

[90] W. Obitayo and T. Liu, “A review: carbon nanotube-based piezoresistive strain sensors,” *J. Sensors*, vol. 652438, pp. 1–15, 2012.

[91] M.-F. Yu, O. Lourie, M. J. Dyer, K. Moloni, T. F. Kelly, and R. S. Ruoff, “Strength and breaking mechanism of multiwalled carbon nanotubes under tensile load,” *Science (80-.).*, vol. 287, pp. 637–640, 2000.

[92] N. Yao, V. Lordi, “Young’s modulus of single-walled carbon nanotubes,"," *J. Appl. Physics,* vol. 84, pp. 1939–1943, 1998.

[93] K. Sun, M. A. Stroscio, and M. Dutta, “Thermal conductivity of carbon nanotubes,” *J. Appl. Phys.*, vol. 105, 2009.

[94] Jkw. Sandler, J. E. Kirk, I. A. Kinloch, M. S. P. Shaffer, and A. H. Windle, “Ultra-low electrical percolation threshold in carbon-nanotube-epoxy composites,” *Polymer (Guildf).*, vol. 44, no. 19, pp. 5893–5899, 2003.

[95] W. Zhang, V. Sakalkar, and N. Koratkar, “In situ health monitoring and repair in composites using carbon nanotube additives,” *Appl. Phys. Lett.*, vol. 91, no. 13, 2007.

[96] J.-M. Park, D.-S. Kim, J.-R. Lee, and T.-W. Kim, “Nondestructive damage sensitivity and reinforcing effect of carbon nanotube/epoxy composites using electro-micromechanical technique,” *Mater. Sci. Eng. C*, vol. 23, no. 6–8, pp. 971–975, 2003.

[97] A. Montazeri, J. Javadpour, A. Khavandi, A. Tcharkhtchi, and A. Mohajeri, “Mechanical properties of multi-walled carbon nanotube/epoxy composites,” *Mater. Des.*, vol. 31, no. 9, pp. 4202–4208, 2010, doi: https://doi.org/10.1016/j.matdes.2010.04.018.

[98] E. T. Thostenson and T. Chou, “Carbon nanotube networks: sensing of distributed strain and damage for life prediction and self healing,” *Adv. Mater.*, vol. 18, no. 21, pp. 2837–2841, 2006.

[99] E. T. Thostenson and T.-W. Chou, “Real-time in situ sensing of damage evolution in advanced fiber composites using carbon nanotube networks,” *Nanotechnology*, vol. 19, no. 21, p. 215713, 2008.

[100] G. T. Pham, Y.-B. Park, Z. Liang, C. Zhang, and B. Wang, “Processing and modeling of conductive thermoplastic/carbon nanotube films for strain sensing,” *Compos. Part B Eng.*, vol. 39, no. 1, pp. 209–216, 2008.

[101] A. Naghashpour and S. Van Hoa, “A technique for real-time detection, location and quantification of damage in large polymer composite structures made of electrically non-conductive fibers and carbon nanotube networks,” *Nanotechnology*, vol. 24, no. 45, p. 455502, 2013.

[102] D. S. W. Ting, Y. Liu, P. Burlina, X. Xu, N. M. Bressler, and T. Y. Wong, “AI for medical imaging goes deep,” *Nat. Med.*, vol. 24, no. 5, pp. 539–540, 2018, doi: 10.1038/s41591-018-0029-3.

[103] A. Kumar and R. Kumar, “Adaptive artificial intelligence for automatic identification of defect in the angular contact bearing,” *Neural Comput. Appl.*, vol. 29, no. 8, pp. 277–287, 2018, doi: 10.1007/s00521-017-3123-4.

[104] S. Zhao, F. Blaabjerg, and H. Wang, “An Overview of Artificial Intelligence Applications for Power Electronics,” *IEEE Trans. Power Electron.*, vol. 36, no. 4, pp. 4633–4658, 2021, doi: 10.1109/TPEL.2020.3024914.

[105] N. H. M. M. Shrifan, M. F. Akbar, and N. A. M. Isa, “Prospect of Using Artificial Intelligence for Microwave Nondestructive Testing Technique: A Review,” *IEEE Access*, vol. 7, pp. 110628–110650, 2019, doi: 10.1109/ACCESS.2019.2934143.

[106] M. W. Libbrecht and W. S. Noble, “Machine learning applications in genetics and genomics,” *Nat. Rev. Genet.*, vol. 16, no. 6, pp. 321–332, 2015, doi: 10.1038/nrg3920.

[107] M.-K. Kazi, F. Eljack, and E. Mahdi, “Predictive ANN models for varying filler content for cotton fiber/PVC composites based on experimental load displacement curves,” *Compos. Struct.*, vol. 254, p. 112885, 2020, doi: https://doi.org/10.1016/j.compstruct.2020.112885.

[108] C. He, M. Ma, and P. Wang, “Extract interpretability-accuracy balanced rules from artificial neural networks: A review,” *Neurocomputing*, vol. 387, pp. 346–358, 2020, doi: https://doi.org/10.1016/j.neucom.2020.01.036.

[109] U. M. R. Paturi, S. Cheruku, and N. S. Reddy, “The role of artificial neural networks in prediction of mechanical and tribological properties of composites—a comprehensive review,” *Arch. Comput. Methods Eng.*, pp. 1–41, 2022.

[110] M. Gayatri Vineela, A. Dave, and P. Kiran Chaganti, “Artificial Neural Network based Prediction of Tensile Strength of Hybrid Composites,” *Mater. Today Proc.*, vol. 5, no. 9, Part 3, pp. 19908–19915, 2018, doi: https://doi.org/10.1016/j.matpr.2018.06.356.

[111] K. M. A. Hossain, M. S. Anwar, and S. G. Samani, “Regression and artificial neural network models for strength properties of engineered cementitious composites,” *Neural Comput. Appl.*, vol. 29, no. 9, pp. 631–645, 2018, doi: 10.1007/s00521-016-2602-3.

[112] M. Kurpinska and L. Kułak, “Predicting Performance of Lightweight Concrete with Granulated Expanded Glass and Ash Aggregate by Means of Using Artificial Neural Networks,” *Materials* , vol. 12, no. 12. 2019. doi: 10.3390/ma12122002.

[113] A. Hammoudi, K. Moussaceb, C. Belebchouche, and F. Dahmoune, “Comparison of artificial neural network (ANN) and response surface methodology (RSM) prediction in compressive strength of recycled concrete aggregates,” *Constr. Build. Mater.*, vol. 209, pp. 425–436, 2019, doi: https://doi.org/10.1016/j.conbuildmat.2019.03.119.

[114] M. Jalal and A. A. Ramezanianpour, “Strength enhancement modeling of concrete cylinders confined with CFRP composites using artificial neural networks,” *Compos. Part B Eng.*, vol. 43, no. 8, pp. 2990–3000, 2012, doi: https://doi.org/10.1016/j.compositesb.2012.05.044.

[115] S. M. Hejazi, M. Sheikhzadeh, S. M. Abtahi, V. Malekian, and S. Mahmoodi, “Using slippage theory to analyze shear behavior of loop-formed fiber reinforced soil composites,” *J. Ind. Text.*, vol. 43, no. 3, pp. 415–439, Sep. 2012, doi: 10.1177/1528083712458304.

[116] K.-L. Xiang, P.-Y. Xiang, and Y.-P. Wu, “Prediction of the fatigue life of natural rubber composites by artificial neural network approaches,” *Mater. Des.*, vol. 57, pp. 180–185, 2014, doi: https://doi.org/10.1016/j.matdes.2013.12.044.

[117] Z. Jiang, Z. Zhang, and K. Friedrich, “Prediction on wear properties of polymer composites with artificial neural networks,” *Compos. Sci. Technol.*, vol. 67, no. 2, pp.

168–176, 2007, doi: https://doi.org/10.1016/j.compscitech.2006.07.026.

[118] A. Vinoth and S. Datta, “Optimization of Mechanical Characteristics of UHMWPE Composites Using Computational Intelligence BT - Structural Integrity Assessment,” 2020, pp. 211–220.

[119] U. Devadiga, R. K. R. Poojary, and P. Fernandes, “Artificial neural network technique to predict the properties of multiwall carbon nanotube-fly ash reinforced aluminium composite,” *J. Mater. Res. Technol.*, vol. 8, no. 5, pp. 3970–3977, 2019, doi: https://doi.org/10.1016/j.jmrt.2019.07.005.

[120] M. Amirjan, H. Khorsand, M. H. Siadati, and R. Eslami Farsani, “Artificial Neural Network prediction of Cu–Al2O3 composite properties prepared by powder metallurgy method,” *J. Mater. Res. Technol.*, vol. 2, no. 4, pp. 351–355, 2013, doi: https://doi.org/10.1016/j.jmrt.2013.08.001.

[121] A. Canakci, S. Ozsahin, and T. Varol, “Modeling the influence of a process control agent on the properties of metal matrix composite powders using artificial neural networks,” *Powder Technol.*, vol. 228, pp. 26–35, 2012, doi: https://doi.org/10.1016/j.powtec.2012.04.045.

[122] L. Natrayan and M. Senthil Kumar, “An integrated artificial neural network and Taguchi approach to optimize the squeeze cast process parameters of AA6061/Al2O3/SiC/Gr hybrid composites prepared by novel encapsulation feeding technique,” *Mater. Today Commun.*, vol. 25, p. 101586, 2020, doi: https://doi.org/10.1016/j.mtcomm.2020.101586.

[123] M. Akbari, P. Asadi, P. Zolghadr, and A. Khalkhali, “Multicriteria optimization of mechanical properties of aluminum composites reinforced with different reinforcing particles type,” *Proc. Inst. Mech. Eng. Part E J. Process Mech. Eng.*, vol. 232, no. 3, pp. 323–337, Apr. 2017, doi: 10.1177/0954408917704994.

[124] O. T. Adesina *et al.*, “Mechanical property prediction of SPS processed GNP/PLA polymer nanocomposite using artificial neural network,” *Cogent Eng.*, vol. 7, no. 1, Jan. 2020, doi: 10.1080/23311916.2020.1720894.

[125] C. C. Nwobi-Okoye and B. Q. Ochieze, “Age hardening process modeling and optimization of aluminum alloy A356/Cow horn particulate composite for brake drum application using RSM, ANN and simulated annealing,” *Def. Technol.*, vol. 14, no. 4, pp. 336–345, 2018, doi: https://doi.org/10.1016/j.dt.2018.04.001.

[126] M. S. Kabbani and H. A. El Kadi, “Predicting the effect of cooling rate on the mechanical properties of glass fiber–polypropylene composites using artificial neural networks,” *J. Thermoplast. Compos. Mater.*, vol. 32, no. 9, pp. 1268–1281, Aug. 2018, doi: 10.1177/0892705718792351.

[127] S. Ye, B. Li, Q. Li, H.-P. Zhao, and X.-Q. Feng, “Deep neural network method for predicting the mechanical properties of composites,” *Appl. Phys. Lett.*, vol. 115, no. 16, p. 161901, Oct. 2019, doi: 10.1063/1.5124529.

[128] M. İnal, S. Sahin, and Y. Sahin, “Optimization of the Young’s Modulus of Low Flow Polypropylene Talc/Colemanite Hybrid Composite Materials with Artificial Neural Networks,” *IFAC-PapersOnLine*, vol. 51, no. 30, pp. 277–281, 2018, doi: https://doi.org/10.1016/j.ifacol.2018.11.301.

[129] S. Tiryaki and C. Hamzaçebi, “Predicting modulus of rupture (MOR) and modulus of elasticity (MOE) of heat treated woods by artificial neural networks,” *Measurement*, vol. 49, pp. 266–274, 2014, doi: https://doi.org/10.1016/j.measurement.2013.12.004.

[130] X. Xu, M. Elgamal, M. Doddamani, and N. Gupta, “Tailoring composite materials for nonlinear viscoelastic properties using artificial neural networks,” *J. Compos. Mater.*, vol. 55, no. 11, pp. 1547–1560, Nov. 2020, doi: 10.1177/0021998320973744.

[131] Z. X. Tan, D. P. Thambiratnam, T. H. T. Chan, M. Gordan, and H. Abdul Razak, “Damage detection in steel-concrete composite bridge using vibration characteristics and artificial neural network,” *Struct. Infrastruct. Eng.*, vol. 16, no. 9, pp. 1247–1261, Sep. 2020, doi: 10.1080/15732479.2019.1696378.

[132] X. Xu and N. Gupta, “Artificial Neural Network Approach to Predict the Elastic Modulus from Dynamic Mechanical Analysis Results,” *Adv. Theory Simulations*, vol. 2, no. 4, p. 1800131, Apr. 2019, doi: https://doi.org/10.1002/adts.201800131.

[133] M. C. Messner, “Convolutional Neural Network Surrogate Models for the Mechanical Properties of Periodic Structures,” *J. Mech. Des.*, vol. 142, no. 2, pp. 1–6, Oct. 2019, doi: 10.1115/1.4045040.

[134] N. Baldo, E. Manthos, and M. Pasetto, “Analysis of the Mechanical Behaviour of Asphalt Concretes Using Artificial Neural Networks,” *Adv. Civ. Eng.*, vol. 2018, p. 1650945, 2018, doi: 10.1155/2018/1650945.

[135] L. Rueda-García, J. L. Bonet Senach, P. F. Miguel Sosa, and M. Á. Fernández Prada, “Experimental analysis of the shear strength of composite concrete beams without web reinforcement,” *Eng. Struct.*, vol. 229, p. 111664, 2021, doi: https://doi.org/10.1016/j.engstruct.2020.111664.

[136] D. Harsha Vardhan, A. Ramesh, and B. Chandra Mohana Reddy, “Effect of ceramic fillers on flexural strength of the GFRP composite material,” *Mater. Today Proc.*, vol. 37, pp. 1739–1742, 2021, doi: https://doi.org/10.1016/j.matpr.2020.07.356.

[137] S. Shyam, S. Kaul, N. Kalsara, and T. N. Babu, “Mechanical behaviour and microscopic analysis of epoxy and E-glass reinforced banyan fibre composites with the application of artificial neural network and deep neural network for the automatic prediction of orientation,” *J. Compos. Mater.*, vol. 55, no. 2, pp. 213–234, Aug. 2020, doi: 10.1177/0021998320947136.

[138] G. L. E. Prasad, B. S. K. Gowda, and R. Velmurugan, “Prediction of Flexural Properties of Coir Polyester Composites by ANN BT - Mechanics of Composite and Multi-functional Materials, Volume 7,” 2016, pp. 173–180.

[139] S. Jayabal, S. Rajamuneeswaran, R. Ramprasath, and N. S. Balaji, “Artificial Neural Network Modeling of Mechanical Properties of Calcium Carbonate Impregnated Coir-Polyester Composites,” *Trans. Indian Inst. Met.*, vol. 66, no. 3, pp. 247–255, 2013, doi: 10.1007/s12666-013-0255-9.

[140] L. Ponraj Sankar, S. Sivasankar, M. Shunmugasundaram, and A. Praveen Kumar, “Predicting the polymer modified ferrocement ultimate flexural strength using artificial neural network and adaptive network based fuzzy inference system,” *Mater. Today Proc.*, vol. 27, pp. 1375–1380, 2020, doi: https://doi.org/10.1016/j.matpr.2020.02.760.

[141] H. Naderpour, O. Poursaeidi, and M. Ahmadi, “Shear resistance prediction of concrete beams reinforced by FRP bars using artificial neural networks,” *Measurement*, vol. 126, pp. 299–308, 2018, doi: https://doi.org/10.1016/j.measurement.2018.05.051.

[142] V. Aguilar, C. Sandoval, J. M. Adam, J. Garzón-Roca, and G. Valdebenito, “Prediction of the shear strength of reinforced masonry walls using a large experimental database and artificial neural networks,” *Struct. Infrastruct. Eng.*, vol. 12, no. 12, pp. 1661–1674, Dec. 2016, doi: 10.1080/15732479.2016.1157824.

[143] H. Mashhadban, S. S. Kutanaei, and M. A. Sayarinejad, “Prediction and modeling of mechanical properties in fiber reinforced self-compacting concrete using particle swarm optimization algorithm and artificial neural network,” *Constr. Build. Mater.*, vol. 119, pp. 277–287, 2016, doi: https://doi.org/10.1016/j.conbuildmat.2016.05.034.

[144] Z. Jiang, L. Gyurova, Z. Zhang, K. Friedrich, and A. K. Schlarb, “Neural network based prediction on mechanical and wear properties of short fibers reinforced polyamide composites,” *Mater. Des.*, vol. 29, no. 3, pp. 628–637, 2008, doi: https://doi.org/10.1016/j.matdes.2007.02.008.

[145] A. Sharma and V. Kushvaha, “Predictive modelling of fracture behaviour in silica-filled polymer composite subjected to impact with varying loading rates using artificial neural network,” *Eng. Fract. Mech.*, vol. 239, p. 107328, 2020, doi: https://doi.org/10.1016/j.engfracmech.2020.107328.

[146] C. Yang, Y. Kim, S. Ryu, and G. X. Gu, “Using convolutional neural networks to predict composite properties beyond the elastic limit,” *MRS Commun.*, vol. 9, no. 2, pp. 609–617, 2019, doi: 10.1557/mrc.2019.49.

[147] T. Jia-li, L. Yi-jun, and W. Fang-sheng, “Neural network for prediction of composite mechanical properties based on niche genetic algorithm,” in *2010 International Conference on Networking and Digital Society*, 2010, vol. 1, pp. 130–133. doi: 10.1109/ICNDS.2010.5479616.

[148] I. Tabian, H. Fu, and Z. Sharif Khodaei, “A Convolutional Neural Network for Impact Detection and Characterization of Complex Composite Structures,” *Sensors* , vol. 19, no. 22. 2019. doi: 10.3390/s19224933.

[149] C. Yang, Y. Kim, S. Ryu, and G. X. Gu, “Prediction of composite microstructure stress-strain curves using convolutional neural networks,” *Mater. Des.*, vol. 189, p. 108509, 2020, doi: https://doi.org/10.1016/j.matdes.2020.108509.

[150] A. Bezazi, S. G. Pierce, K. Worden, and E. H. Harkati, “Fatigue life prediction of sandwich composite materials under flexural tests using a Bayesian trained artificial neural network,” *Int. J. Fatigue*, vol. 29, no. 4, pp. 738–747, 2007, doi: https://doi.org/10.1016/j.ijfatigue.2006.06.013.

[151] T. M. Ahmed, P. L. Green, and H. A. Khalid, “Predicting fatigue performance of hot mix asphalt using artificial neural networks,” *Road Mater. Pavement Des.*, vol. 18, no. sup2, pp. 141–154, May 2017, doi: 10.1080/14680629.2017.1306928.

[152] G. Allegri, “Modelling fatigue delamination growth in fibre-reinforced composites: Power-law equations or artificial neural networks?,” *Mater. Des.*, vol. 155, pp. 59–70, 2018, doi: https://doi.org/10.1016/j.matdes.2018.05.049.

[153] C. Bhat, M. R. Bhat, and C. R. L. Murthy, “Characterization of Failure Modes in CFRP Composites — An ANN Approach,” *J. Compos. Mater.*, vol. 42, no. 3, pp. 257–276, Feb. 2008, doi: 10.1177/0021998307086209.

[154] M. Al-Assadi, H. A. El Kadi, and I. M. Deiab, “Using Artificial Neural Networks to Predict the Fatigue Life of Different Composite Materials Including the Stress Ratio Effect,” *Appl. Compos. Mater.*, vol. 18, no. 4, pp. 297–309, 2011, doi: 10.1007/s10443-010-9158-7.

[155] B. B. V. de Sena and R. C. S. F. Júnior, “Criteria for the use of modular networks: fatigue in composite materials,” *J. Compos. Mater.*, vol. 46, no. 23, pp. 2973–2985, Feb. 2012, doi: 10.1177/0021998311434968.

[156] B. da C. Diniz and R. C. S. Freire Júnior, “Study of the fatigue behavior of composites using modular ANN with the incorporation of a posteriori failure probability,” *Int. J. Fatigue*, vol. 131, p. 105357, 2020, doi: https://doi.org/10.1016/j.ijfatigue.2019.105357.

[157] H. El Kadi and Y. Al-Assaf, “Energy-based fatigue life prediction of fiberglass/epoxy composites using modular neural networks,” *Compos. Struct.*, vol. 57, no. 1, pp. 85–89, 2002, doi: https://doi.org/10.1016/S0263-8223(02)00071-5.

[158] A. Naghashpour and S. Van Hoa, “A technique for in-situ detection of random failure in composite structures under cyclic loading,” *J. Compos. Mater.*, vol. 53, no. 23, pp. 3243–3255, Apr. 2019, doi: 10.1177/0021998319839131.

[159] N. K. Chauhan and K. Singh, “A Review on Conventional Machine Learning vs Deep Learning,” in *2018 International Conference on Computing, Power and Communication Technologies (GUCON)*, 2018, pp. 347–352. doi: 10.1109/GUCON.2018.8675097.

[160] R. Kohavi, “Glossary of terms,” *Spec. issue Appl. Mach. Learn. Knowl. Discov. Process*, vol. 30, no. 271, pp. 127–132, 1998.

[161] S. Setiowati, E. L. Franita, and I. Ardiyanto, “A review of optimization method in face recognition: Comparison deep learning and non-deep learning methods,” in *2017 9th International Conference on Information Technology and Electrical Engineering (ICITEE)*, 2017, pp. 1–6.

[162] N. Aloysius and M. Geetha, “A review on deep convolutional neural networks,” in *2017 international conference on communication and signal processing (ICCSP)*, 2017, pp. 588–592.

[163] Y. LeCun, Y. Bengio, and G. Hinton, “Deep learning,” *Nature*, vol. 521, no. 7553, pp. 436–444, 2015.

[164] R. Ramachandran, D. C. Rajeev, S. G. Krishnan, and P. Subathra, “Deep learning an overview,” *Int. J. Appl. Eng. Res.*, vol. 10, no. 10, pp. 25433–25448, 2015.

[165] J. H. Mikkelsen, “Ltspice–an introduction,” *Tech. report, Inst. Electron. Syst. Aalborg Univ. Aalborg*, 2005.

[166] A. Naghashpour and S. Van Hoa, “A technique for real-time detecting, locating, and quantifying damage in large polymer composite structures made of carbon fibers and carbon nanotube networks,” *Struct. Heal. Monit.*, vol. 14, no. 1, pp. 35–45, Sep. 2014,

doi: 10.1177/1475921714546063.

[167] I. D. Rosca and S. V Hoa, “Highly conductive multiwall carbon nanotube and epoxy composites produced by three-roll milling,” *Carbon N. Y.*, vol. 47, no. 8, pp. 1958–1968, 2009, doi: https://doi.org/10.1016/j.carbon.2009.03.039.

[168] M. Banzi and M. Shiloh, *Getting started with Arduino*. Maker Media, Inc., 2022.

[169] D. A. van Dyk and X.-L. Meng, “The Art of Data Augmentation,” *J. Comput. Graph. Stat.*, vol. 10, no. 1, pp. 1–50, Mar. 2001, doi: 10.1198/10618600152418584.

[170] Arun K, “What is Data Augmentation & how it works?” https://www.mygreatlearning.com/blog/understanding-data-augmentation

[171] J. C. Pouncey and J. M. Lehr, “A spark gap model for LTspice and similar circuit simulation software,” *Dig. Tech. Pap. Int. Pulsed Power Conf.*, vol. 2015-Octob, Oct. 2015, doi: 10.1109/PPC.2015.7296883.

[172] V. I. Kubov, Y. Y. Dymytrov, and R. M. Kubova, “LTspice-model of thermoelectric Peltier-Seebeck element,” in *2016 IEEE 36th International Conference on Electronics and Nanotechnology (ELNANO)*, 2016, pp. 47–51. doi: 10.1109/ELNANO.2016.7493007.

[173] D. Kuhlman, *A Python Book: Beginning Python, Advanced Python, and Python Exercises*. 2013. Accessed: Nov. 24, 2021. [Online]. Available: https://web.archive.org/web/20120623165941/http://cutter.rexx.com/~dkuhlman/python_book_01.html

[174] T. M. Mitchell, *Machine Learning*. New York: McGraw-Hill, 1997.

[175] E. Alpaydin, *Introduction to machine learning*, Fourth edi. Cambridge Massachusetts: The MIT Press, 2020.

[176] Google, “Colaboratory: Frequently Asked Questions.” https://research.google.com/colaboratory/faq.html

[177] P. Kanani and M. Padole, “Deep learning to detect skin cancer using google colab,” *Int. J. Eng. Adv. Technol. Regul. Issue*, vol. 8, no. 6, pp. 2176–2183, 2019.

[178] T. Carneiro, R. V. M. Da NóBrega, T. Nepomuceno, G.-B. Bian, V. H. C. De Albuquerque, and P. P. R. Filho, “Performance Analysis of Google Colaboratory as a Tool for Accelerating Deep Learning Applications,” *IEEE Access*, vol. 6, pp. 61677–61685, 2018, doi: 10.1109/ACCESS.2018.2874767.

[179] N. Shukla and K. Fricklas, *Machine learning with TensorFlow*. Manning Greenwich, 2018.

[180] TensorFlow, “An end-to-end open source machine learning platform.” https://www.tensorflow.org/

[181] Wikipedia, “Keras.” https://en.wikipedia.org/wiki/Keras

[182] L. Torrey and J. Shavlik, “Transfer learning,” in *Handbook of research on machine learning applications and trends: algorithms, methods, and techniques*, IGI global, 2010, pp. 242–264.

[183] S. J. Pan and Q. Yang, “A survey on transfer learning,” *IEEE Trans. Knowl. Data Eng.*, vol. 22, no. 10, pp. 1345–1359, 2010, doi: 10.1109/TKDE.2009.191.

[184] H. Kang, Y. Nam, and S. Choi, “Composite common spatial pattern for subject-to-subject transfer,” *IEEE Signal Process. Lett.*, vol. 16, no. 8, pp. 683–686, 2009, doi: 10.1109/LSP.2009.2022557.

[185] W. Tu and S. Sun, “A subject transfer framework for EEG classification,” *Neurocomputing*, vol. 82, pp. 109–116, 2012.

[186] A. Atyabi, M. H. Luerssen, and D. M. W. Powers, “PSO-based dimension reduction of EEG recordings: Implications for subject transfer in BCI,” *Neurocomputing*, vol. 119, pp. 319–331, 2013, doi: https://doi.org/10.1016/j.neucom.2013.03.027.

[187] D. Wu, B. J. Lance, and T. D. Parsons, “Collaborative filtering for brain-computer interaction using transfer learning and active class selection,” *PLoS One*, vol. 8, no. 2, p. e56624, 2013.

[188] W. Dai, Q. Yang, G. R. Xue, and Y. Yu, “Boosting for transfer learning,” in *ACM International Conference Proceeding Series*, 2007, vol. 227, pp. 193–200. doi: 10.1145/1273496.1273521.

[189] A. Quattoni, M. Collins, and T. Darrell, “Transfer learning for image classification with sparse prototype representations,” *26th IEEE Conf. Comput. Vis. Pattern Recognition, CVPR*, 2008, doi: 10.1109/CVPR.2008.4587637.

[190] J. Deng, Z. Zhang, E. Marchi, and B. Schuller, “Sparse autoencoder-based feature transfer learning for speech emotion recognition,” *Proc. - 2013 Hum. Assoc. Conf. Affect. Comput. Intell. Interact. ACII 2013*, pp. 511–516, 2013, doi: 10.1109/ACII.2013.90.

[191] Y.-P. Lin and T.-P. Jung, “Improving EEG-based emotion classification using conditional transfer learning,” *Front. Hum. Neurosci.*, vol. 11, p. 334, 2017.

[192] K. Hara, D. Saito, and H. Shouno, “Analysis of function of rectified linear unit used in deep learning,” in *2015 international joint conference on neural networks (IJCNN)*, 2015, pp. 1–8.

[193] I. Kouretas and V. Paliouras, “Simplified hardware implementation of the softmax activation function,” in *2019 8th international conference on modern circuits and systems technologies (MOCAST)*, 2019, pp. 1–4.

[194] Dwivedi Priya, “Understanding and Coding a ResNet in Keras.” https://towardsdatascience.com/understanding-and-coding-a-resnet-in-keras-446d7ff84d33

[195] “Advanced Guide to Inception v3.” https://cloud.google.com/tpu/docs/inception-v3-advanced

[196] C. Szegedy, V. Vanhoucke, S. Ioffe, J. Shlens, and Z. Wojna, “Rethinking the Inception Architecture for Computer Vision,” in *2016 IEEE Conference on Computer Vision and Pattern Recognition (CVPR)*, 2016, pp. 2818–2826. doi: 10.1109/CVPR.2016.308.

[197] Y. Wu *et al.*, “Google’s neural machine translation system: Bridging the gap between

human and machine translation," *arXiv Prepr. arXiv1609.08144*, 2016.

[198] K. Papineni, S. Roukos, T. Ward, and W. J. Zhu, *BLEU: a method for automatic evaluation of machine translation*. 2002. Accessed: Nov. 13, 2021. [Online]. Available: http://aclweb.org/anthology/P/P02/P02-1040.pdf